CHARACTERIZING HETEROGENEITY IN THE REGENERATIVE CAPACITY OF HUMAN MUSCLE PROGENITOR CELLS

A Dissertation

Presented to the Faculty of the Graduate School

of Cornell University

In Partial Fulfillment of the Requirements for the Degree of

Doctor of Philosophy

by

Emily Suzanne Riddle

August 2018

CHARACTERIZING HETEROGENEITY IN THE REGENERATIVE CAPACITY OF HUMAN MUSCLE PROGENITOR CELLS

Emily Suzanne Riddle, Ph.D.

Cornell University 2018

Skeletal muscle regeneration following muscle damage is imperative to maintain skeletal muscle structure and function throughout the lifespan. Regeneration requires a complex series of events including activation of skeletal muscle specific stem cells (satellite cells) followed by proliferation and differentiation of committed myoblasts [muscle progenitor cells (MPCs)], and formation/repair of functional multinucleated muscle cells. Activation of satellite cells and expansion of MPCs is essential to generate a sufficient number of viable cells to repair damaged skeletal muscle. In animal models, age is associated with reduced MPC expansion capacity *in vitro*. Additionally, male mouse-MPCs (*m*MPCs) exhibit higher proliferation rates than female *m*MPCs. However, the impact of age and sex on expansion of human MPCs (*h*MPCs) remains unknown.

To evaluate the age- and sex-related differences in expansion capacity of primary *h*MPCs, we compared markers of expansion between young and old, male and female primary *h*MPC cultures. *h*MPCs from older males have reduced expansion capacity compared to their younger counterparts, but *h*MPCs from females are largely unaffected by age. Proliferating MPCs have high energetic and biosynthetic material requirements, and the ability to utilize oxidative phosphorylation (OXPHOS) and/or glycolysis may affect the expansion capacity of MPCs. Results from our study suggest that reduced expansion capacity in OM-*h*MPCs is accompanied by alterations in measurements of OXPHOS while glycolysis is maintained.

However, we and others have demonstrated that not all old *h*MPCs have impaired expansion capacity and similarly, not all young *h*MPCs expand better than old *h*MPCs.

Using K-means cluster analysis and measurements of culture population doubling time and saturation density, we are the first to unbiasedly cluster cultures with similar growth parameters and to identify drivers of expansion capacity that weren't related to categorical age or sex. Our primary findings demonstrate that cultures with enhanced expansion capacity have DEgenes enriched in functional classifications, pathways and networks that suggest promotion of the cell cycle, reduced apoptosis and cellular senescence, and enhanced DNA replication.

Acute inflammation following muscle injury is essential to activate satellite cells. However, chronic muscle inflammation likely contributes to impaired regenerative capacity in skeletal muscle. Previous research has identified muscle inflammatory susceptibility, or the ability to manage and respond to inflammation, as a predictor of failed muscle regeneration and regrowth following surgery. We determined a transcript profile that distinguishes human muscle progenitor cell (*h*MPC) cultures with high and low inflammatory susceptibility. DEgene enrichment suggested that MuIS+ cells had promotion of inflammatory pathways and inhibition of muscle differentiation pathways. Novel (KISS1) and known (SMARCA4, MYOD1, IL1β) genes emerged as regulators for identified functional pathways. When compared to other transcriptomics datasets, MuIS+ cultures share overlap in transcript profiles to both individuals who do not respond to progressive resistance exercise training and to older adults with diminished muscle strength.

This dissertation highlights the heterogeneity that exists between humans throughout the muscle regenerative process. Uncovering the molecular underpinnings of this heterogeneity is essential as the field of medicine moves towards a personalized approach.

BIOGRAPHICAL SKETCH

Emily completed her undergraduate degree in nutritional sciences from Penn State University in 2008. While there, she completed her honor thesis with Dr. Mary Jane De Souza in the Women's Health and Exercise Lab at Penn State. In this lab, she co-authored a peer-reviewed, published manuscript on the effects of inadequate energy intake on menstrual status and bone health in active women. As her lab work progressed, she became increasingly interested in the mechanisms driving the effects she discovered. Inspired by this curiosity and motivated to learn molecular research techniques, she joined Dr. Penny Kris-Etherton's lab group during her senior year. While in this lab, she analyzed the effects of a lipopolysaccharide inflammatory challenge on cytokine release from 3T3L1 cells under various conditions. Recognizing her dual interests in scientific research and applied dietetics work, she enrolled in the Coordinated Master's Program in Nutrition and Dietetics at the University of Utah. While there she completed both the RD internship and a basic science master's thesis. Her master's thesis focused on adipose tissue dysfunction and epigenetic modifications in intrauterine growth restricted rats. While in this lab, she published her second peer-reviewed manuscript, "Intrauterine Growth Restriction Programs Adipocyte Dysfunction in Male Rat Pups." At Cornell, she continued to pursue her interests in cellular metabolism and chronic disease through her work with Dr. Anna Thalacker-Mercer. Simultaneously with her doctoral training, Emily practiced as a registered dietitian in the Ithaca area and pursued training in translating science into policy through the WHO/Cochrane/Cornell Summer Institute for Systematic Reviews in Nutrition for Global Policy Making. In her free time, Emily enjoys a variety of outdoor pursuits including alpine skiing, mountain biking, trail running, and backpacking.

ACKNOWLEDGMENTS

I would like to thank my advisor, Dr. Anna Thalacker-Mercer, for her endless mentorship throughout the dissertation process. I am so grateful for the opportunities and support she has given me over the past four years. I would not be moving forward in my career, in the direction I am, without her support and encouragement.

I would like to thank my committee members, Dr. Marie Caudill, Dr. Bethany Cummings, and Dr. Rebecca Seguin, for encouraging me to think about my research across the translational spectrum.

I would like to thank members of the Cornell Statistical Consulting Unit for their help with the statistical analyses in this dissertation.

I would like to thank Heather Roman for her assistance with method development and cell culture.

Finally, this dissertation would not have been possible without the support of my lab-mates, family, and friends. A special thank you to Jamie Blum, Brandon Gheller, Diwaker Gupta, and Lauren Varvatos for all the science discussions, lab work assistance, and laughs.

TABLE OF CONTENTS

LIST OF FIGURES

LIST OF TABLES

LIST OF ABBREVIATIONS

2-deoxygluclse-6-phosphate	2DG6P
7-Aminoactinomycin D	7AAD
Amphiregulin	AREG
Analysis of variance	ANOVA
Breast cancer type 1 susceptibility protein	BRCA1
Calcium-calmodulin-dependent protein kinases	CaMK
Cluster of differentiation 36	CD36
Chitinase-3-protein 1	CHI3L1
Cyclin A1	CCNA1
Cyclin-dependent kinase inhibitor 1A	CDKN1A
Differentially expressed genes	DEgenes
Differentiation media	DM
DNA-methyltransferase 3 beta	DNMT3B
Dulbecco's Modified Eagle Media	DMEM
E2F transcription factor 2	E2F2
Extracellular acidification rate	ECAR
Extracellular signal-regulated kinases	ERK1/2
Early growth response 1	EGR1
F-box only protein 32	FBX032
False discovery rate	FDR
Fast growing cluster	FAST

Fluorescence activated cell sorting	FACS
Forkhead box protein M1	FOXM1
Fragments Per Kilobase of transcript per Million mapped reads	FPKM
Glucose transporter 1	GLUT1
Glucose transporter 4	GLUT4
Growth hormone	GH
Growth media	GM
Hepatocyte growth factor	HGF
High proliferative clones	HPC
Immunity-related GTPase family M protein 1	IRGM1
Ingenuity Pathway Analysis	IPA
Insulin-like growth factor-1	IGF-1
Integrin beta-1	CD29
Integrin-linked kinase	ILK
Interleukin 1 beta	IL1B
Interleukin 6	IL6
Kisspeptin 1	KISS1
Lipopolysaccharide	LPS
Low proliferative clones	LPC
Muscle inflammatory susceptibility negative	MuIS-
Muscle inflammatory susceptible positive	MuIS+
Muscle progenitor cell	MPC
Myocyte enhancer factor 2C	MEF2C

Myogenic differentiation 1	MYOD1
Myogenin	MYOG
Net area under the curve	nAUC
Neural cell adhesion molecule	CD56
Notch homolog 1	NOTCH1
Nuclear factor kappa-light-chain-enhancer of activated B cells	NF-κB
Old female-*h*MPCs	OF-*h*MPCs
Old male-*h*MPCs	OM-*h*MPCs
Oxidative phosphorylation	OXPHOS
Oxygen consumption rate	OCR
P21-activated kinases	PAK
Peroxisome proliferator-activated receptor gamma coactivator 1-alpha	PPARGC1A
Platelet-derived growth factor receptor alpha	PDGFRA
Phosphate buffered saline	PBS
Polymerase chain reaction	PCR
Principal component analysis	PCA
Principal component 1	PC1
Principal component 2	PC2
RAB, Member RAS Onocgene Family Like 6	RABL6
Retinoblastoma	Rb
RNA quality number	RQN
Satellite cells	SC
Slow growing cluster	SLOW

SWI/SNF related matrix associated actin dependent regulator of chromatin	SMARCA4
SWItch/ Sucrose Non-Fermentable	SWI/SNF
TATA-box-binding protein	TBP
TNF receptor associated protein 1	TRPA1
TNF superfamily member 12	TNFSF12
TNF-related weak inducer of apoptosis	TWEAK
Total area under the curve	tAUC
Transforming growth factor beta	TGFβ
Tripartitie motif containing 63	TRIM63
Tumor necrosis factor alpha	TNFα
Young male-*h*MPCs	YM-*h*MPCs
Young female-*h*MPCs	YF-*h*MPCs

CHAPTER 1. REVIEW OF LITERATURE

1.1 Skeletal muscle function and structure

Skeletal muscle (SkM) is the largest organ system in the body (132). Functionally, the skeletal muscle is best known for its roles in maintaining posture, producing movement, and protecting bones and joints. Additionally, the SkM plays important roles in metabolism. The SkM acts as a secretory organ; it releases cytokines ("myokines") that have autocrine, paracrine, and endocrine effects (132). The SkM is the largest glucose sink in the body accounting for ~75% of insulin-stimulated glucose uptake, it stores carbohydrate in the form of glycogen (17), and it contains 50-75% of all body proteins (59).

Structurally, the SkM is composed of multinucleated, post mitotic muscle cells (myofibers) that are formed by the differentiation and fusion of myoblasts in a process known as myogenesis. The myofibers are surrounded by a cell membrane or sarcolemma. Myofibers are bundled into muscle fascicles and surrounded by the perimysium, another layer of connective tissue. The entire muscle is surrounded by a third layer of connective tissue called the epimysium. The size of a muscle is determined largely by the number and size of the individual myofibers; however, infiltrating fat and connective tissue can also alter the size of the muscle (56, 81). The structural composition of SkM is shown in **Figure 1**.

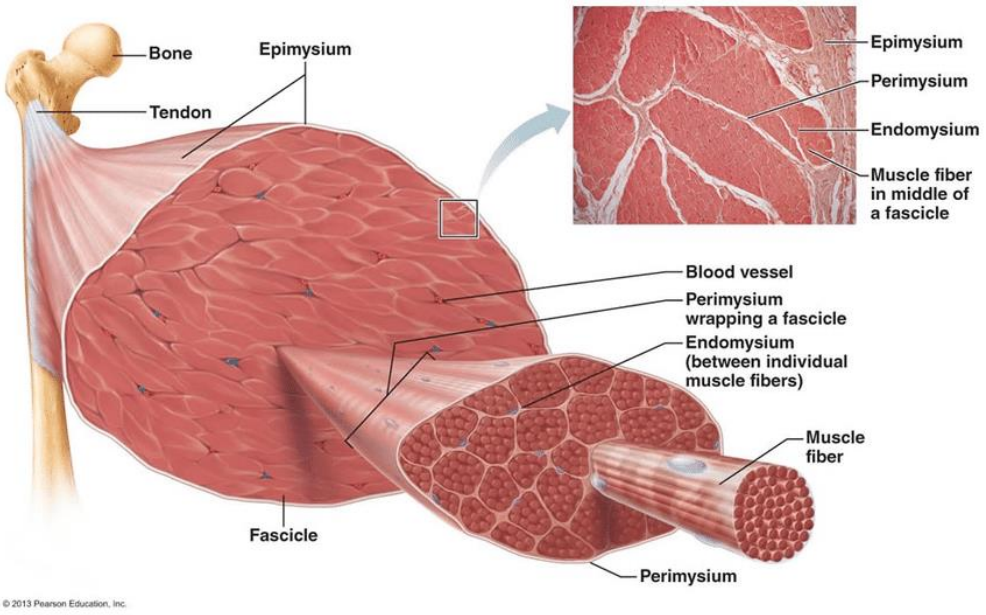

Figure 1. Skeletal Muscle Structure (photo taken from Pearson Education © 2013)

1.2. Skeletal muscle regeneration

Over a lifetime, skeletal muscle may be injured in various ways including burns, wounds, surgical trauma, and exercise injuries. Importantly, subtle myofiber injuries routinely occur secondary to regular activities (39). Adequate repair and regeneration following damage are necessary to maintain muscle structure, function, and metabolic homeostasis throughout the lifespan (170). When the SkM is injured, satellite cells [(SC), the adult stem cells found in the skeletal muscle] are activated to repair the damaged tissue. SCs are located between the sarcolemma and the basal lamina in a quiescent state until activated by stimulating factors. Once activated, SCs proliferate, differentiate, and fuse with other myogenic cells or with existing myofibers to repair and/or regenerate injured tissue (**Figure 2**). When damage is subtle, SCs or their progeny fuse with existing myofibers; however, when damage is severe, SCs or their progeny fuse with each other to form new myofibers (73, 76).

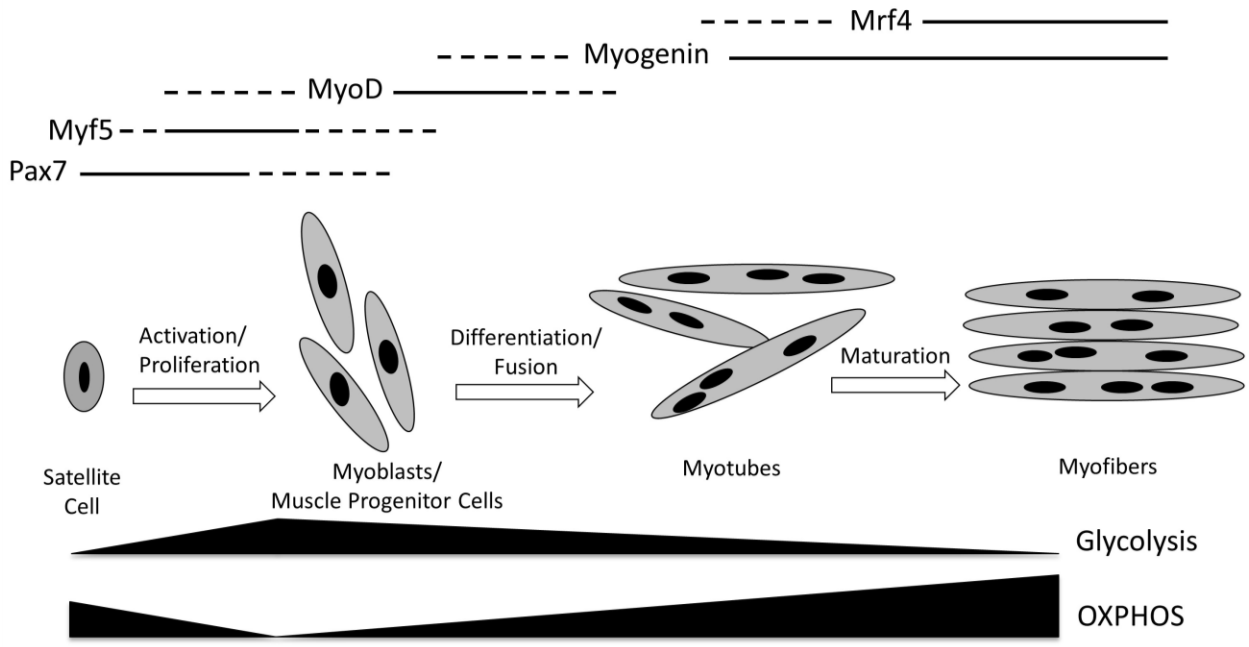

Figure 2. Changes in Myogenic Regulatory Factors and Metabolism throughout Muscle Regeneration

SCs express PAX7, an essential transcription factor for regulating myogenic potential, or the potential of cells to progress through the major phases of SkM formation. *In vivo*, $Pax7^{-/-}$ mice have a complete absence of SCs in SkM (160), and muscles in $Pax7^{-/-}$ mice are reduced in size and contain 50% the normal number of nuclei (127, 142, 160). Deletion of Pax7+ cells *in vivo* also results in impaired regeneration, marked by reduced formation of myotubes and increased deposition of fibrotic tissue (19, 94). In the absence of injury, Pax7+ cells also fuse with existing myotubes and contribute to the homeostatic maintenance of SkM over time, especially in aged muscle (174). *In vitro*, deletion of Pax7 in primary myoblasts inhibits proliferation and results in complete growth arrest (180). Thus, Pax7+ SCs are essential for both homeostatic maintenance and regeneration of SkM.

Upon injury, Pax7+ cells are activated by stimulating factors [e.g. fibroblast growth

factor (FGF), hepatocyte growth factor (HGF), insulin-like growth factor (IGF), interleukin-6 (IL6), or tumor necrosis factor-alpha (TNFα)]. Once activated, SCs express the transcription factors MYF5 and MYOD and proliferate. MPCs progress through proliferation, and committed MPCs differentiate, exit the cell cycle, and fuse to form myotubes that repair injured muscle. Adequate expansion of the MPC population is essential for muscle regeneration. It is postulated that expansion of the MPC population promotes the formation of myotubes with greater numbers of nuclei and larger mass (99). *In vivo*, inhibiting expansion of the MPC population via radiation-induced damage (140) or pharmacological inhibition (151) prevents muscle regeneration.

Following expansion, a subset of cells differentiate into mature myofibers. MPCs that enter differentiation express the transcription factors myogenin (MYOG), a master regulator of the differentiation process, and MRF4. *In vivo*, a subset of SCs do not proceed to differentiation but instead reinstate the quiescent state and self-renew the SC pool (5). In summary, successful SkM regeneration requires this well-orchestrated series of events from activation of the quiescent SC, to expansion and differentiation of the committed myoblast or MPC, and formation of multinucleated cells.

1.3 Age and skeletal muscle regenerative capacity

Life-expectancy from birth and from the age of 60 years continues to increase; the average life-expectancy in the United States is 78.8 years and 83.2 years for men and women, respectively, an approximate 16 year increase since 1940 (24). However, in 2010, over 25% of those aged ≥ 65 years reported difficulty walking and climbing stairs, while 18.5% reported difficulty conducting errands independently (187). In healthy, young men and women, SkM accounts for approximately 42% and 34% of human body weight, respectively (80). However,

this percentage declines with age to SkM accounting for 36% and 30% of human body weight in 70+ year old men and women, respectively (80). The overall reduction in the size of SkM is accompanied by an increase in fat infiltration with age, independent of sex (43), and a decline in power, strength and endurance (54, 157). Over time, the decline in the structural and functional properties of SkM results in physical disability and loss of mobility and independence, especially in the elderly (9, 46, 138). Thus, although human life-expectancy is increasing, older adults and adults with chronic disease may face a larger window of diminished quality of life.

Loss of SkM is accompanied by a decrease in the size and number of myofibers (50, 91). A decrease in the number of myonuclei has also been reported in aged muscle (18). A myonuclei can only support a certain volume of cytoplasm, and changes in myofiber cross-sectional area are paralleled by changes in the number of myonuclei (197). Since SCs donate their nuclei to myofibers, a decline in the number of SCs with age could be one mechanism explaining the decrease in the number of myonuclei with age. However, studies comparing the numbers of SCs in aged muscle have reported varying results, likely due to differences in the species studied and the methods used (e.g. immunohistochemistry versus fluorescence activated cell sorting). Several studies have reported a decrease in SC number with age (20, 156, 161, 164), while others report no change (35). Most likely, altered regenerative potential in aged muscle is a result of changes in both SC number and SC function with age.

Loss of the ability to return to quiescence and to self-renew with age may be one mechanism through which SC number and function decrease with age. If aged SCs lose their intrinsic capacity to self-renew, the SC pool shrinks. p38α/β signaling is involved in SC activation, and p38α/β is overstimulated in aged SCs (16). Over-activation of the p38α/β pathway induces SC activation and reduces self-renewal. Activation of the p38α/β pathway is not

altered when old SCs are transplanted into a young niche (16, 36), suggesting over-activation of the p38 pathway may be an intrinsic defect in aged SCs. Additionally, Cosgrove et al. reported that two thirds of aged SCs fail to successfully transplant even when placed into a young mouse (36), further supporting the presence of intrinsic defects in aged SCs.

Following injury or transplantation, activated SCs must proliferate to generate sufficient cell numbers to fuse or repair damaged tissue. However, SCs from aged mice have higher rates of apoptosis and senescence when cultured; thus, expansion of the SC population from aged mice is impaired (34). In aged animals, SC activation is delayed and proliferation is impaired, resulting in fewer cells available to fuse with injured tissue (13). Additionally, following injury *in vivo*, fewer myoblasts are generated in myofiber explant cultures from aged compared to young or adult mice (35). In rats, muscle regeneration following injury is prolonged (3 weeks in old versus 1 week in young), and myofibers formed are smaller in size (155). Thus, although the reasons for impaired regeneration with age are multi-factorial, impairments in MPC expansion capacity are an important factor affecting the success of aged SkM regeneration and transplantation. Despite evidence in mouse and rat models, data on human MPCs (*h*MPCs) and the effect of chronological age on *h*MPC expansion capacity remains limited.

1.4 Sex and skeletal muscle regenerative capacity

Sex differences in SkM health have been reported throughout the lifespan. On average, males have greater SkM mass and larger muscle cross-sectional area compared to females (114, 152). Transcriptomics has been used to understand baseline differences in the size of male and female SkM from healthy adults (aged 20-75 years). In total, over 3,000 genes were reported as differentially expressed (DEgenes) between male and female SkM (185). However, only a few of

the DEgenes were obvious candidates for explaining the sex-related difference in SkM mass (185). For example, differences in *IGF1* and *GDF8* (myostatin) expression could contribute to the sex difference in muscle size (185).

At the whole tissue level, sex-related SkM differences in function with age are mixed. Studies report that males lose SkM mass at a faster rate with age than females (195). Additionally, males lose almost twice the strength that females lose with age (69). However, other reports suggest that females have an increased probability of encountering age-related functional disability (79), a greater likelihood of experiencing frailty (118), and a greater chance of developing metabolic disease (141). While sex-related differences in SkM are present throughout the lifespan, it is not obvious why differences in measures of functional outcomes occur.

At the cellular level, male and female SCs have comparable contributions to muscle regeneration after transplantation in mice (122). However, 3 month and 1 year old male mice have more SCs per myofiber than age-matched female mice, suggesting that male mice have a greater pool of SCs (122). Additionally, Manzano et al. reported that SCs isolated from 40, 60, and 120 day old male mice have higher proliferation rates compared to SCs isolated from female mice (108). With age, the reduction in SCs per myofiber is more prominent in female mice compared to male mice (39). Although evidence from animal models suggest sex-specific differences in the MPC population, data comparing male and female *h*MPCs remains limited.

1.5 Metabolism and muscle regenerative capacity

Throughout the lifespan, metabolism of macronutrients provides substrates and energy necessary to regenerate injured muscle and to maintain muscle mass. Inadequate energy and/or

protein intake results in loss of lean body mass and can lead to increased injury risk (130, 131). At the cellular level, the metabolism of macronutrients plays an important role in the control of SC stemness and in the expansion and differentiation of activated SCs (65). A simplified schematic of macronutrient metabolism is shown in **Figure 3** (153). Our current understanding of glycolytic and oxidative phosphorylation (OXPHOS), throughout myogenesis/ the regenerative process, is shown in Figure 2. Glucose is metabolized, in the cytoplasm, to pyruvate through glycolysis, a process that does not require oxygen. Although each round of anaerobic glycolysis only produces two net molecules of ATP, glycolysis also produces essential biosynthetic building blocks; byproducts of glycolysis are necessary for nucleotide, lipid, and amino acid biosynthesis (Figure 3). Pyruvate, the glycolytic end product, can either be converted to lactate in the cytoplasm or shuttled into the mitochondria and converted to acetyl CoA for OXPHOS. Additionally, pyruvate can be converted to oxaloacetate, a TCA cycle intermediate, by pyruvate carboxylase in an anaplerotic reaction. The metabolism of fatty acids and amino acids can also produce acetyl CoA for OXPHOS. OXPHOS generates large amounts of ATP (up to 36 ATP molecules).

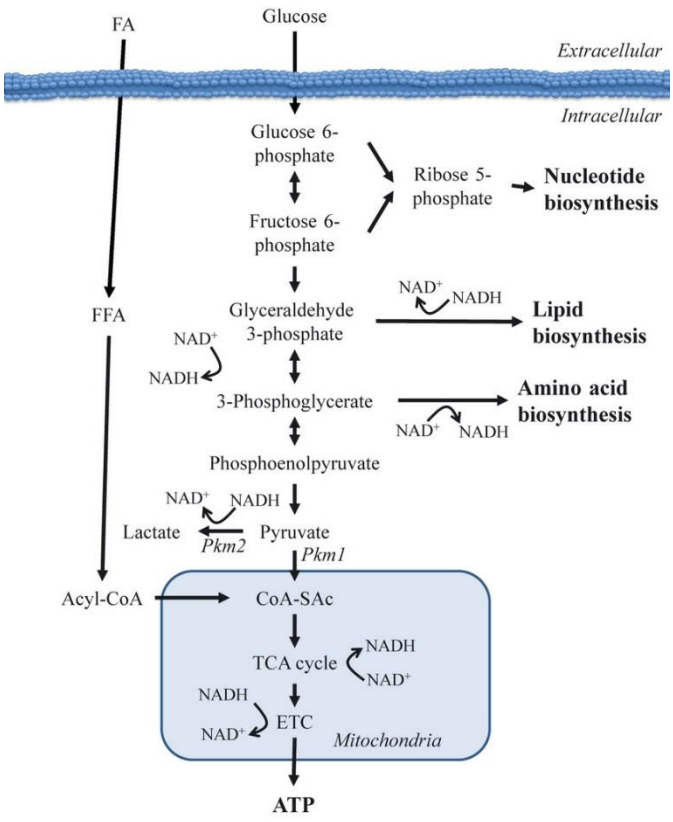

Figure 3. Macronutrient Metabolism Pathways. Taken from Ryall et. al, 2013

Quiescent SCs reside in a state of little or no basal cellular turnover and have very low energy needs (42). Quiescent SCs co-localize with capillaries and nerves, which suggests an aerobic niche (65). Compared to activated SCs, quiescent SCs have an enrichment of genes that regulate lipid transport (62). It is postulated that unlike other stem cells, quiescent SCs may primarily oxidize fatty acids through OXPHOS (65). Because oxidative stress occurs secondary to OXPHOS, long-lived SCs need a mechanism to protect against oxidative damage (65). SCs respond to oxidative stress by removing damaged mitochondria via autophagy (the controlled degradation and recycling of cellular components) (186); autophagy is essential to maintain the stem-cell quiescent state in mice (63). Compared to quiescent SCs, proliferating murine

myoblasts [C2C12 and mouse primary MPCs (*m*MPCs)] have higher metabolic rates and greater lactate production (93, 154). *m*MPCs, during early proliferation (3 and 24 h after plating), also have greater extracellular acidification rates (ECAR, a measure of glycolysis) and greater expression of genes involved in glycolysis compared to freshly isolated SCs (154). Furthermore, Ryall et al. demonstrated that SCs transition from utilizing primarily fatty acid oxidation to utilizing primarily glycolysis during the switch from quiescent to proliferating SCs (154). Although glycolysis is inefficient for energy generation compared to OXPHOS, use of glycolysis allows cells to generate essential biosynthetic materials and to respond quickly to energy demands (104). Cellular metabolism is reprogrammed from OXPHOS to glycolysis during activation. Evidence suggests the enzymatic activity of sirtuin 1 (SIRT1) plays a role in this reprogramming (154). SIRT1 has also been shown to regulate autophagy during activation; autophagic flux is induced during activation and inhibition of autophagic flux delays SC activation (167). Increased autophagy during activation provides substrates for ATP generation to meet the increased energy needs of activation (167).

As expansion proceeds, proliferating *m*MPCs significantly increase mitochondrial content and the expression of genes associated with the TCA cycle (154). Thus, while glycolysis plays a role in MPC activation, MPCs may rely more on OXPHOS as expansion continues. OXPHOS is essential for differentiation; inhibiting the assembly of the electron transport chain inhibits myotube formation (146). Differentiated cells do not need to sustain high rates of replication and therefore have a lower anabolic demand. However, they do require significant energy to support homeostasis and muscle contraction; it is well accepted that fully differentiated myotubes rely heavily on OXPHOS to meet their high metabolic needs (93, 181). Thus, both glycolysis and OXPHOS are important for varying stages of MPC expansion, differentiation, and

fusion into mature multinucleated cells.

Impairments in metabolism may underlie poor muscle regeneration by limiting the substrates or energy necessary to complete cellular processes of regeneration. Aged SkM has reduced energy, glucose, protein, and fat metabolism (68). Genes related to mitochondrial function and the TCA cycle are also reduced in SkM from older adults when compared to younger adults, with the lowest expression levels in frail older adults (51). Expression of genes related to mitochondrial function including peroxisome proliferator-activated receptor gamma coactivator 1-alpha (PGC1α) target genes are also reduced in older adults when compared to younger adults (51); PGC1α is a transcription factor that promotes mitochondrial biogenesis. At the cellular level, replicative aging (continuing to passage cells until senescence) reduces whole cell ATP production (116). Aging via replication has been shown to alter glycolytic enzymes (12), downregulate OXPHOS (128), and decrease glucose uptake, glycogen synthesis, and fatty acid oxidation (123). However, despite evidence in whole tissue and in *h*MPCs aged via replication, the effect of chronological or biological age on metabolism in *h*MPCs remains unknown.

1.6 Inflammation and skeletal muscle regeneration

Inflammation plays a key role in muscle regeneration. Upon injury, the body initiates an acute phase inflammatory response characterized by upregulation of the pro-inflammatory cytokines interleukin 1β (IL-1β) and tumor necrosis factor alpha (TNFα) (107, 172). These cytokines can be released by both resident macrophages or by the muscle itself and act through nuclear factor kappa-light-chain-enhancer of activated B cells (NF-κB) to upregulate expression of additional pro-inflammatory genes (**Figure 4**) (132, 172). These cytokines also act as

chemoattractants to attract additional macrophages from the circulation and increase proteolysis of the injured muscle (139). Attracted macrophages release growth factors that promote muscle repair through promoting SC proliferation (145). TNFα itself also activates SCs and promotes the transition from G1 to S phase of the cell cycle (95).

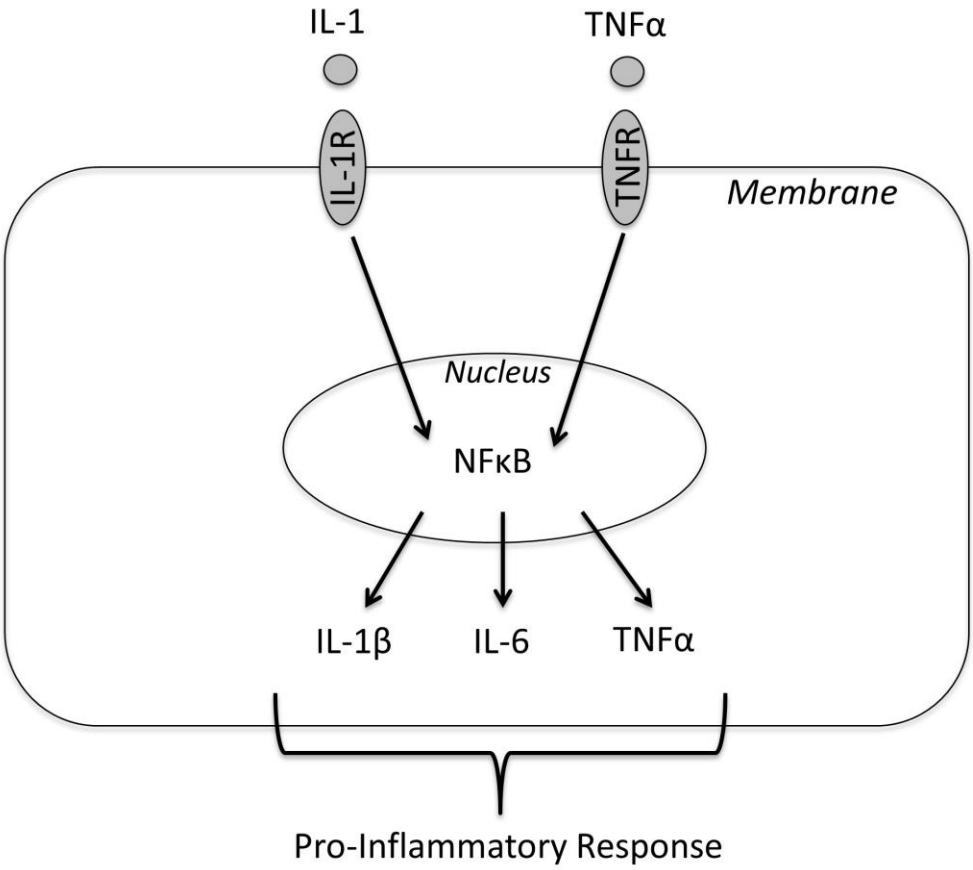

Figure 4. Inflammatory Cytokine Signaling

Although an acute inflammatory response is essential for muscle repair, chronic inflammation can result in myopathies including muscle wasting and tissue remodeling (89). Infusion of IL-1β or TNFα inhibits muscle protein synthesis and induces skeletal muscle

catabolism in rats (98). Looking downstream of IL-1β or TNFα, NF-κB increases the expression of murine ring finger-1 (MuRF1), a critical mediator of muscle atrophy (22). TNFα also inhibits myoblast differentiation and fusion by post-transcriptionally repressing MYOD (74, 115). Inhibiting NF-κB *in vivo* or *in vitro* improves proliferation and myogenic differentiation (102). The effects of chronic inflammatory cytokine exposure promote protein degradation and inhibit successful muscle regeneration.

Higher baseline levels of muscle inflammation and higher proinflammatory signaling in response to damage [termed muscle inflammatory susceptibility (MuIS+)] have been associated with impaired differentiation and fusion in *h*MPCs from older human adults (112). In a follow-up study, those with MuIS+ also experienced lower rates of muscle protein synthesis following surgery (10). Thus, localized MuIS+ may be a contributing factor to long-term disability in some individuals following trauma or surgical procedures. However, why some individuals develop MuIS+ while others do not is not understood. An –omics based approach may provide insight into the molecular underpinnings of the MuIS+ phenotype.

1.7 Transcriptomics

High-throughput sequencing methods, such as RNA-sequencing (RNAseq), can be used to comprehensively measure changes in an organism's transcriptome (the sum of all its transcripts) with time, cell type, or condition. Genetic information is carried on DNA. This information is transcribed and carried by mRNA. RNAseq generates cDNA sequences derived from all RNA molecules in a sample. These cDNA sequences are then constructed into a library and sequenced using massive parallel deep sequencing technologies. Expression level of mRNA targets can be quantified in an unbiased way with high resolution (single base pair resolution)

(183). This process is outlined in **Figure 5**.

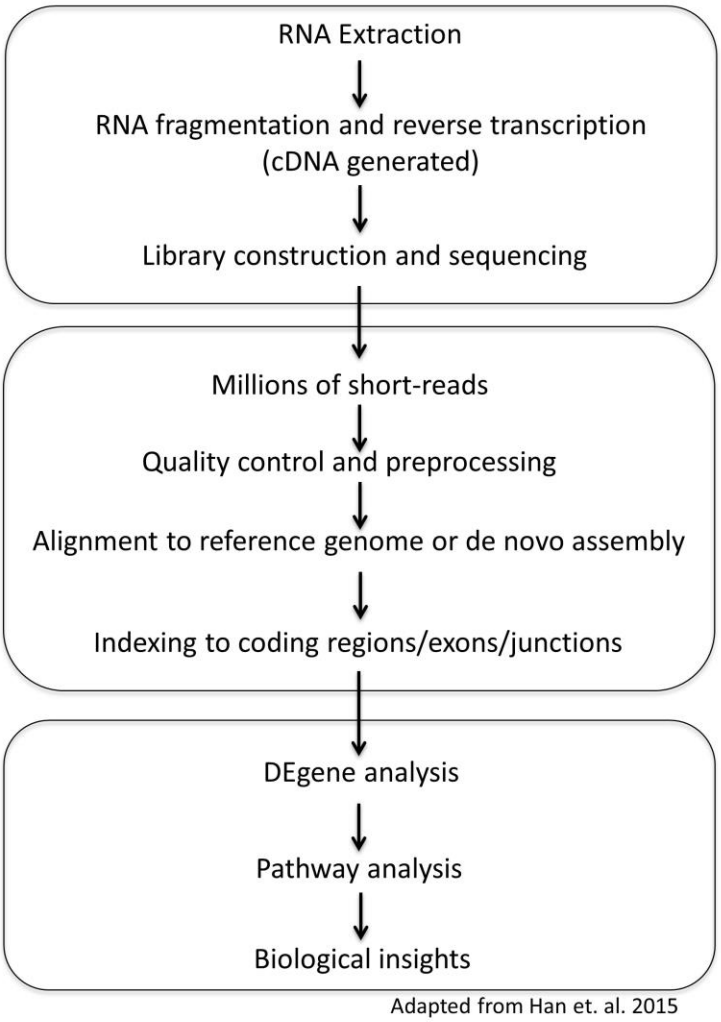

Figure 5. Overview of Typical RNAseq Pipeline

RNAseq can be used to determine genes that are differentially expressed (DEgenes) between samples, time-points, or conditions. Fragments Per Kilobase of transcript per Million mapped reads (FPKM) values are determined for each gene within a sample. These FPKM values account for the number of fragment reads with respect to the overall mapped read number

and the gene length. FPKM values are then compared and the significance and the fold change differences between groups are determined.

While lists of DEgenes are informative, DEgene lists may overlook important biological changes. Minor changes in multiple genes in a pathway may have large biological consequences but may be overlooked by DEgene comparisons alone. Pathway analysis is a powerful tool that connects expression changes to the function of individual genes and the roles of these genes in biological pathways. Analyses of differentially expressed biological pathways often provide more insight than lists of seemingly unrelated DEgenes (137). Programs such as Ingenuity Pathway Analysis (IPA) develop outputs identifying top canonical pathways, functional categories, and networks of DEgenes between conditions. Based on the directional changes of DEgenes (i.e. up- or down-regulated), the directionality of the identified pathway, category, or network can be predicted. IPA also predicts upstream regulators that may control the DEgenes and alter biological functions of interest. In this way, RNAseq can be used as an exploratory tool to generate hypotheses about upstream regulators controlling DEgene expression. Although RNAseq and pathway analysis can be useful in hypothesis generation, it is important to remember that this tool only provides information at the level of transcription. Changes at the mRNA level do not always translate into changes in the level of functional proteins.

1.8 Benefits and limitations of the model

Use of a cell culture model for understanding human SkM regeneration has important benefits and limitations. *h*MPC populations largely retain the donor metabolic phenotype and have the most relevant genetic background to address age- and sex-related differences in MPC expansion capacity and metabolism (1). However, our model is also limited by the use of

isolated satellite cells; the tissue niche has been shown to play a critical role in the muscle regeneration process (193). It is unlikely that impaired muscle regeneration is solely a function of alterations in SCs. Rather, it is a combination of intrinsic changes within SCs and extrinsic changes within the tissue niche that alter regenerative capacity. Additionally, a potential limitation of our research model is use of passage six *h*MPCs. It is recognized that proliferative capacity declines with passaging (106).

1.9 Summary

Animal models have been widely used to investigate the effects of age, sex, and inflammation on different stages of SkM regeneration. However, *h*MPCs largely retain the donor metabolic phenotype and have the most relevant genetic background to address questions related to human variance in muscle regeneration (1). Upon critical evaluation of the literature, it is apparent that to better understand how human heterogeneity impacts muscle regeneration, whether based on categorical variables such as age or sex or phenotypic variables such as growth speed or inflammatory susceptibility, studies using human primary cultures need to be conducted. The results of these experiments are presented in Chapters 2, 3, and 4.

CHAPTER 2: EXPANSION CAPACITY OF HUMAN MUSCLE PROGENITOR CELLS DIFFERS BY AGE, SEX, AND METABOLIC FUEL PREFERENCE

Emily S Riddle, Erica L Bender, Anna E Thalacker-Mercer

Author Affiliations: Division of Nutritional Sciences, Cornell University, Ithaca, NY, 14853, USA (ER, HR, EB, ATM)

Abbreviated Title for Running Head: Muscle Progenitor Cell Growth and Metabolism

Corresponding Author: Dr. Anna Thalacker-Mercer, aet74@cornell.edu, 109 Savage Hall, Cornell University, Ithaca, NY 14850

Emily S Riddle: Experimental design, data collection, data analysis, and interpretation
Erica L Bender: Data collection
Anna E Thalacker-Mercer: Experimental design, data collection, data analysis, and interpretation

Keywords: Muscle progenitor cells, metabolism, cell proliferation, sex differences

2.1 Abstract

Activation of satellite cells and expansion of the muscle progenitor cell (MPC) population is essential to generate a sufficient number of cells to repair damaged skeletal muscle (SkM). Proliferating MPCs have high energetic and biosynthetic material requirements, and the ability to utilize oxidative phosphorylation (OXPHOS) and/or glycolysis may affect expansion capacity of MPCs. In the present study, we investigated the effect of donor age and sex on human MPC (*h*MPCs) expansion capacity and metabolic fuel preference. *h*MPCs from young and old males and females were grown for 408 h (17 days). Percent confluency, live nuclei count, and dead cell count were measured every 24 h. Metabolic phenotype was assessed using glucose uptake, expression of genes related to glycolysis and OXPHOS, and the Seahorse XF24 Phenotype Test Kit during the exponential phase of growth. *h*MPCs from old male donors had impaired expansion capacity secondary to heightened cell death early in expansion compared to *h*MPCs from young male donors, an effect not observed in female *h*MPCs. Age-related differences in metabolism were also sex-dependent; markers of OXPHOS were altered in old (vs. young) male *h*MPCs while markers of metabolism were largely unaffected by age in female *h*MPCs. For the first time, we identify sex-specific differences in cell death and OXPHOS that contribute to impaired expansion capacity of *h*MPC cell populations with age.

2.2 Introduction

The regenerative process following skeletal muscle (SkM) damage is necessary to maintain SkM composition and function throughout the lifespan. Impaired SkM regeneration post injury is related to pathological tissue remodeling and deterioration of the muscle with age (60). Successful regeneration requires a well-orchestrated series of events including activation of quiescent, SkM specific stem cells [satellite cells (SCs)] followed by proliferation and differentiation of committed myoblasts [muscle progenitor cells (MPCs)], and formation/repair of functional multinucleated muscle cells (29). Activation of SCs and expansion of MPCs is essential to generate a sufficient number of viable cells to repair damaged SkM (4). *In vitro,* MPC expansion encompasses cell division and cell death, as well as the ability of cells to reach confluence. Greater expansion of MPCs is postulated to promote the formation of myotubes with higher numbers of nuclei and increased mass (99); inhibiting expansion of the MPC population via radiation-induced damage (140) or pharmacological inhibition (151) prevents muscle regeneration.

Throughout MPC expansion, catabolism of macronutrients provides the substrates and energy needed to support the generation of new cells and cellular structures (153). Although glycolysis is inefficient for energy generation compared to oxidative phosphorylation (OXPHOS), use of glycolysis allows cells to generate essential biosynthetic materials and to respond quickly to energy demands (104). Compared to quiescent and differentiating cells, proliferating murine myoblasts [C2C12 cells and mouse primary MPCs (*m*MPCs)] have higher metabolic rates and higher lactate production (93, 154). *m*MPCs during early proliferation (3 and 24 h after plating) also have greater extracellular acidification rates (ECAR, a measure of glycolysis) and greater gene expression of enzymes involved in glucose catabolism compared to

freshly isolated SCs (154). Later in expansion (48 h after plating), proliferating *m*MPCs significantly increase mitochondrial content and the expression of genes associated with the TCA cycle (154). Thus, both glycolysis and OXPHOS appear to be important throughout myoblast expansion.

In animal models, age is associated with reduced MPC expansion capacity *in vitro* (28, 34). MPCs derived from young rats attain more population doublings compared to MPCs derived from old rats (28). Similarly, human MPCs (*h*MPCs) "aged" via replication have longer population doubling times compared to their "younger" counterparts that have undergone fewer replications (123). Evidence also suggests that sex may impact MPC expansion capacity; throughout the lifespan in mice, male *m*MPCs exhibit higher proliferation rates than female *m*MPCs (108). Although the effects of chronological age and sex on expansion of MPCs from animals are accepted, the effects of chronological age and sex on expansion of *h*MPCs remains unknown. Furthermore, although studies have compared the metabolism of proliferating cells to the metabolism of quiescent or differentiating cells, no studies to date have determined the effects of chronological age and sex on *h*MPC metabolic fuel preference throughout expansion. Therefore, the aim of the present study was to determine the effect of age and sex on expansion capacity and metabolism in *h*MPCs.

2.3 Methods

2.3.1 Ethical approval

All studies were approved by the Cornell University, Institutional Review Board. Written informed consent was obtained from all participants.

2.3.2 Human donors

Human MPCs from healthy, ambulant young and old, males and females were used to address the objectives of this research. Average weight, BMI, and age of participants in each group are presented in Table 1. There were no significant differences in weight between young and old participants within sex, and there were no significant differences in BMI between any of the groups. All individuals completed a comprehensive health history and physical activity questionnaire and were independently ambulatory and cognitively intact (as determined by the examining nurse practitioner). All individuals were relatively active; individuals in all age-by-sex groups participated in endurance and/or resistance exercise ≥ 2 days per week. All subjects were requested to refrain from exercise within 24 h of the biopsy. Individuals were excluded for contagious infections and any chronic end-stage disease expected to limit life-expectancy to less than one year, induce anorexia, or restrict physical activity. Individuals with seated resting systolic blood pressure ≥140 mmHg or diastolic blood pressure ≥90 mmHg and individuals receiving anabolic (e.g., GH, IGF-I) therapy were also excluded.

Table 1. **Subject Characteristics**

Group	Number in Group	Average Weight (kg)	Average BMI (kg/m^2)	Average Age (y)
Young Males (YM-*h*MPCs)	6	80.2 ± 16.6	25.3 ± 4.2	28.5 ± 7.1
Old Males (OM-*h*MPCs)	3	78.3 ± 8.9	27.9 ± 4.3	72.0 ± 7.0
Young Females (YF-*h*MPCs)	6	64.2 ± 12.0	24.2 ± 6.0	30.0 ± 5.7
Old Females (OF-*h*MPCs)	6	65.0 ± 7.5	24.3 ± 4.0	70.8 ± 6.9

Data are presented as mean +/- SD.

2.3.3 Purified, primary human muscle progenitor cells

Primary human SCs were obtained from the vastus lateralis muscle using the percutaneous biopsy technique. The biopsy tissue was cleaned of any extraneous fascia and adipose tissues. Approximately 75-100 mg of the total muscle biopsy was stored in Gibco® Hibernate®A (Thermo Fisher Scientific) at 4°C until tissue disassociation was performed. After mincing and washing via gravity with Ca-Mg free D-PBS, the tissue was disassociated in digest medium [2mg/mL Collagenase D (Roche) in low-glucose DMEM]. After 30 minutes in digest medium, fresh digest medium and Dispase (Sigma) were added. The disassociating pellet was titurated until a uniform slurry was achieved. Growth medium [(GM) Hams F12 + 20% FBS + 5ng/mL bFGF (Promega) + 1% Pen/Strep (Gibco)] was added to the slurry and passed through a 70 μm cell strainer into a sterile tube. The cell suspension was centrifuged. The pellet was resuspended in Recovery® freezing medium (Gibco) and cryopreserved at -80°C. Thawed cells were seeded on a type-I collagen coated culture dish (initial cell confluency ~15%). After 24 h, the GM was replaced with fresh GM and further replenished every 48 h. Once cells reached ~70% confluency, they were removed from the plate using 0.05% trypsin and passaged. Cells were expanded to passage four, then cryopreserved in 10% DMSO + GM.

2.3.4 Fluorescence activated cell sorting

Approximately 1-1.5 million cells were labeled with fluorescently-conjugated antibodies specific for myoblast cell surface antigens CD56 (NCAM; PE-Cy7-conjugated) and CD29 (β1-integrin; AlexaFluor488-conjugated) and the viability stain 7-Aminoactinomycin D (7AAD) (191). Individual samples yield 150,000 – 800,000 viable CD56+/CD29+ *h*MPCs per 1 million cells sorted using a BD FACS Aria™ Fusion flow cytometer. Sorted CD56+/CD29+ cells (>98%

positive) were expanded in culture by passaging twice and then used in experiments; all *in vitro* experiments were performed using sorted cells at passage six. Due to high rates of cell death, only three old male cultures yielded a sufficient number of cells to be sorted and used in experiments.

2.3.5 Growth curves

Sorted *h*MPCs were seeded at a density of approximately 10% (~2000 cells) and proliferated in GM for 408 h (17 days) in 96 well plates. GM was changed every 48 h. Live cell count, percent dead, and percent confluency in each culture were measured every 24 h after seeding using the Celigo® S Imaging Cytometer (Nexcelom Bioscience). Use of the Celigo® S enabled the imaging of all cells in each well with little disruption to the culture. Confluency was measured using a minimum of 2 wells per day (confluency of 2-9 wells was averaged per day) with the exception of the final day of growth, in which only one well was measured. To validate growth curve measurements, on a separate day, growth curves were generated in duplicate for a subset of samples; no differences in growth curves were observed between separate day, duplicated growth curves [(n=7), data not shown]. Live cells were measured every 24 h by co-staining cells with Hoescht 33342 (to identify nuclei) and fluorescently labeled propidium iodide (to identify dead cells). Propidium iodide positive cells were subtracted from Hoescht 33342 positive cells to determine the total number of live cells. The number of propidium iodide positive cells were divided by the number of Hoescht 33342 positive cells to determine the percentage of dead cells. Using live nuclei counts, percent dead, and percent confluency, we determined live nuclei net area under the curve (nAUC), percent dead, total area under the curve (tAUC), confluency nAUC, population doubling time [duration*log(2)/log(final concentration) –

log(initial concentration)], and saturation density (the number of live nuclei at growth plateau divided by area of the well) for each culture.

2.3.6 RNAseq

An existing RNAseq database was leveraged to support observed differences in expansion phenotype. Importantly, the questions we asked and the analyses we used were completely different from our previous use of this RNAseq dataset (143). Briefly, TruSeq-barcoded RNAseq libraries were generated with the NEBNext Ultra II RNA Library Prep Kit (New England Biolabs). Each library was quantified with a Qubit 2.0 (dsDNA HS kit; Thermo Fisher) and the size distribution was determined with a Fragment Analyzer (Advanced Analytical) prior to pooling. Libraries were sequenced on a NextSeq500 instrument (Illumina). At least 20M single-end 75 bp reads were generated per library. Reads were trimmed for low quality and adaptor sequences with cutadapt v1.8 (parameters: parameters: -m 50 -q 20 -a AGATCGGAAGAGCACACGTCTGAACTCCAG --match-read-wildcards) (109). Reads were mapped to the reference genome/ transcriptome using tophat v2.1 (parameters: --library-type=fr-firststrand --no-novel-juncs -G <ref_genes.gtf>) (85). Cufflinks v2.2 (cuffnorm/cuffdiff) was used to generate the fragments per kilobase of transcript per million mapped reads (FPKM) values and statistical analysis of differentially expressed genes (DEgenes) (176). Ingenuity Pathway Analysis (IPA) was used to identify canonical pathways and molecular and cellular functions of DEgenes. The software was set to analyze transcripts with an FDR corrected q value ≤ 0.01.

2.3.7 Seahorse flux analysis

The Seahorse XF24 Flux Analyzer and the Seahorse Phenotype Test Kit (Agilent) were used, following manufacturer's instructions, to measure the baseline metabolic phenotype, the stressed metabolic phenotype, and the metabolic potential of the *h*MPC cultures during expansion. Metabolic phenotype was characterized by the extracellular acidification rate [(ECAR), a proxy measure of glycolysis] and the oxygen consumption rate [(OCR), a proxy measure of OXPHOS] of each culture. Cells were seeded at 17,000 cells per well in phenol red free DMEM (10 mM glucose, 2 mM glutamine, 1 mM pyruvate) with 10% FBS and grown for 72 h (media was changed at 24 h). After 72 h, media was changed to bicarbonate free phenol red free DMEM (10 mM glucose, 2 mM glutamine, 1 mM pyruvate). After the baseline metabolic phenotype (OCR and ECAR) was measured, 1μM of each of the stress inducing compounds, oligomycin which maximizes glycolysis and carbonylcyanide-4-(trifluoromethoxy)-phenylhydrazone (FCCP) which maximizes OXPHOS, were injected simultaneously into each well to induce an energy demand. After injection of the stress inducing compounds, OCR and ECAR were measured again (stressed OCR and stressed ECAR) to determine the stressed metabolic phenotype. The metabolic potentials for OXPHOS and glycolysis were calculated using the ratio of stressed OCR/baseline OCR and stressed ECAR/baseline ECAR, respectively. Metabolic potential (the percent change from baseline to stressed after the addition of stressor compounds) is presented as % baseline. Each sample was run in triplicate. OCR and ECAR values were normalized by the number of live cells in the well. After Seahorse measurements were obtained, Hoescht 33342 and propidium iodide were used to stain for the number of total nuclei and dead nuclei, respectively. Propidium iodide positive cells were subtracted from total nuclei to determine the number of live cells in each well. All Seahorse measurements were run in triplicate and normalized to the number of live cells in each well.

2.3.8 Gene expression in early proliferation

RNA was harvested from sorted cells using TRK lysis buffer (Omega) following manufacturer's instructions at the first day and third day of rapid expansion. The first day of rapid expansion was defined as the first increase in percent confluency of ≥ 5%. Confluency in OM-*h*MPCs never increased by ≥ 5% in a 24 h interval. Thus, after 72 and 120 h of growth, RNA from OM-*h*MPCs was harvested. An EZNA total RNA kit (Omega) was used for total RNA extraction following the manufacturer's instructions. Total RNA quantity and quality was determined spectrophotometrically, followed by cDNA synthesis using the High Capacity cDNA Reverse Transcription Kit (Applied Biosystems). We analyzed key targets related to glucose uptake and metabolism, fatty acid transport and metabolism, and mitochondrial biogenesis. We used real-time, quantitative PCR performed using the LightCycler 480 system (Roche) with the TaqMan Fast Advanced Master Mix and TaqMan® Gene Expression Assays (Applied Biosystems) to identify differences in gene expression of select genes. Assays were used to quantify mRNA levels of glucose transporters [*GLUT1* (Hs00892681_a1), *GLUT4* (Hs00168966_m1)], a fatty acid transporter [*CD36* (Hs00169627_m1)], and a marker of mitochondrial biogenesis [*PPARGC1* (Hs01016719_m1)]. *TBP* (Hs00427621_m1) was used as the housekeeper. Each PCR reaction was run in triplicate.

2.3.9 Glucose uptake

The Glucose Uptake-Glo Assay (Promega) was used following manufacturer's instructions to quantify glucose uptake in proliferating cells. Briefly, cells were seeded at 17,000 cells per well in phenol red free DMEM (10 mM glucose, 2 mM glutamine, 1 mM pyruvate) and grown for 72 h (media was changed after 24 h). After 72 h of growth, medium was removed and

cells were washed with glucose free media. Media was replaced with 1mM diluted 2-deoxyglucose (diluted in glucose and phenol red free DMEM). Cells were incubated in 2-deoxyglucose for 1 h, before the addition of stop buffer, neutralization buffer, and 2-deoxyglucose-6-phosphate (2DG6P) detection reagent. Cells were incubated in 2DG6P detection reagent for 1 h at room temperature, and luminescence was measured using a microplate reader. Luminescence was normalized to total cell number in each well, determined using Hoescht 33342. All samples were run in duplicate.

2.3.10 Statistics

Two-way analysis of variance (ANOVA) (age-by-sex) for unbalanced designs with Tukey post hoc tests was used to compare growth and metabolic parameters in YM-, YF-, OM-, and OF-*h*MPCs. The growth parameters compared include percent dead tAUC, live nuclei nAUC, confluency nAUC, saturation density, and population doubling time. To normally distribute the residuals, percent dead tAUC, live nuclei nAUC, and confluency nAUC values were log transformed prior to calculating the two-way ANOVA. The metabolic parameters include baseline OCR, stressed OCR, OCR metabolic potential, baseline ECAR, stressed ECAR, ECAR metabolic potential, OCR/ECAR ratio, and glucose uptake. Three-way ANOVA (age-by-sex-by-time) was used with a Tukey post hoc test and a Bonferroni correction to compare YM-*h*MPCs, YF-*h*MPCs, OM-*h*MPCs, and OF-*h*MPCs for percent dead, live nuclei count, and percent confluency over time. Three-way ANOVA (age-by-sex-by-time) was also used with a Bonferroni correction to compare mRNA levels of *PPARGC1α*, *CD36*, *GLUT1*, and *GLUT4* over time. All statistical tests for mRNA data were performed on the delta Cp values for all genes. Biologically meaningful comparisons (YM-*h*MPCs vs. YF-*h*MPCs, YM-*h*MPCs vs. OM-

*h*MPCs, YF-*h*MPCs vs. OF-*h*MPCs, and OM-*h*MPCs vs. OF-*h*MPCs) are reported for all parameters measured. Pairwise results for two- and three-way ANOVAs are presented if the interaction term is significant. Statistics were completed using R. All values are reported as mean ± s.d. Significance was determined at $p < 0.05$.

2.4 Results

2.4.1 Effect of age and sex on hMPC expansion capacity

To determine whether age and sex impact expansion capacity, we compared expansion parameters of YM-, YF-, OM- and OF-*h*MPCs over 408 h, while cells were incubated in GM. To capture cell death throughout expansion, we determined the percentage of dead cells every 24 h for 408 h. For percentage of dead cells throughout expansion **(Figure 1A)**, we observed a significant age-by-sex-by-time interaction ($p<0.001$). Post hoc analysis revealed that within young-*h*MPCs, YF-*h*MPCs had a greater percentage of dead cells early in proliferation (24 and 48 h, $p<0.05$, Figure 1A) compared to YM-*h*MPCs. Within old-*h*MPCs, OM-*h*MPCs had a greater percentage of dead cells throughout proliferation (24, 120, 168, and 216 h; $p<0.05$) when compared to OF-*h*MPCs. Within male-*h*MPCs, OM-*h*MPCs had a greater percentage of dead cells throughout proliferation (24-120, 168, 216 h; $p<0.05$) compared to YM-*h*MPCs. Within female-*h*MPCs, OF-*h*MPCs had a greater percentage of dead cells at 72 and 96 h of proliferation (72-96 h, $p<0.05$) when compared to YF-*h*MPCs. To determine the magnitude of total cell death throughout expansion, we also determined the percent dead total area under the curve (tAUC) for each group **(Figure 1B)**; we observed a significant age-by-sex interaction ($p<0.001$). Post hoc analysis indicated that within young-*h*MPCs, YF-*h*MPCs had significantly greater percent dead tAUC compared to YM-*h*MPCs ($p<0.01$). Within male-*h*MPCs, OM-*h*MPCs had significantly

greater percent dead tAUC compared to YM-*h*MPCs ($p<0.001$). We observed no significant differences in percent dead tAUC between old- or female-*h*MPCs.

To fully characterize growth characteristics over time, we measured live nuclei count and percent confluency every 24 h for 408 h. For live nuclei count **(Figure 1C)**, we observed a significant age-by-sex-by-time interaction ($p<0.001$). Post hoc analysis indicated that within young-*h*MPCs, YF-*h*MPCs had a fewer number of live cells throughout expansion (192-260, 408 h; $p<0.05$). Within male-*h*MPCs, OM-*h*MPCs had fewer live nuclei throughout expansion (168-408 h, $p<0.05$) compared to YM-*h*MPCs. We observed no significant post hoc analyses within old-*h*MPCs or within female-*h*MPCs. We calculated live nuclei net area under the curve (nAUC) as a measure of the overall magnitude of live cell count throughout expansion **(Figure 1D).** For live nuclei nAUC, we observed a significant age-by-sex interaction ($p<0.01$). Post hoc analysis revealed that within young-*h*MPCs, YF-*h*MPCs had a trending lower nAUC ($p=0.06$). Within male *h*MPCs, OM-*h*MPCs had a significantly lower live nuclei nAUC ($p<0.001$). We observed no sex-related differences in the old-*h*MPCs or age-related differences in female-*h*MPCs for live nuclei nAUC. For percent confluency **(Figure 1E)**, we observed a significant age-by-sex-by-time interaction ($p<0.001$). Post hoc analysis revealed that within young-*h*MPCs, YF-*h*MPCs had a lower percent confluency throughout proliferation (168-264 h, $p<0.05$) when compared to YM-*h*MPCs. Within male-*h*MPCs, OM-*h*MPCs had a lower percent confluency throughout proliferation (144-408 h, $p<0.05$) compared to YM-*h*MPCs. We observed no difference in percent confluency between female- or old-*h*MPCs. For percent confluency nAUC **(Figure 1F)**, we observed a significant age-by-sex interaction ($p<0.01$). We observed no difference in percent confluency nAUC between YF-hMPCs and YM-hMPCs. Within male-*h*MPCs, OM-*h*MPCs had a significantly lower percent confluency nAUC compared to YM-*h*MPCs ($p<0.001$). We

observed no difference in percent confluency nAUC between old- or female-*h*MPCs.

Our final measured growth parameters were population doubling time **(Figure 1G)** and saturation density **(Figure 1H)**. For population doubling time, we observed a significant age-by-sex interaction ($p<0.001$). Post hoc analysis revealed that within old-*h*MPCs, OM-*h*MPCs had significantly longer population doubling times compared to OF-*h*MPCs. Within male hMPCs, OM-*h*MPCs had a significantly longer population doubling time compared to YM-hMPCs. We observed no differences within young-*h*MPCs or within female-*h*MPCs. For saturation density, we observed a significant age-by-sex interaction ($p<0.01$). Post hoc analysis revealed a significantly lower saturation density in YF-*h*MPCs compared to YM-*h*MPCs ($p<0.05$) and significantly lower saturation density in OM-*h*MPCs compared to YM-*h*MPCs ($p<0.001$). We observed no significant differences within old-*h*MPCs or within female-*h*MPCs.

Collectively, this evidence suggests that within young-*h*MPCs, YF-*h*MPCs have a lower expansion capacity than YM-*h*MPCs. Additionally, male-*h*MPCs are severely impacted with age; OM-*h*MPCs have impaired expansion capacity when compared to YM-*h*MPCs. To the contrary, female-hMPCs are largely unaffected with age; OF-*h*MPCs do not have significantly impaired expansion capacity compared to YF-*h*MPCs.

2.4.2 Effect of age and sex on markers of cell cycle and cell apoptosis

To probe more deeply into alterations in pathways related to cell expansion, we leveraged an existing RNAseq dataset that included all YM-, YF-, OM-, and OF-*h*MPC samples at the 3rd day of rapid expansion. Based on our cell expansion data, we were particularly interested in identifying canonical pathways and cellular and molecular functions that were differentially

expressed between OM- and YM-*h*MPCs and between YF- and YM-*h*MPCs. We identified 571 DEgenes between OM- and YM-*h*MPCs that had a q value (False Discovery Rate) <0.01. We identified 395 DEgenes between YF- and YM-hMPCs that had a q value of <0.01. Significantly up- and down-regulated canonical pathways are reported in Table 2 and Table 3 for the age comparison in males and sex comparison in young, respectively. Significantly up- and down-regulated molecular and cellular functions are reported in Table 4 and Table 5 for the age comparison in males and sex comparison in young, respectively. Briefly, the canonical pathways and cellular and molecular functions support decreased cell cycling and increased cell death in OM- compared to YM-*h*MPCs and in YF- compared to YM-*h*MPCs.

2.4.3 Effect of age and sex on markers of metabolism throughout expansion

After determining that expansion capacity is altered with age and sex, especially in male-*h*MPCs, we next asked whether *h*MPC metabolism is impacted by age and sex during expansion. We measured both oxygen consumption rate (OCR) and extracellular acidification rate (ECAR) to capture the metabolic phenotype under baseline and stressed (stimulated to maximize energy production) conditions. The metabolic phenotype of each age-by-sex *h*MPC comparison, under baseline and stressed conditions, is shown in **Figure 2.** For baseline OCR **(Figure 3A)**, we observed a significant age-by-sex interaction ($p<0.01$). Post hoc analysis revealed that within young-*h*MPCs, YF-*h*MPCs had a significantly lower baseline OCR when compared to YM-*h*MPCs. Within male-*h*MPCs, OM-*h*MPCs had a trending lower baseline OCR ($p=0.09$). We observed no significant post hoc differences within female-*h*MPCs or old-*h*MPCs. We observed no significant main-effects or interactions for stressed OCR **(Figure 3B)**. For OCR metabolic potential, we observed a significant age-by-sex interaction ($p<0.05$) **(Figure 3C)**. Post hoc

analysis revealed that within old-*h*MPCs, OM-*h*MPCs had a significantly greater OCR metabolic potential when compared to OF-*h*MPCs. Within male-*h*MPCs, OM-*h*MPCs had a significantly greater OCR metabolic potential ($p<0.01$), suggesting OM-*h*MPCs used less of their OXPHOS capacity during expansion. There were no significant differences in OCR metabolic potential within young- or female-*h*MPCs. We observed no significant main-effects or interactions for any ECAR measure **(Figure 3D-3F)**, the OCR/ECAR ratio **(Figure 3G)**, or glucose uptake **(Figure 3H)**. Interestingly, the ECAR metabolic potential was significantly greater than the OCR metabolic potential during expansion (age-by-sex-by-measure interaction $p<0.05$, **Figure 4**), suggesting that cells used the majority of their OXPHOS capacity during expansion but had a glycolytic reserve that could be used to meet an energy demand. Post hoc analysis revealed significantly higher ECAR metabolic potential versus OCR metabolic potential in YM-*h*MPCs ($p=0.1$), YF-*h*MPCs ($p<0.05$), and OF-*h*MPCs ($p<0.05$). OCR and ECAR metabolic potential was not significantly different in OM-*h*MPCs.

Importantly, we identified that baseline OCR was negatively correlated with percent dead tAUC **(Figure 5)**. This suggests that *h*MPCs that had the lowest baseline OCR also had the greatest cell death throughout expansion and further supports the importance of OCR during *h*MPC expansion.

To complement the Seahorse measurements, we also quantified the expression of genes related to substrate uptake *(CD36, GLUT1* and *GLUT4)* and mitochondrial biosynthesis (*PPARGC1A*). We observed significant main-effects of time ($p<0.05$) for both *PPARGC1A* **(Figure 6A)** and *CD36* **(Figure 6B)**. Expression of both genes significantly increased over time in all groups, indicating that *h*MPCs may increase OXPHOS and fatty acid uptake throughout proliferation. For glucose uptake genes, we observed significant age-by-sex interactions for

GLUT1 ($p<0.0001$) **(Figure 6C)** and *GLUT4* ($p<0.05$) **(Figure 6D)**. Post hoc analysis revealed that within old-*h*MPCs, OM-*h*MPCs had significantly greater expression of *GLUT1* ($p<0.001$) and *GLUT4* ($p<0.001$) compared to OF-*h*MPCs. Within male-*h*MPCs, OM-*h*MPCs had significantly greater expression of *GLUT1* ($p<0.001$) and *GLUT4* ($p<0.001$) compared to YM-*h*MPCs. No significant difference in *GLUT1* or *GLUT4* expression was detected within young- and female-*h*MPCs. We did not observe changes in glucose uptake in accompaniment to observed increases in *GLUT1* gene expression. However, this may be due to the sensitivity of our glucose uptake assay.

Table 2. Differentially Expressed Canonical Pathways between OM- and YM-*h*MPCs

OM- vs. YM-*h*MPCs		
Canonical Pathways	*P-value*	*Z-score*
Mitotic Roles of Polo-Like Kinase	1.0E-07	-2.1
Cell Cycle: G2/M DNA Damage Checkpoint Regulation	3.8E-05	1.4
Cyclins and Cell Cycle Regulation	2.3E-04	-2.3
P53 Signaling	2.3E-03	1.9
Pyrodixal 5'-phosphate Salvage Pathway	1.4E-03	-1.9
Pyrimidine Deoxyribonucleotides De Novo Biosynthesis I	2.6E-03	-2.0
Salvage Pathways of Pyrimidine Ribonucleotides	3.5E-03	-2.1

Table 3. Differentially Expressed Canonical Pathways Between YF- and YM-*h*MPCs

YF- vs. YM-*h*MPCs		
Canonical Pathways	*P-value*	*Z-score*
Mitotic Roles of Polo-Like Kinase	2.2E-08	-1.7
Cell Cycle: G2/M DNA Damage Checkpoint Regulation	2.2E-07	1.7
Cyclins and Cell Cycle Regulation	9.8E-05	-2.1
Pyridoxal 5'-phosphate Salvage Pathway	1.1E-03	-2.5
Role of BRAC1 in DNA Damage Response	9.0E-05	-1.3
Salvage Pathways of Pyrimidine Ribonucleotides	1.8E-03	-2.6
Cell Cycle: G1/S Checkpoint Regulation	6.9E-03	1.3

Table 4. Molecular and Cellular Functions of DEgenes (OM- vs. YM-*h*MPCs)

Molecular and Cellular Functions	*P-value*	*Z-score*	*# Molecules*
Cell cycle progression	4.2E-29	-1.2	121
M phase	9.7E-21	-1.7	44
Interphase	1.2E-20	-1.6	80
Segregation of chromosomes	4.4E-20	-2.0	32
G1/S phase transition	9.5E-09	-1.7	26
Senescence of cells	1.7E-08	2.4	31
Necrosis	9.4E-30	2.3	217
Cell death	7.6E-27	2.0	248
Apoptosis	1.4E-26	2.0	209

Table 5. **Molecular and Cellular Functions of DEgenes (YF- vs. YM-*h*MPCs)**

Molecular and Cellular Functions	*P-value*	*Z-score*	*# Molecules*
Cell cycle progression	5.8E-28	-1.7	96
Mitosis	8.9E-28	-1.2	64
Segregation of chromosomes	9.5E-24	-2.1	31
M phase	2.7E-21	-1.9	38
Interphase	3.0E-13	-2.0	53
S phase	1.8E-09	-1.7	25
G1/S phase transition	2.0E-06	-2.6	18
Segregation of chromosomes	9.5E-24	-2.1	31
Repair of DNA	1.5E-09	-2.8	28
Apoptosis	3.6E-20	2.2	148

Figure 1. Expansion Characteristics of Young and Old Male and Female *h*MPCs. A) percentage of dead cells every 24 h over 408 h of growth, B) percent dead total area under the curve (AUC), C) live nuclei count every 24 h over 408 h of growth, D) live nuclei net AUC, E) percent confluency every 24 h over 408 h of growth, F) confluency net AUC, G) population doubling time during the exponential growth phase, H) saturation density (number of live nuclei/cm^2 at the proliferation plateau). Two-way ANOVAs were used with Tukey post-hoc tests to compare YM-, YF-, OM-, and OF-*h*MPCs for percent dead tAUC, live nuclei nAUC, confluency nAUC, saturation density, and population doubling time. Three-way ANOVAs were used with Tukey post-hoc tests and Bonferroni corrections to compare percent dead, live nuclei count, and percent confluency over 408 h of growth. All values are reported as mean ± s.d. # YM- vs. YF-*h*MPCs, β YF- vs. OF-*h*MCPs, κ YM- vs. OM-*h*MPCs, α OM- vs. OF-*h*MPCs.

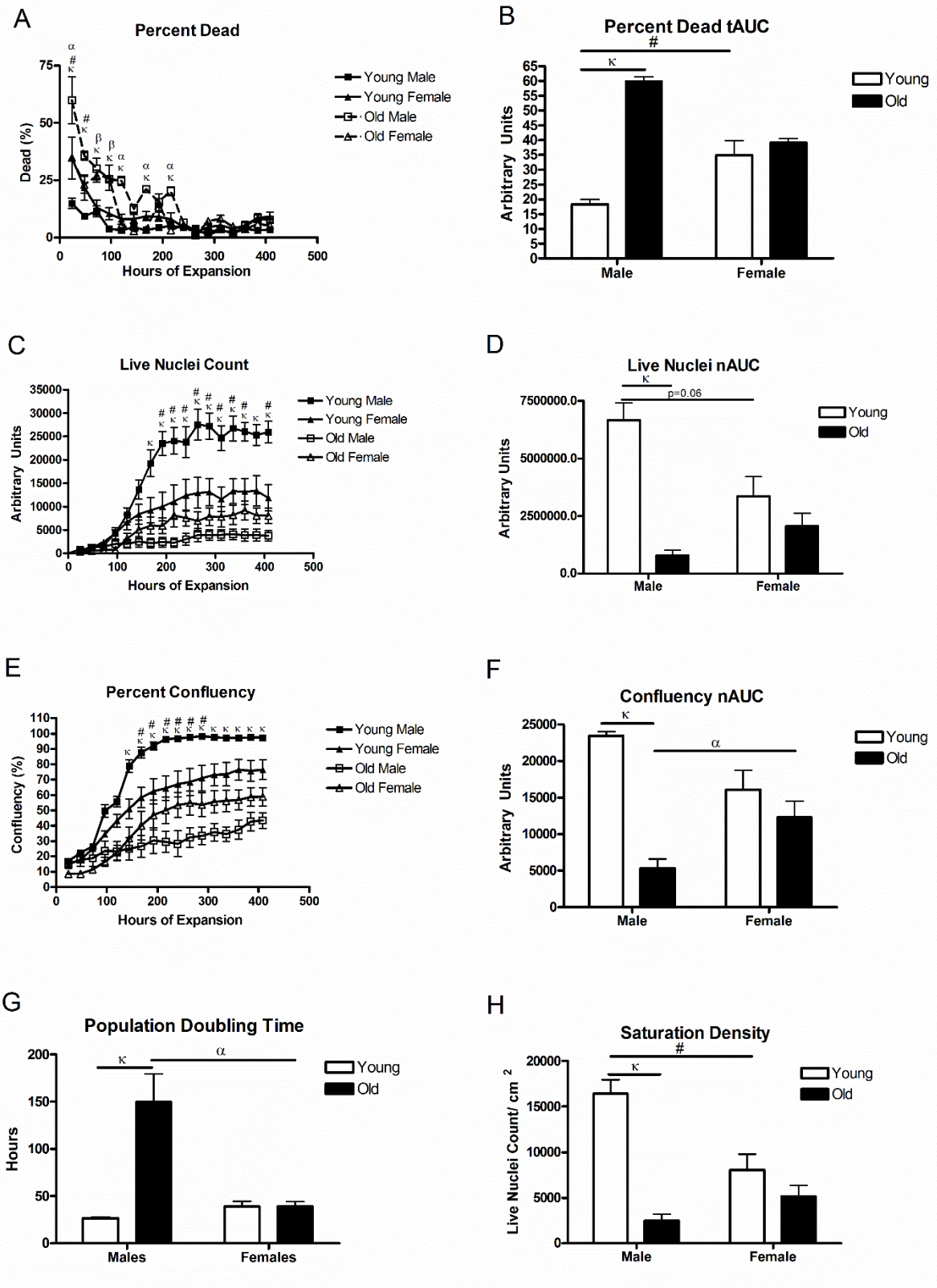
A
Percent Dead
Dead (%)
Hours of Expansion
Young Male
Young Female
Old Male
Old Female
B
Percent Dead tAUC
Arbitrary Units
Male
Female
Young
Old
C
Live Nuclei Count
Arbitrary Units
Hours of Expansion
Young Male
Young Female
Old Male
Old Female
D
Live Nuclei nAUC
Arbitrary Units
p=0.06
Male
Female
Young
Old
E
Percent Confluency
Confluency (%)
Hours of Expansion
Young Male
Young Female
Old Male
Old Female
F
Confluency nAUC
Arbitrary Units
Male
Female
Young
Old
G
Population Doubling Time
Hours
Males
Females
Young
Old
H
Saturation Density
Live Nuclei Count/ cm 2
Male
Female
Young
Old

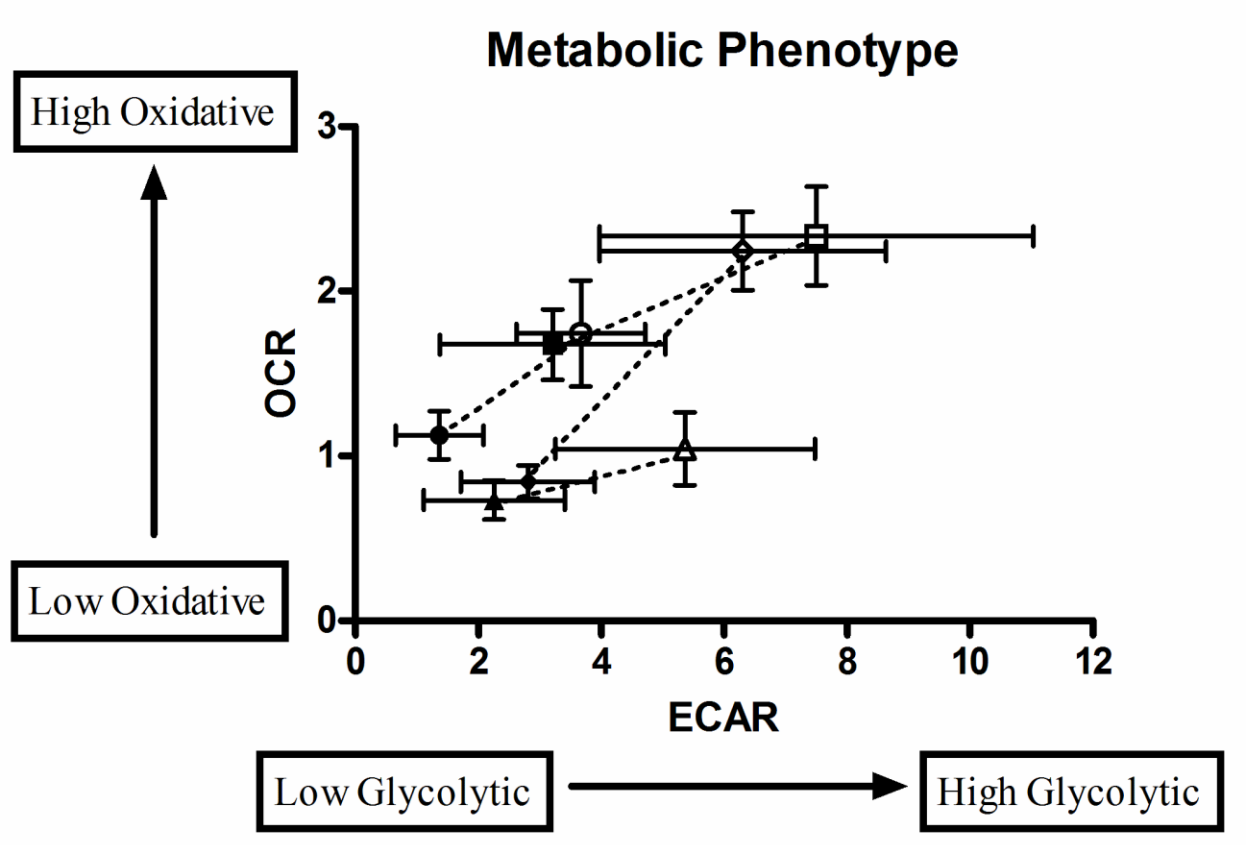

Figure 2. Metabolic Phenotype of Young and Old Male and Female *h*MPCs. Baseline metabolic phenotype of YM-, YF-, OM-, and OF-*h*MPCs are designated by solid shapes (■ = YM-, ▲= YF-, ♦ = OM-, ● = OF-*h*MPCs). Stressed metabolic phenotype of YM-, YF-, OM-, and OF-hMPCs are designated by open shapes (□ = YM-, Δ = YF-, ◊ = OM-, ○ = OF-*h*MPCs).

Figure 3. Metabolic Characteristics of Young and Old Male and Female *h*MPCs. A) Baseline oxygen consumption rate (OCR), B) stressed OCR, C) OCR metabolic potential (stressed – baseline), D) baseline extracellular acidification rate (ECAR), E) stressed ECAR, F) ECAR metabolic potential, G) baseline ratio of OCR/ECAR, H) glucose uptake. Two-way ANOVAs were used with Tukey post-hoc tests to compare YM-, YF-, OM-, and OF-*h*MPCs for all parameters. All values are reported as mean ± s.d. # YM- vs. YF-*h*MPCs, β YF- vs. OF-*h*MCPs, κ YM- vs. OM-*h*MPCs, α OM- vs. OF-*h*MPCs. $p<0.05$

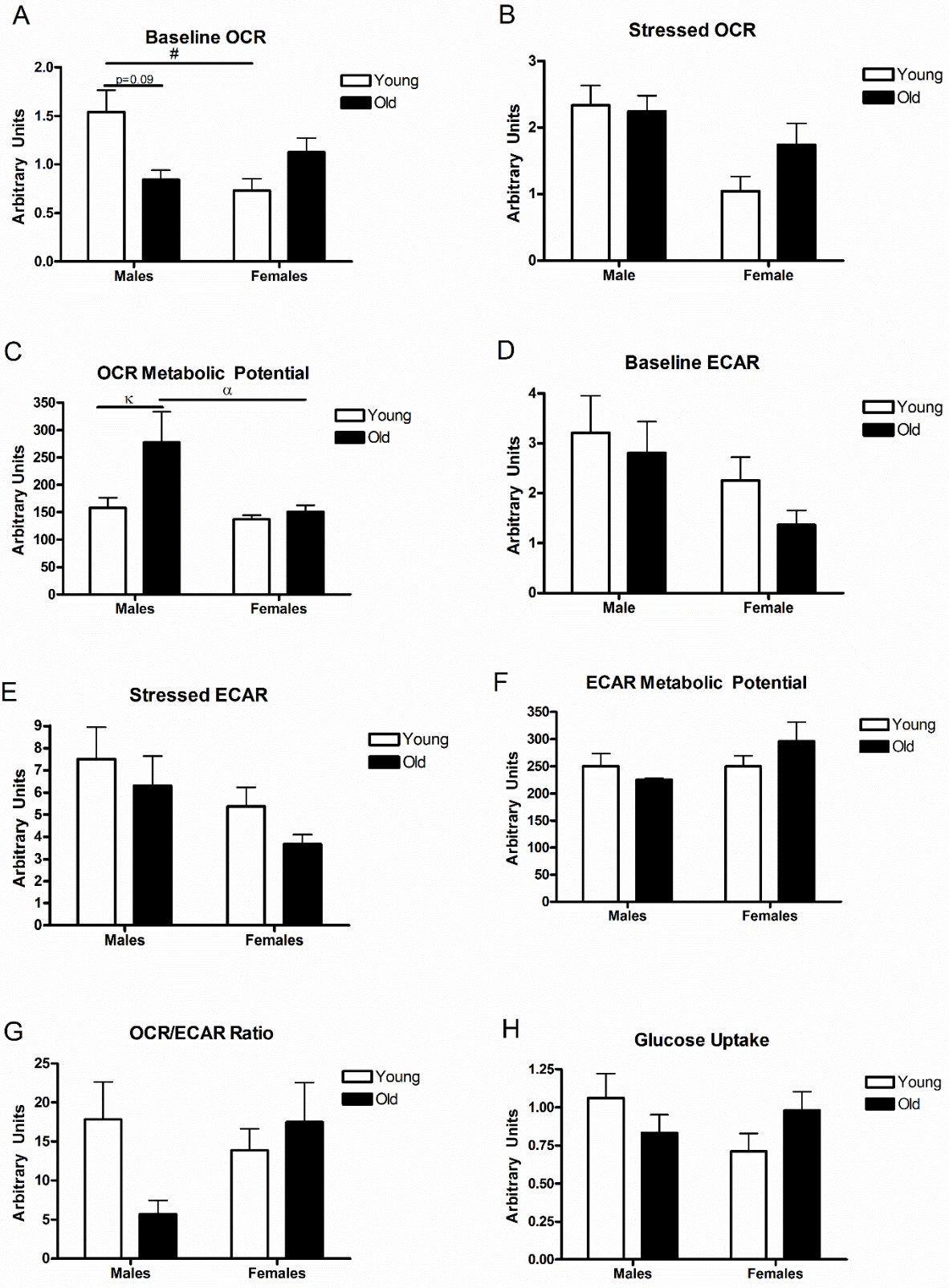
A
Baseline OCR
#
p=0.09
Young
Old
Arbitrary Units
2.0
1.5
1.0
0.5
0.0
Males
Females
B
Stressed OCR
Young
Old
Arbitrary Units
3
2
1
0
Male
Female
C
OCR Metabolic Potential
κ
α
Young
Old
Arbitrary Units
350
300
250
200
150
100
50
0
Males
Females
D
Baseline ECAR
Young
Old
Arbitrary Units
4
3
2
1
0
Male
Female
E
Stressed ECAR
Young
Old
Arbitrary Units
9
8
7
6
5
4
3
2
1
0
Males
Females
F
ECAR Metabolic Potential
Young
Old
Arbitrary Units
350
300
250
200
150
100
50
0
Males
Females
G
OCR/ECAR Ratio
Young
Old
Arbitrary Units
25
20
15
10
5
0
Males
Females
H
Glucose Uptake
Young
Old
Arbitrary Units
1.25
1.00
0.75
0.50
0.25
0.00
Males
Females

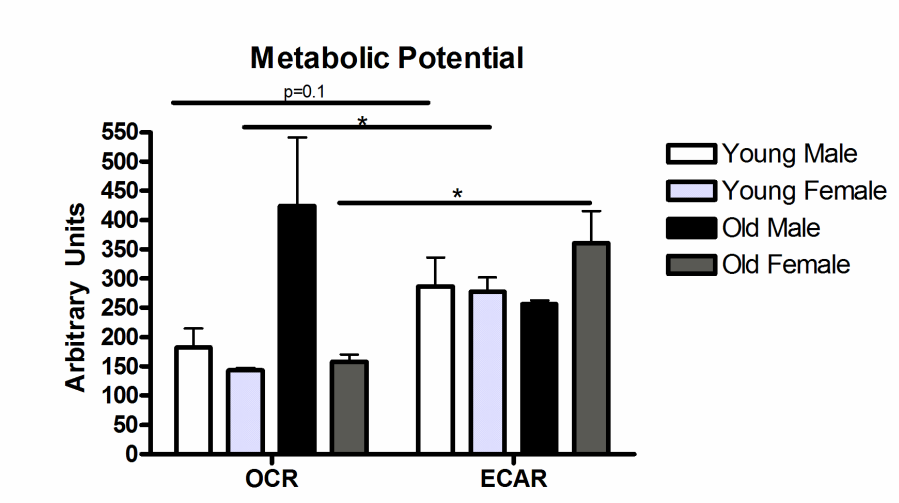

Figure 4. OCR and ECAR Metabolic Potential. Metabolic potential of OCR vs. ECAR in all groups. A two-way ANOVA was used with Tukey post-hoc tests to compare OCR and ECAR metabolic potential in all groups. All values are reported as mean ± s.d. * $p<0.05$

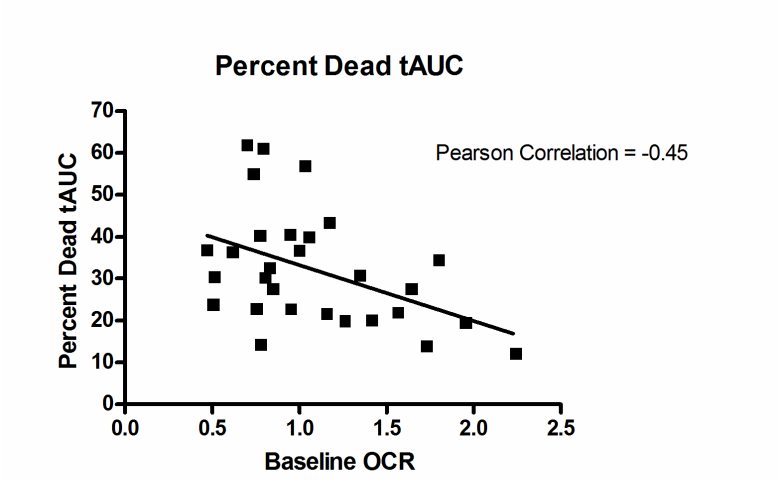

Figure 5. Baseline OCR and Percent Dead Correlation. Pearson correlation of percent dead tAUC and baseline OCR. $p<0.05$

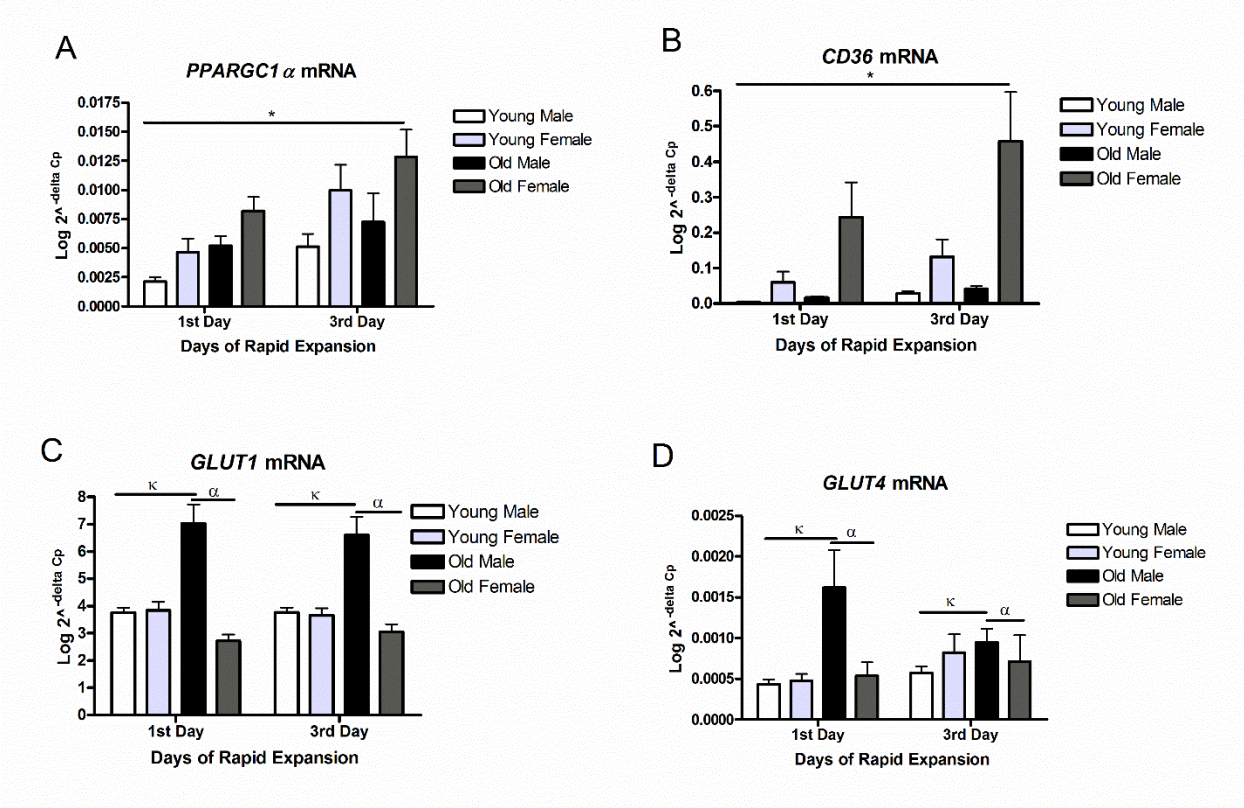

Figure 6. Gene Expression in Young and Old Male and Female *h*MPCs A) *PPARGC1α*, B) *CD36*, C) *GLUT1* and D) *GLUT4* mRNA levels at 1st and 3rd day of rapid expansion. Three-way ANOVAs were used with Tukey post-hoc tests and Bonferroni corrections for all mRNA targets. All values are reported as mean ± s.d. # YM- vs. YF-*h*MPCs, β YF- vs. OF-*h*MCPs, κ YM- vs. OM-*h*MPCs, α OM- vs. OF-*h*MPCs. $p<0.05$

2.5 Discussion

This is the first research to evaluate age- and sex-related differences in the expansion capacity of primary *h*MPCs and to identify differences in metabolism that underlie and thus likely impact *h*MPC expansion capacity. Expansion capacity is the ability of cells to undergo cell division but minimize cell death, senescence, or premature differentiation, thus, maximizing the number of cells that are able to be used for repair and regeneration of tissue. Expansion of the *h*MPC pool following injury is an essential component of the SkM regeneration process (4). It has been documented that aged SkM has a decreased capacity for recovery following injury (21). *In vitro*, animal MPC models have demonstrated age-related reductions in total nuclei count and elevation in cell death during expansion (34, 159). However, our experiments using *h*MPCs suggest that age-related differences in MPC expansion are sex-specific and not due to a main-effect of chronological aging *per se*. Importantly, *h*MPCs largely retain the human donor, metabolic phenotype and have the most relevant genetic background to address age- and sex-related differences in *h*MPC expansion capacity and metabolism (1). Use of isolated and cultured SCs do limit the ability to understand the role of the tissue niche, which has been shown to play a critical role in the muscle regeneration process (193). Impaired muscle regeneration with age is likely due to a combination of intrinsic changes within SCs and extrinsic changes within the tissue niche (193).

2.5.1 Continual, heightened cell death impairs expansion capacity of old male hMPCs

*h*MPCs from healthy older males had reduced expansion capacity compared to their younger counterparts, but *h*MPCs from healthy females were largely unaffected by age. Both OF- and OM-*h*MPCs had heightened cell death early in expansion. However, OF-*h*MPCs were

able to minimize cell death and largely maintain their expansion capacity. This contrasts with OM-*h*MPCs that had continued, heightened cell death and impaired expansion capacity as evidenced by lengthened population doubling times, impaired confluency, and a lowered saturation density. The impaired expansion phenotype of the OM-hMPCs was supported by differential expression of genes that are related to (i) increased DNA damage checkpoint control, p53 signaling, apoptosis, and senescence; and (ii) decreased cyclins and cell cycle control.

Heightened cell death was also observed as a contributor to reduced expansion capacity in YF-*h*MPCs compared to YM-*h*MPCs. While YF-*h*MPCs (vs. YM-*h*MPCs) also had differential expression of genes involved in (i) increased DNA damage checkpoint control and apoptosis; and (ii) decreased cyclins and cell cycle control, the number of DEgenes related to these functions was lower than the aging male-*h*MPC comparison. Additionally, in the YF-*h*MPCs vs. YM-*h*MPCs comparison, senescence of cells was not identified as a functional category for DEgenes. Intriguingly, unlike the male-*h*MPCs, female-*h*MPCs were largely unaffected by age. This contrasts evidence from mouse models. Mouse primary MPCs (*m*MPCs) derived from male mice at 40, 60, or 120 days of age all exhibited higher proliferation rates than age-matched female *m*MPCs, suggesting male *m*MPCs have greater expansion capacity, independent of age (108). However, sex-related differences in expansion capacity were based on total nuclei counts only; the number of dead cells was not quantified. As we have identified in this study, there are significant age- and sex- related differences in cell death that greatly impact total *h*MPC number. Thus, measuring only total nuclei as a proxy of cell expansion may overestimate the culture's expansion capacity. Differences between studies may also indicate species-specific differences in MPC expansion. Overall, we identified heightened cell death in *h*MPCs from old males, which diminished the number of cells available for myogenesis.

Notably, only three old male cultures expanded well enough to be used in the experiments reported here. Thus, the difference between OM- and YM-, YF-, or OF-*h*MPCs may be even greater in the general population than suggested in this study. Age related changes at the whole tissue and cellular level in muscle have been previously dichotimized by sex (144). *In vivo*, SkM mass makes up a greater percentage of total body mass in males compared to females; however, males lose SkM mass at a faster rate and lose almost twice the strength that females lose with age (69, 80, 135, 144, 195). Additionally, females tend to preserve muscle quality (strength per unity of muscle) better than males with age (97). The data we present here agree with these previous reports; *h*MPCs from males have the greatest alterations in phenotype and expansion capacity with age. Thus, the predominant mechanisms driving muscle loss with age appear sex dependent.

2.5.2 OXPHOS is impaired in old male hMPCs

Results from our study also suggest that reduced expansion capacity in OM-*h*MPCs was accompanied by alterations in measurements of OXPHOS while glycolysis was maintained. The OM-*h*MPCs that remained viable had slightly reduced OXPHOS, but similar glycolytic activity and greater *GLUT1* mRNA levels compared to YM-*h*MPCs. It is unclear whether the cells that survived in OM-*h*MPC cultures were protected or harmed by lower OXPHOS. Lower OXPHOS reduces the potential for oxidative stress and related cell damage, assuming there are no impairments in any of the electron transport chain complexes (3). Thus, reduced OXPHOS may have protected surviving OM-*h*MPCs. Similarly, surviving SCs, isolated from cadavers four days post mortem, consumed less oxygen, produced lower levels of ATP, and existed at a lower metabolic state compared to freshly isolated cells (92); reduced metabolic activity may promote

cell survival. An alternative and more likely hypothesis is that lower basal respiration indicates an inability to meet energy demands and/or an impairment in one or more of the electron transport chain complexes. Impairments in the electron transport chain can increase reactive oxygen species (ROS) production and decrease energy production (120). Increased ROS generation and/or reduced energy production may subsequently impair *h*MPC expansion capacity. Interestingly, following an OXPHOS stressor, OM-*h*MPCs had the equivalent oxygen consumption capacity as YM-*h*MPCs, suggesting that OM-*h*MPCs preferentially used glycolysis over OXPHOS. In support of this theory, SCs that underwent replicative aging also had alterations in mitochondrial OXPHOS and favored glycolysis (128). Furthermore, a metabolite analysis of whole SkM demonstrated lower TCA cycle intermediates and lower ATP levels in healthy older males compared to young males (51). Additionally, our study suggests that higher rates of baseline OXPHOS are correlated with a lower percent dead throughout expansion. Collectively, this evidence suggests that OXPHOS is necessary to meet energy demands and promote cell survival throughout *h*MPC expansion.

Contrary to the OM-*h*MPCs, OF-*h*MPCs maintained markers of both OXPHOS and glycolysis at similar levels as those in YF-*h*MPCs, despite lower expression levels of the glucose transporters *GLUT1* and *GLUT4*. Similarly, SCs isolated from a female infant and passaged until replicative senescence displayed increased OCR and reduced glucose flux as cells approached senescence (12). Overall, our results suggest that sex-specific alterations in metabolism occur with age and may underlie sex-specific alterations in expansion capacity.

Supporting the importance of OXPHOS for expansion, expression of genes related to fatty acid uptake and OXPHOS (*CD36* and *PPARGC1A*) increased throughout expansion in all age-by-sex *h*MPC cultures. In accordance, Ryall et al. reported an increase in mitochondrial

fluorescence and an enrichment of genes known to regulate the TCA cycle in primary *m*MPCs after 48 h in culture (154). Additionally, Cerletti et al. demonstrated that enhanced OXPHOS capacity in *m*MPCs achieved through caloric restriction increased proliferation and improved transplant efficiency (25). Thus, while studies have reported the importance of glycolysis early in cell proliferation (93, 154), our results as well as those of others support that increasing OXPHOS capacity may be important for later stages of proliferation (148, 154) and differentiation (93, 162).

2.5.3 Heterogeneity within cell cultures

An alternative hypothesis to the observed sex-specific, age-related differences in *h*MPCs is that there is metabolic heterogeneity in our cultures despite sorting for SC specific markers (191). Rossi et al. recently characterized two distinct SC populations using cells freshly isolated from Sprague-Dawley wild-type rats (150). The two populations, termed Low Proliferative Clones [(LPC) myogenic fate] and High Proliferative Clones [(HPC) spontaneously produce adipocytes], were separated according to their proliferative capacity and metabolic profiles (150). While both LPC and HPC cells were isolated using SC specific markers, only LPC cells expressed a marker of myogenic commitment (MyoD) after 10 days in culture and had a greater myogenic regeneration potential when transplanted *in vivo* (150). Interestingly, LPC cells had elevated mitochondrial ATP production and OXPHOS, while HPC cells were more likely to be sensitive to oxidative stress (150). Similarly, Rocheteau et al. identified two subpopulations of SCs in Tg:Pax7-nGFP mice *in vivo* and *in vitro*; the $Pax7^{Hi}$ population of SCs (vs. $Pax7^{Lo}$ cells) had greater expression of genes related to stemness and lower metabolic activity as evidenced by lower ATP levels (147). It is likely that similar metabolic heterogeneity exists in *h*MPC cultures

and the heterogeneity changes with age and sex of the donor. However, the presence of subpopulations in human cultures remains unexplored.

2.6 Conclusion

In summary, this is the first research to identify heightened cell death and altered metabolism as age-related intrinsic differences that contribute to altered expansion capacity of *h*MPCs. Importantly, these age-related differences in expansion and metabolism were sex-specific. *h*MPCs derived from older males exhibited the greatest cell death and expansion impairment while *h*MPCs derived from older females were largely unaffected by age. Our results highlight the importance of quantifying both live and dead cell counts when measuring expansion capacity. Furthermore, OM-*h*MPCs exhibited alterations in markers of OXPHOS while OF-*h*MPCs maintained OXPHOS function. We conclude that the underlying contributors to impairments in expansion capacity that occur with age are largely sex-dependent and may be a function of altered metabolism.

2.7 Acknowledgements

We thank Cornell University, Biotechnology Resource Center Imaging Facility for their help with fluorescence activated cell sorting. We thank Heather Roman, M.S. for her assistance with maintaining the *h*MPC cultures. We also thank Melinda Lem for her help with participant recruitment. Finally, we thank the participants for their time and participation in the study. This study was funded by PCCW and Cornell Division of Nutritional Sciences funds.

CHAPTER 3: TRANSCRIPT PROFILE DISTINGUISHES VARIABILITY IN HUMAN MYOGENIC PROGENITOR CELL EXPANSION CAPACITY

Emily S Riddle, Erica L Bender, Anna E Thalacker-Mercer

Author Affiliations: Division of Nutritional Sciences, Cornell University, Ithaca, NY, 14853, USA (ER, EB, ATM)

Abbreviated Title for Running Head: Myoblast Expansion Capacity Transcriptome

Corresponding Author: Dr. Anna Thalacker-Mercer, aet74@cornell.edu, 109 Savage Hall, Cornell University, Ithaca, NY 14850

Emily S Riddle: Experimental design, data collection, data analysis, and interpretation
Erica L Bender: Data collection
Anna E Thalacker-Mercer: Experimental design, data collection, data analysis, and interpretation

Keywords: cell proliferation, variation, gene expression, muscle progenitor cells

3.1 Abstract

Primary human muscle progenitor cells (*h*MPCs) are commonly used to understand skeletal muscle biology, including the regenerative process. Variability from unknown origin in *h*MPC expansion capacity occurs independent of disease, age, or sex of the donor. We sought to determine the transcript profile that distinguishes *h*MPC cultures with greater expansion capacity and to identify biological underpinnings of these transcriptome profile differences. Sorted (CD56+/CD29+) *h*MPC cultures were clustered using unbiased, K-means cluster analysis into FAST and SLOW based on growth parameters (saturation density and population doubling time). FAST had greater expansion capacity indicated by significantly reduced population doubling time (-60%) and greater saturation density (+200%), nuclei area under the curve (AUC, +250%), and confluency AUC (+120%). Additionally, FAST had fewer % dead cells AUC (-44%, $p<0.05$). RNAseq was conducted on RNA extracted during the expansion phase. Principal component analysis distinguished FAST and SLOW based on the transcript profiles. There were 2205 differentially expressed genes (DEgenes) between FAST and SLOW (q value ≤ 0.05); 362 DEgenes met a more stringent cut-off (q value ≤ 0.001 and 2.0 fold-change). DEgene enrichment suggested FAST (vs. SLOW) had promotion of the cell cycle, reduced apoptosis and cellular senescence, and enhanced DNA replication. Novel (*RABL6, IRGM1,* and *AREG*) and known (*FOXM1, CDKN1A, Rb*) genes emerged as regulators of identified functional pathways. Collectively the data suggest that variation in *h*MPC expansion capacity occurs independent of age and sex and is driven, in part, by intrinsic mechanisms that support the cell cycle.

3.2 Introduction

Stem cells [satellite cells (SC)] are essential for skeletal muscle repair and regeneration following damage. SC and a well-orchestrated program leads to muscle progenitor cells (MPCs) that develop into multinucleated muscle cells (myofibers) or self-renew the SC pool. *In vivo*, dysfunction and loss of SCs leads to pathological remodeling and eventually to functional decline of the muscle (60). To date, much research has used animal models to understand SC biology and skeletal muscle regeneration (34, 36, 108, 122, 147). Characterization of human MPC (hMPC) biology is currently limited and is necessary to understand the basic biology of human skeletal muscle regeneration and to develop and use hMPCs in stem cell therapies.

Interindividual variability in skeletal muscle regeneration is becoming more appreciated (41, 182); however, the biological underpinnings of regenerative variability are unclear. hMPCs maintain properties of their *in vivo* state (1, 71); thus, hMPCs are advantageous for the study of human variability in the regenerative response. Regeneration requires the proliferation and expansion of MPCs to create adequate cells to fuse into mature myofibers (99, 140, 151). In mice, depletion of SCs by genetic modification impedes myocyte fusion and skeletal muscle regeneration (88). Previous reports demonstrate that age of human/mouse MPCs impacts primary MPC proliferation rates (15, 28, 34, 108). We and others have demonstrated, however, that not all old hMPCs have impaired expansion capacity and similarly, not all young hMPCs expand better than old hMPCs (165). This raises the question, what are the biological underpinnings of expansion capacity of hMPCs?

Using unbiased statistical clustering tools, such as K-means cluster analysis, samples can be clustered by phenotypic similarity versus by the commonly used categorical similarity. Clustering by phenotypic similarity allows us to identify and understand basic biological

differences that underlie a phenotype (11, 169). Using tools such as principal components analysis (PCA), we can also unbiasedly cluster samples based on transcript profile similarity to determine whether the transcript profile underlies observed differences in phenotype (124, 190). The overarching goals of the proposed research were to determine the transcript profile(s) that distinguishes the expansion capacity of hMPCs independent of age and sex, and to identify biological underpinnings of expansion capacity. Understanding and even predicting hMPC expansion capacity of donor cells will further our understanding and utilization of hMPCs for research and therapy.

3.3 Methods

3.3.1 Ethical approval

All studies were approved by the Cornell University, Institutional Review Board. Written informed consent was obtained from all participants.

3.3.2 Human skeletal muscle procurement

Young and old, males and females were recruited for participation in this study. Young and old participants met the screening age range cutoffs of 22-40 y and 60-85 y respectively. All individuals completed a comprehensive health history and physical activity questionnaire and were independently ambulatory and cognitively intact (as determined by the examining nurse practitioner). Individuals were excluded for contagious infections and any chronic, end-stage disease expected to limit life-expectancy to less than one year, induce anorexia, or restrict physical activity. Individuals with seated resting systolic blood pressure >140 mmHg or diastolic blood pressure >90 mmHg and individuals receiving anabolic (e.g., GH, IGF-I) therapy were

also excluded.

Skeletal muscle biopsies were performed by a nurse practitioner in the Human Metabolic Research Unit (HMRU) at Cornell University. After an overnight fast, subjects reported to the HMRU, vitals were measured, and subjects rested in the supine position. A percutaneous needle biopsy of the vastus lateralis was taken using a 5.0 mm Bergstrom biopsy needle with suction under local anesthetic (1% lidocaine). Tissue was quickly blotted with sterile gauze, and visible adipose and connective tissues were removed. Skeletal muscle aliquots were either snap frozen in liquid nitrogen and stored at -80°C or were placed in Gibco® Hibernate®A (Thermo Fisher Scientific) and stored at 4°C.

3.3.3 Purified, primary human skeletal satellite cells

Primary human SCs were obtained from the biopsy tissue of young males (n=6, average age = 29 y), old males (n=3, average age = 72 y), young females (n=13, average age = 29 y), and old females (n=7, average age = 71 y). Approximately 75-100 mg of muscle biopsy tissue was stored in Gibco® Hibernate®A (Thermo Fisher Scientific) at 4°C until tissue disassociation was performed; dissociation occurred within 48 h of the biopsy. After mincing and washing via gravity with Ca-Mg free D-PBS, the tissue was disassociated in digest medium [2 mg/mL Collagenase D (Roche) in low-glucose DMEM]. After 30 minutes in digest medium, fresh digest medium and dispase were added. The disassociating pellet was titurated until a uniform slurry was achieved. Growth medium [(GM) Hams F12 + 20% FBS + 5ng/mL bFGF (Promega) + 1% Pen/Strep (Gibco)] was added to the slurry and passed through a 70 um cell strainer into a sterile conical tube. The cell suspension was centrifuged and the achieved pellet was resuspended in Recovery® freezing medium (Gibco) and cryopreserved at -80°C. Thawed cells were seeded on

a type-I collagen coated culture dish (initial cell confluency ~15%) (178). After 24 h, the GM was replaced with fresh GM and further replenished every 48 h. Once cells reached ~70% confluency, they were removed from the plate using 0.05% trypsin and passaged. Cells were expanded to passage four, then cryopreserved in 10% DMSO + GM.

To purify the culture, approximately 1-1.5 million cells were labeled with fluorescently-conjugated antibodies specific for myoblast cell surface antigens CD56 (NCAM; PE-Cy7-conjugated) and CD29 (β1-integrin; AlexaFluor488-conjugated) and the viability stain 7-Aminoactinomycin D (7AAD) (191). Individual samples yield 150,000 – 800,000 viable CD56+/CD29+ *h*MPCs per 1 million cells sorted using a BD FACS Aria™ Fusion flow cytometer. Sorted CD56+/CD29+ cells (>98% positive) were expanded in culture by passaging twice and then used in experiments; all *in vitro* experiments were performed using sorted cells at passage six. Due to high rates of cell death, only three old male cultures yielded sufficient *h*MPCs to be sorted and used in experiments.

3.3.4 Expansion measurements

Sorted *h*MPCs were seeded at a density of approximately 10% and proliferated in GM for 408 h. GM was changed every 48 h. Confluency, nuclei count, and percent dead in each culture were measured every 24 h after seeding using the Celigo® S, Imaging Cytometer (Nexcelom Bioscience), a high-throughput, microplate based, brightfield and fluorescent imaging system. In this way, we performed repeated measures of confluence, nuclei counts, and live/dead cell counts. Live cells were measured every 24 h by co-staining cells with Hoescht 33342 (to identify nuclei) and fluorescently labeled propidium iodide (to identify dead cells). Propidium iodide positive cells were subtracted from Hoescht 33342 positive cells to determine the total number of

live cells. The number of propidium iodide positive cells were divided by the number of Hoescht 33342 positive cells to determine the percentage of dead cells. Using percent confluency and live nuclei counts, we determined live nuclei net area under the curve (AUC), net confluency AUC, percent dead total AUC, population doubling time, and saturation density (the number of live nuclei at growth plateau divided by area of the well) for each culture.

3.3.5 Clustering hMPC cultures via growth parameters

K-means clustering using Euclidean distance was used to unbiasedly separate cultures into two clusters [fast growing cluster (FAST) and slow growing cluster (SLOW)] based on the growth parameters population doubling time and saturation density. The data was checked for outliers by identifying any samples that had a distance ≥ 2.5 standard deviations from the cluster mean; no outliers were identified. FAST had significantly faster population doubling times (**Figure 1A**) and greater saturation densities (**Figure 1B**) compared to SLOW. It is important to highlight that K-means clustering separated the *h*MPC cultures independent of age and sex of the donor. The number of males and females as well as the average age, weight, and BMI of the participants in each cluster are presented in Table 1. Although the age range was similar between clusters, the average age of participants in the FAST cluster was significantly younger than participants in the SLOW cluster.

Table 1. Participant Demographics

Cluster	Sex (M/F)	Age (years)*	Age Range (years)	Weight (kg)	BMI (kg/m^2)
FAST	6/7	31 ± 13	21-68	70.9 ± 14.6	23.7 ± 3.3
SLOW	3/13	53 ± 22	25-80	67.0 ± 12.2	25.1 ± 5.1

All values are Mean ± SD.
* $p<0.05$
Total n = 29

3.3.6 RNA isolation and integrity

RNA was harvested from sorted cells using TRK lysis buffer (Omega) following manufacturer's instructions at the third day of rapid expansion. The first day of rapid expansion was defined as the first increase in percent confluency that was ≥ 5%. RNA was harvested after 120 h of proliferation for samples that never had an increase in percent confluency ≥ 5% in a 24 h interval. Total RNA was purified using an EZNA total RNA kit (Omega) following manufacturer's instructions. Total RNA quantity was determined spectrophotometrically and an RNA quality number (RQN) was generated via sample quality control (QC). A subgroup of samples from each cluster was chosen for RNA sequencing (RNAseq). Samples were chosen based on RNA quality, age, and sex. To eliminate biased age and sex effects, we aimed to balance age and sex in each cluster. All RNA samples submitted for RNA sequencing had an RQN > 7. The number of males and females as well as the average age, weight, and BMI of participants that were sequenced in each cluster are presented in Table 2.

Table 2. Participant Demographics from RNAseq Samples

Cluster	Sex (M/F)	Age (years)*	Age Range (years)	Weight (kg)	BMI (kg/m^2)
FAST	4/3	35 ± 17	21-68	73.8 ± 16.0	24.0 ± 3.2
SLOW	3/5	63 ± 21	26-80	66.8 ± 13.3	25.2 ± 5.0

All values are Mean ± SD.
* $p<0.05$
Total n = 15

3.3.7 RNAseq

TruSeq-barcoded RNAseq libraries were generated with the NEBNext Ultra II RNA Library Prep Kit (New England Biolabs). Each library was quantified with a Qubit 2.0 (dsDNA HS kit; Thermo Fisher) and the size distribution was determined with a Fragment Analyzer (Advanced Analytical) prior to pooling. Libraries were sequenced on a NextSeq500 instrument (Illumina). At least 20M single-end 75 bp reads were generated per library. Reads were trimmed for low quality and adaptor sequences with cutadapt v1.8 (parameters: parameters: -m 50 -q 20 -a AGATCGGAAGAGCACACGTCTGAACTCCAG --match-read-wildcards) (109). Reads were mapped to the reference genome/ transcriptome using tophat v2.1 (parameters: --library-type=fr-firststrand --no-novel-juncs -G <ref_genes.gtf>) (85). Cufflinks v2.2 (cuffnorm/cuffdiff) was used to generate the fragments per kilobase of transcript per million mapped reads (FPKM) values and statistical analysis of differentially expressed genes (DEgenes) (176). DEgenes met a minimum q value cut-off of < 0.05.

3.3.8 PCR validation

Total RNA quantity and quality was determined spectrophotometrically, followed by cDNA synthesis using the High Capacity cDNA Reverse Transcription Kit (Applied Biosystems). We selected and validated five DEgenes that were identified as having differential expression between FAST and SLOW in the RNAseq dataset. Genes chosen to validate were selected as follows: four genes were previously shown to be involved in myoblast proliferation (*E2F2, HGF, PDGFRA, FOXM1*), and one gene was randomly selected via a random number generator (*EGR1*). We used real-time, quantitative PCR, performed using the LightCycler 480 system (Roche) with the TaqMan Fast Advanced Master Mix and TaqMan® Gene Expression

Assays (Applied Biosystems), to identify differences in gene expression of select genes. Primer/probes used were as follows: *E2F2* (Hs00918090_m1), *HGF* (Hs00300159_m1), *PDGFRA* (Hs00998018_m1), *EGR1* (Hs00152928_m1), and *FOXM1* (Hs01073586_m1). *TBP* (Hs00427621_m1) was used as the housekeeper.

3.3.9 Principal component analysis

Principal component analysis (PCA) of the log2FPKM values was used to reduce the dimensionality and unbiasedly cluster the RNAseq data. Briefly, FPKM values were converted to log2FPKM values. The gene list was trimmed to include only genes for which at least two samples had FPKM ≥ 2.0 and the log2FPKM was at least a 2.0-fold change across samples. JMP was used to complete the PCA on the covariances of the trimmed gene list. Eigenvectors, eigenvalues, and principal components were determined.

3.3.10 Pathway analysis

Ingenuity Pathway Analysis (IPA) was used to identify canonical pathways, functional classifications, upstream regulators, and networks discovery. The software was set to analyze transcripts with a fold change ≥ 2.0 and FDR corrected q value ≤ 0.001.

3.3.11 Statistical methods

Statistical tests used to analyze differences in growth parameters were performed using R and Prism 4 (GraphPad). For comparisons between two groups, t-tests were performed in Prism 4.0. For a comparison over time (i.e., confluency, live nuclei count, and percent dead), a two-way ANOVA (cluster-by-time) for unbalanced designs was performed in R. When interactions

were significant, a pairwise comparison with Bonferonni correction was performed for each time-point in R. Significance was determined at $p < 0.05$.

3.4 Results

3.4.1 Expansion phenotype of the FAST and SLOW clusters

After we separated *h*MPC cultures into FAST and SLOW clusters using K-means cluster analysis (based on population doubling time and saturation density), we quantified differences between FAST and SLOW for all expansion measurements. Compared to samples in the SLOW cluster, samples in the FAST cluster had more live cells at each 24 h measurement between 120-408 h of growth (**Figure 2A**) and more live cells in total throughout expansion (**Figure 2B**). Similarly, samples in the FAST cluster had a greater percent confluency every 24 h from 96-408 h of growth (**Figure 2C**) and a greater percent confluency in total throughout growth (**Figure 2D**) compared to samples in the SLOW cluster. Samples in the FAST cluster also had a lesser percentage of dead cells from 24-144 h and 168-192 h of growth (**Figure 2E**) and a lesser percentage of dead cells in total throughout expansion compared to the SLOW (**Figure 2F**).

3.4.2 RNAseq and pathway enrichment

PCA was used to determine whether the transcript profile, determined using RNAseq, could unbiasedly cluster the *h*MPC cultures into the same growth parameter clusters (i.e. FAST vs. SLOW). PC1 accounted for 85% of the variability while PC2 accounted for 4% of the variability in the data (**Figure 3**). While PC1 and PC2 clustered the samples into the same FAST and SLOW clusters, PC2 was largely responsible for this separation. Aligning with the separation of cultures into FAST and SLOW, the top 30 DEgenes driving PC2 (Table 3) were

classified by IPA into Molecular and Cellular Functions (Table 4). PC1 accounted for the largest amount of variability in the data, but it did not distinguish the cultures clearly into FAST and SLOW, suggesting there is a large amount of variability not accounted for by growth parameters. Genes driving PC1 are shown in Table 5.

Table 3. **Top 30 Genes Driving PC2**

Gene Name	**PC Score (Absolute Value)**	**Gene Name**	**PC Score (Absolute Value)**
TNNT2	7.4	*FRMPD1*	4.9
TMEM8C	7.0	*COMP*	4.8
SOX8	6.1	*MYL4*	4.8
MT3	6.0	*KPRP*	4.8
LCE3A	5.7	*FAM101A*	4.7
RARRES2	5.4	*PSG4*	4.7
HLA-DRB1	5.3	*CD24*	4.7
TGM3	5.3	*RTN4RL1*	4.6
CRIP1	5.2	*SPINK13*	4.6
UTS2R	5.1	*PENK*	4.6
STMN2	5.1	*LCE2A*	4.5
PTGDS	5.0	*ATP1A2*	4.5
LOC389033	5.0	*L1CAM*	4.5
SFRP4	4.9	*CA2*	4.4
CPXM1	4.9	*WBSCR27*	4.4

Table 4. Functions of *DEgenes Driving PC2

****Molecular and Cellular Function**	**# DEgenes in Pathway**
Cell Death and Survival	89
Cell Cycle	37
Cellular Assembly and Organization	29
DNA Replication, Recombination, and Repair	36

*DEgenes, differentially expressed genes

**Functional annotation determined using Ingenuity Pathways Analysis

Table 5. Top 30 Genes Driving PC1

Gene Name	PC Score (Absolute Value)	Gene Name	PC Score (Absolute Value)
H19	35.0	*CTSD*	23.3
TGFBI	33.3	*VKORC1*	23.3
FN1	30.5	*ANPEP*	23.3
SERPINE2	30.0	*PTX3*	22.5
ASS1	27.6	*PTTG1IP*	22.3
PLAU	27.3	*TPM1*	22.3
TAGLN	27.1	*MT1E*	22.3
TIMP1	27.1	*IGFBP7*	22.2
HMGA1	27.0	*SNHG5*	21.8
IGFBP3	26.4	*LOX*	21.5
HTRA1	25.8	*DKK1*	21.4
MMP2	25.6	*ALDH1A1*	21.4
PLAT	25.0	*IFITM3*	21.3
SPARC	24.2	*ITGBL1*	21.3
SERPINE1	23.7	*ERRFI1*	21.2

To determine biological underpinnings for observed differences in *h*MPC expansion capacity, DEgenes between FAST and SLOW were determined. We identified 2204 DEgenes with a (FDR) q value < 0.05. All DEgenes were expressed in both FAST and SLOW clusters and met the minimum FPKM cutoff of 2.0. To validate the RNAseq results, five genes were selected for RT-PCR analysis (see methods). Similar to the RNAseq data, all five genes had significantly greater expression in the FAST compared to the SLOW, confirming the RNAseq results (**Figure 4**).

IPA was used to identify pathway enrichment for DEgenes. Of the 2204 DEgenes, 362 DEgenes (173 upregulated and 189 downregulated) met a cutoff of fold change ≥ 2.0 and a stringent FDR of q value ≤ 0.001. The top 10 up- and down-regulated genes are reported in Table 6. A total of 50 functional classifications were identified at the $p < 0.05$ level. Sub-functions within each functional classification are associated with a z-score that indicates predicted activation (increased or decreased) of the sub-function based on the directional change

of the DEgenes. Out of the top 10 functional classifications, four were of particular interest to us (*Cell Cycle, Cellular Assembly and Organization, DNA Replication Recombination and Repair*, and *Cell Death and Survival*). The most highly activated and deactivated sub-functions within these functional classifications are reported in Table 7; redundant sub-functions were collapsed. As anticipated, FAST cultures had functions that suggest activation of *Cell Cycle Progression, Cell Proliferation,* and *Cell Survival,* but deactivation of *Apoptosis* and *Senescence of Cells*. In addition, we analyzed the top networks created by the DEgenes. The top four networks of DEgenes had functions related to *DNA Replication, Recombination and Repair; Cellular Function and Maintenance; Cellular Assembly and Organization* (Network 1, Score = 50, **Figure 5**), *Cell Cycle, Cellular Assembly and Organization, Reproductive System Development and Function* (Network 2, Score = 50, **Figure 6**), *Cell Cycle; DNA Replication, Recombination, and Repair;* and *Cellular Assembly and Organization* (Network 3, Score = 42, **Figure 7**), and *Cell Cycle, Connective Tissue Disorders, and Developmental Disorder* (Network 4, Score = 40, **Figure 8**). Of particular interest, several known and novel regulators of cell proliferation were nodes in the top 4 networks. These nodes include *ERK1/2*, *E2F, FOXM1, CCNA1*, and *Rb*.

Table 6. Top 10 Up- and Down-Regulated DEgenes

DEgene	Expression Log Ratio	Q Value (FDR)
Upregulated in FAST		
TRPA1	3.5	7.21E-04
CHI3L1	3.2	7.21E-04
PENK	2.9	7.21E-04
CA2	2.8	7.21E-04
CPXM1	2.7	7.21E-04
COLEC12	2.5	7.21E-04
PDGFRA	2.3	7.21E-04
FOXF1	2.3	7.21E-04
COL15A1	2.3	7.21E-04
CACNG7	2.2	7.21E-04
Downregulated in FAST		
COMP	-3.6	5.00E-05
TNNT2	-3.6	5.00E-05
SOST	-3.6	5.00E-05
LCE3A	-3.6	5.00E-05
PRRT4	-3.4	5.00E-05
RARRES2	-3.3	5.00E-05
MYOG	-3.3	2.00E-04
TGM3	-3.2	5.00E-05
SORCS1	-2.7	5.00E-05
STMN2	-2.7	5.00E-05

Table 7. Functional Classification of DEgenes

Functional Pathway	Sub-function	P value	*Activation z score
Cell Cycle	Interphase	2.0E-10	3.8
	Cell cycle progression	5.1E-15	2.9
	Senescence of cells	1.2E-05	-2.2
Cellular Development, Cellular Growth and Proliferation	Cell proliferation of tumor cell lines	3.3E-09	3.4
Cell Death and Survival	Cell survival	5.3E-09	3.0
	Cell viability	1.4E-08	2.6
	Apoptosis	2.8E-13	-2.8
DNA Replication, Recombination, and Repair	Chromosomal aberration	3.0E-08	-2.2
	Metabolism of DNA	2.7E-09	2.5
	DNA replication	6.6E-08	2.4

*Positive z score, predicted activation is *increased*; negative z score, predicted activation is *decreased*

A total of 36 canonical pathways were identified at $p < 0.05$. Like sub-functions, increased and decreased activity of canonical pathways is inferred based on the z-score. Highly activated canonical pathways included *Mitotic Roles of Polo-like Kinase* (z-score 2.3, p value 1.09E-08), *Estrogen-Mediated S-phase Entry* (z-score 1.9, p value 1.66E-07), and *Cyclins and Cell Cycle Regulation* (z-score 2.6, p value 3.71E-04). Intriguingly, deactivated canonical pathways included checkpoint regulation of the cell cycle: *CHK Proteins in Cell Cycle Checkpoint Control* (z-score -2.2, p value 4.28E-05), *Cell Cycle G2/M DNA Damage Checkpoint Regulation* (z-score -2.2, p value 1.29E-03) and *Cell Cycle G1/S Checkpoint Regulation* (-1.3, p value 4.81E-03).

Identifying upstream regulators provides additional insight into the modulators responsible for the observed DEgenes between FAST and SLOW. We identified several regulators using both the Upstream Analysis and Regulator Effects tools in IPA (Table 8). Several of the top upstream regulators, identified based on DEgenes, are related to regulation of the cell cycle; regulators that promote cell cycle (e.g. E2F2) had prediction scores that suggested

increased activity in FAST compared to SLOW, while regulators that inhibit the cell cycle (e.g. CDKN1A, Rb) had prediction scores that suggested decreased activity in FAST compared to SLOW.

Table 8. Predicted Upstream Regulators

Gene	Molecule Type	*Activation Z-Score	P Value
FOXM1	Transcription Regulator	4.7	1.5E-21
RABL6	Other	4.9	6.8E-33
Irgm1	Other	-3.3	8.7E-11
MED1	Transcription Regulator	3.1	1.0E-05
AREG	Growth Factor	4.6	1.2E-18
CDKN1A	Kinase	-3.7	1.7E-38
Rb	Group	-3.2	4.1E-15
E2F2	Transcription Regulator	2.4	1.2E-16

*Positive z score, predicted as *activated*; negative z score, predicted as *inhibited*

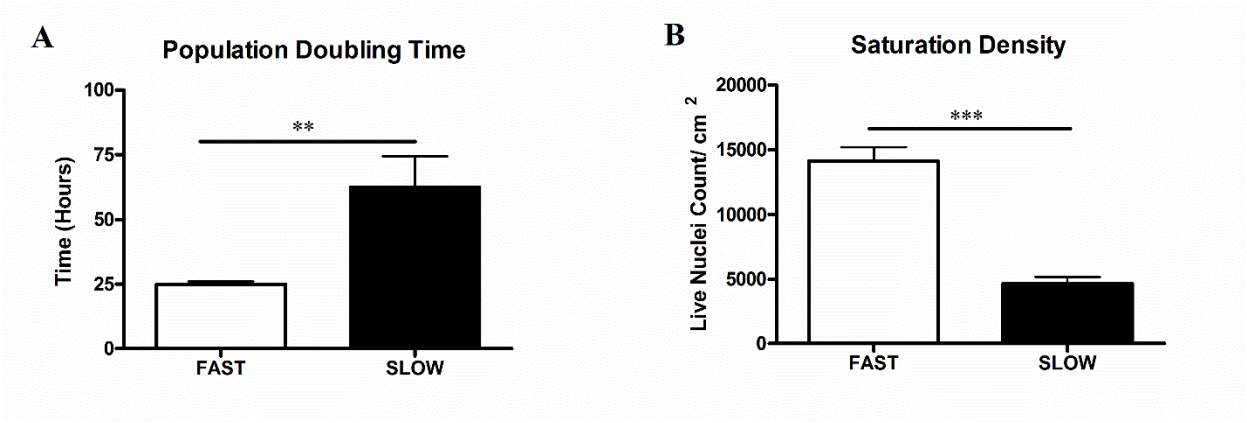

Figure 1. Determinants of FAST and SLOW Clusters. A) Population doubling time during exponential growth and B) saturation density (number of live nuclei/cm^2 at the proliferation plateau) were used to separate FAST and SLOW clusters using K-means clustering. T-tests were used to compare clusters for saturation density and population doubling time. All values are reported as mean ± s.d. **p<0.01, ***p<0.001. Total n=29 (n=13 in FAST, n=16 in SLOW).

Figure 2. Growth Characteristics of FAST and SLOW Clusters. A) Live nuclei count every 24 h over 408 h of growth, B) live nuclei net area under the curve (AUC), C) percent confluency every 24 h over 408 h of growth, D) confluency net AUC, E) percentage of dead cells every 24 h over 408 h of growth, and F) percent dead total AUC. Two-way ANOVA with Bonferroni correction was used to compare clusters at each time point for live nuclei count, percent confluency, and percentage of dead cells. T-tests were used to compare clusters for live nuclei net AUC, confluency net AUC, and percent dead total AUC. All values are reported as mean ± s.d. *$p<0.05$, **$p<0.01$, ***$p<0.001$. Total n=29 (n=13 in FAST, n=16 in SLOW).

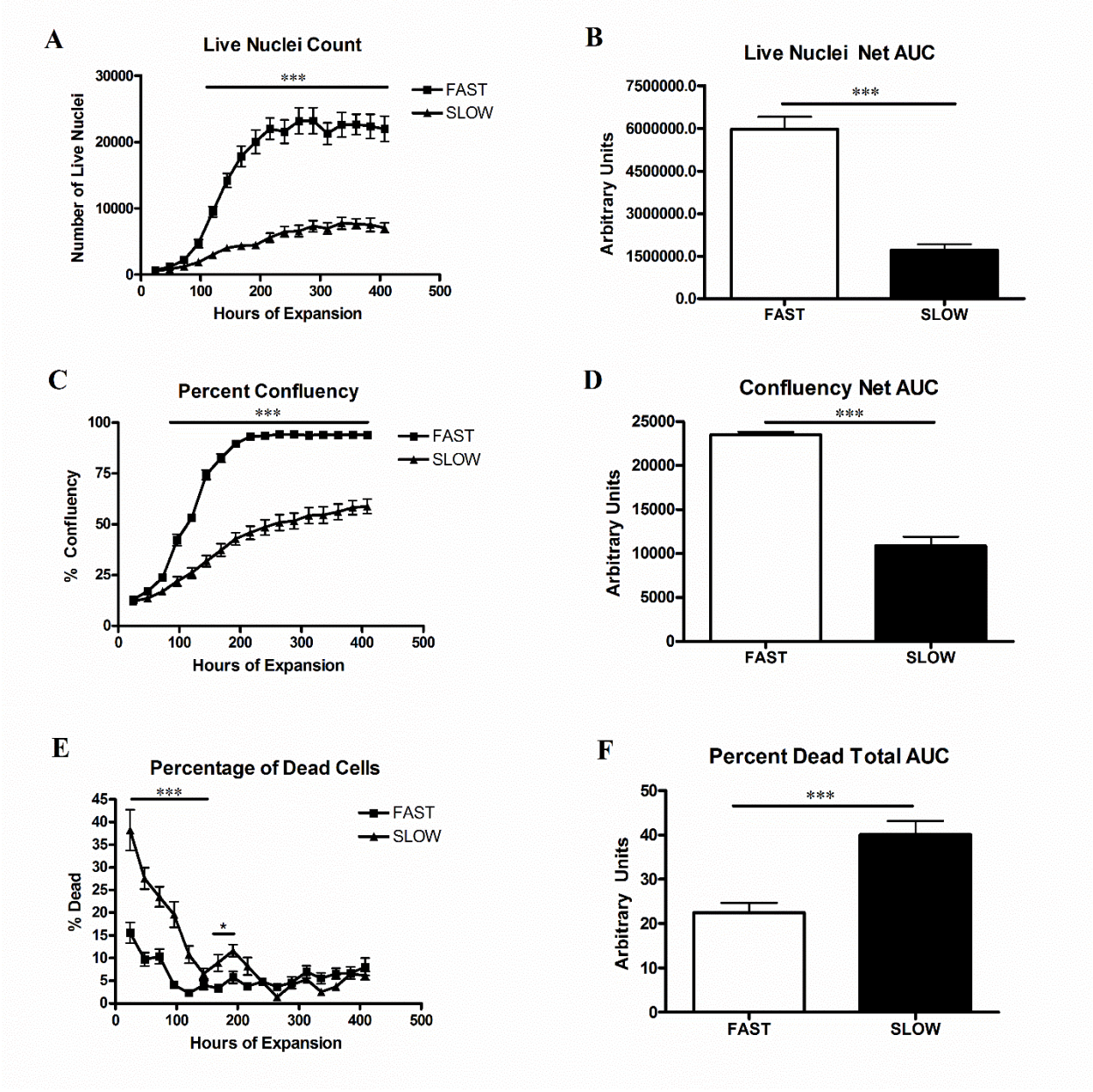
A
Live Nuclei Count
***
FAST
SLOW
Number of Live Nuclei
30000
20000
10000
0
0
100
200
300
400
500
Hours of Expansion
B
Live Nuclei Net AUC
***
Arbitrary Units
7500000.0
6000000.0
4500000.0
3000000.0
1500000.0
0.0
FAST
SLOW
C
Percent Confluency
***
FAST
SLOW
% Confluency
100
75
50
25
0
0
100
200
300
400
500
Hours of Expansion
D
Confluency Net AUC
***
Arbitrary Units
25000
20000
15000
10000
5000
0
FAST
SLOW
E
Percentage of Dead Cells
***
*
FAST
SLOW
% Dead
45
40
35
30
25
20
15
10
5
0
0
100
200
300
400
500
Hours of Expansion
F
Percent Dead Total AUC
***
Arbitrary Units
50
40
30
20
10
0
FAST
SLOW

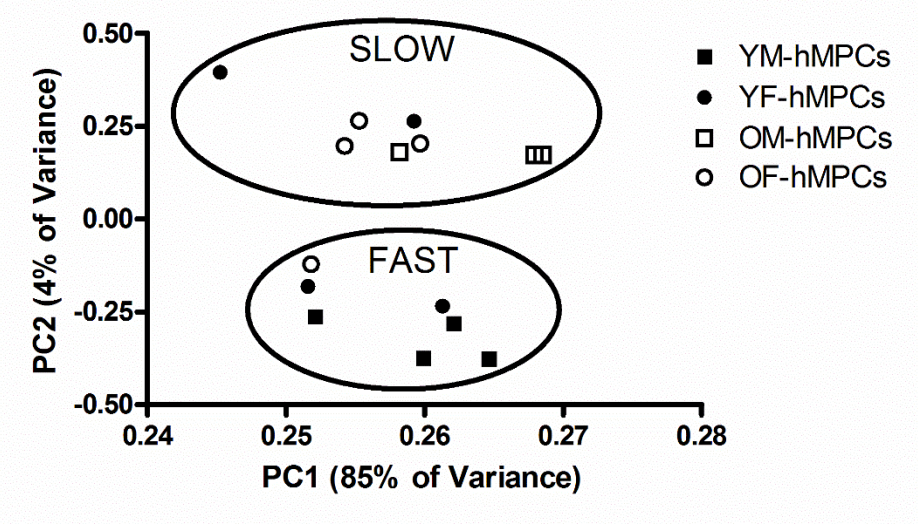

Figure 3. Principal Components Analysis. Principal Component Analysis (PCA) show larger separation of samples between identified growth phenotype clusters than within identified growth phenotype clusters. PCA revealed that 85% of gene expression data could be explained by PC1. PC2 accounted for 4% of the variability in the data. Each dot represents an individual transcriptome from a participant. Closed square = Young Male-*h*MPCs, closed circle = Young Female-*h*MPCs, open square = Old Male-*h*MPCs, open circle = Old Female-*h*MPCs. Total n = 15 (n=7 in FAST, n=8 in SLOW).

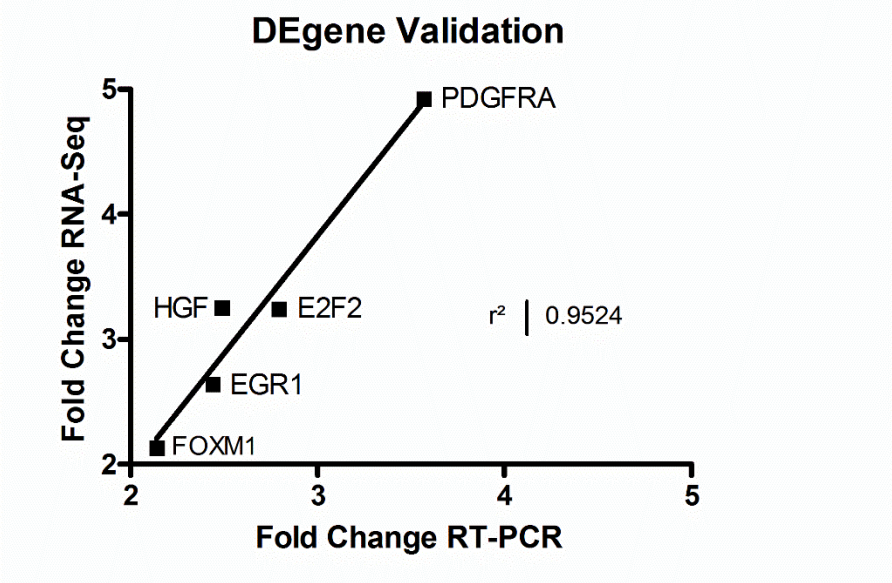

Figure 4. Validation of DEgenes. Plot comparing the fold-change between RT-PCR and RNAseq for 5 genes that were upregulated in the FAST Cluster. Total n = 15 (n=7 in FAST, n=8 in SLOW).

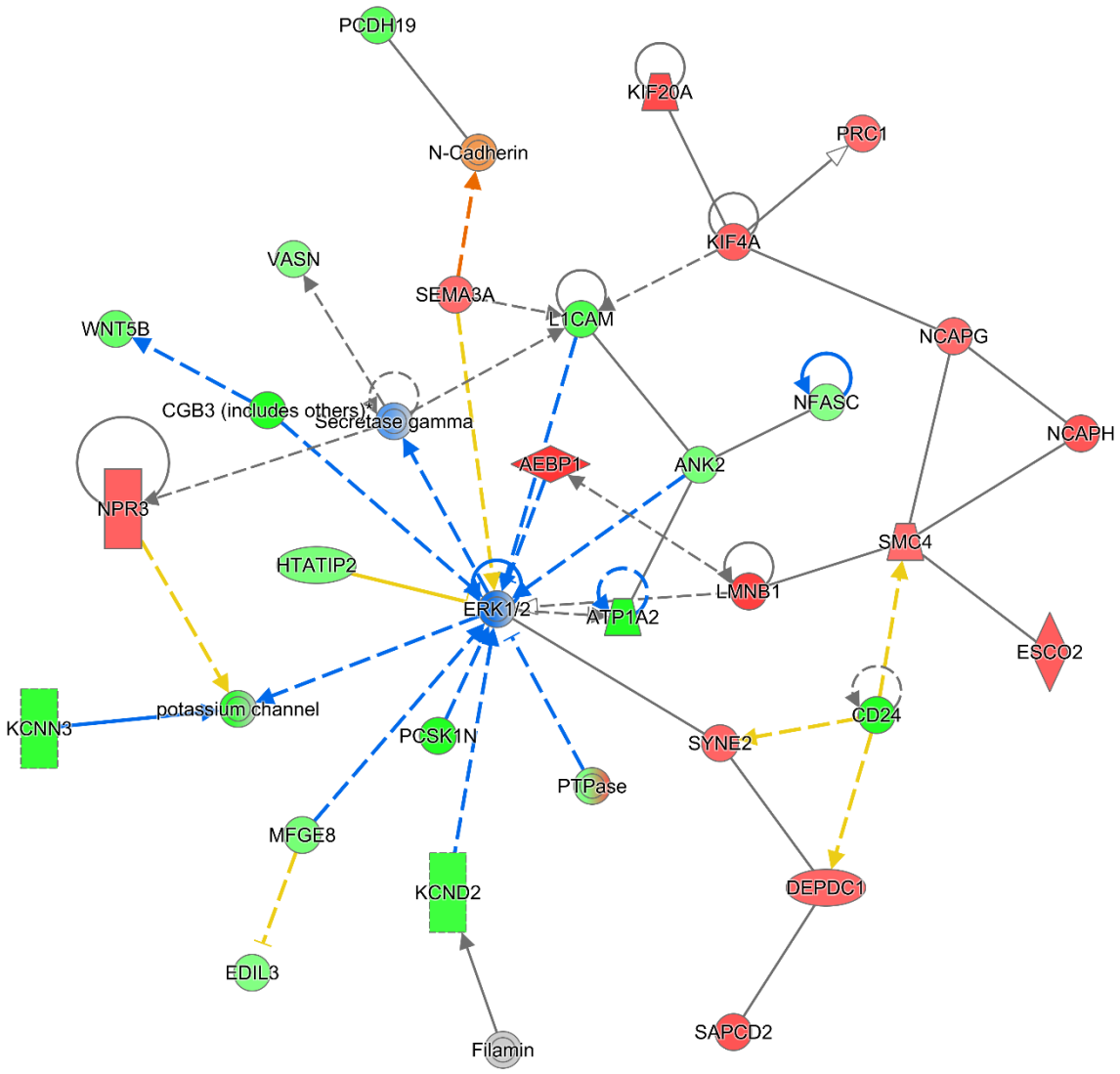

Figure 5. Network 1. The top network of DEgenes had functions related to *DNA Replication, Recombination and Repair; Cellular Function and Maintenance; Cellular Assembly and Organization.* Of particular interest, *ERK1/2* (a known regulator of cell proliferation) was identified as a primary node in this network.

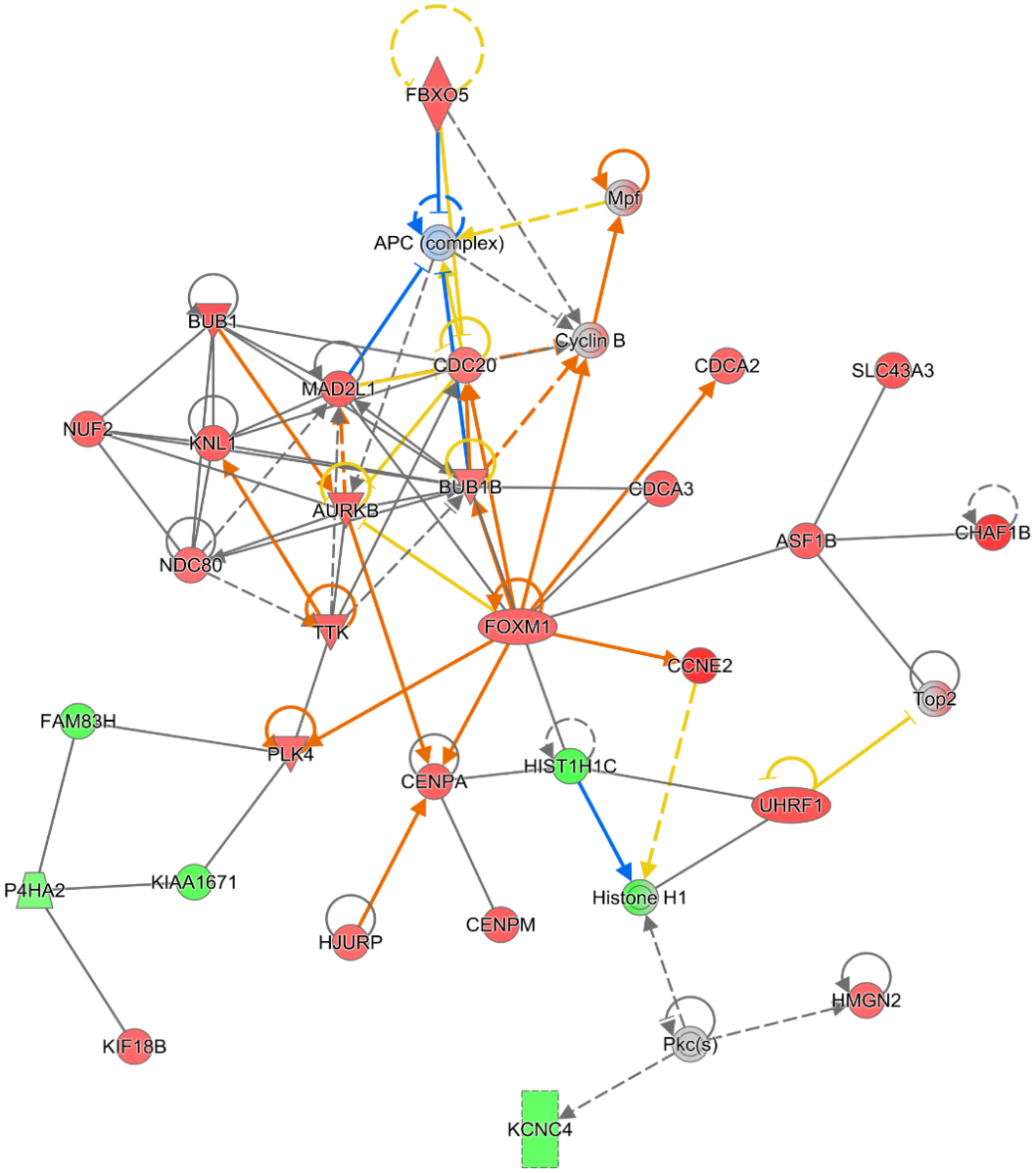

Figure 6. Network 2. The second network of DEgenes had functions related to *Cell Cycle, Cellular Assembly and Organization, Reproductive System Development and Function.* Of particular interest, *FOXM1* (a novel regulator of MPC proliferation) was identified as a primary node in this network.

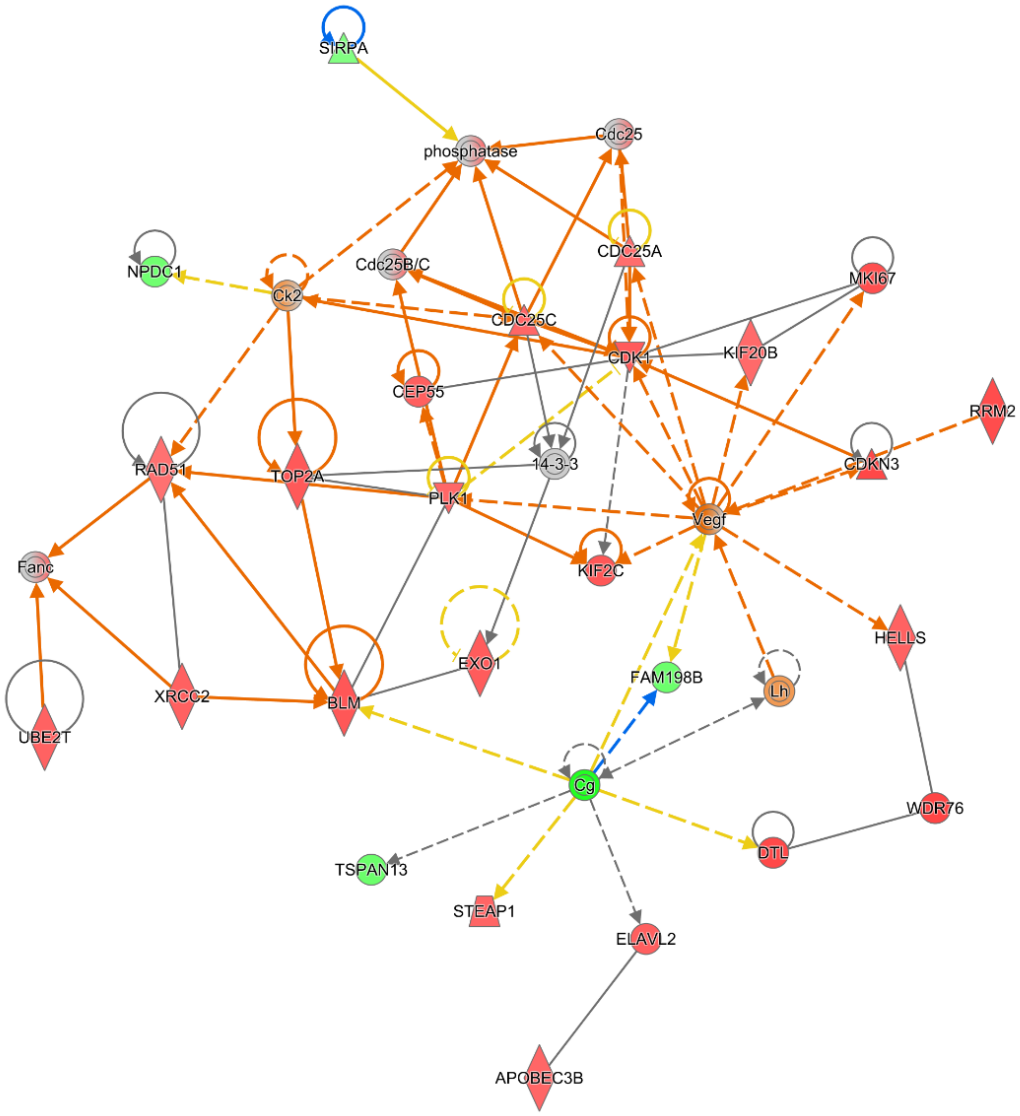

Figure 7. Network 3. The third network of DEgenes had functions related to *Cell Cycle; DNA Replication, Recombination, and Repair;* and *Cellular Assembly and Organization.*

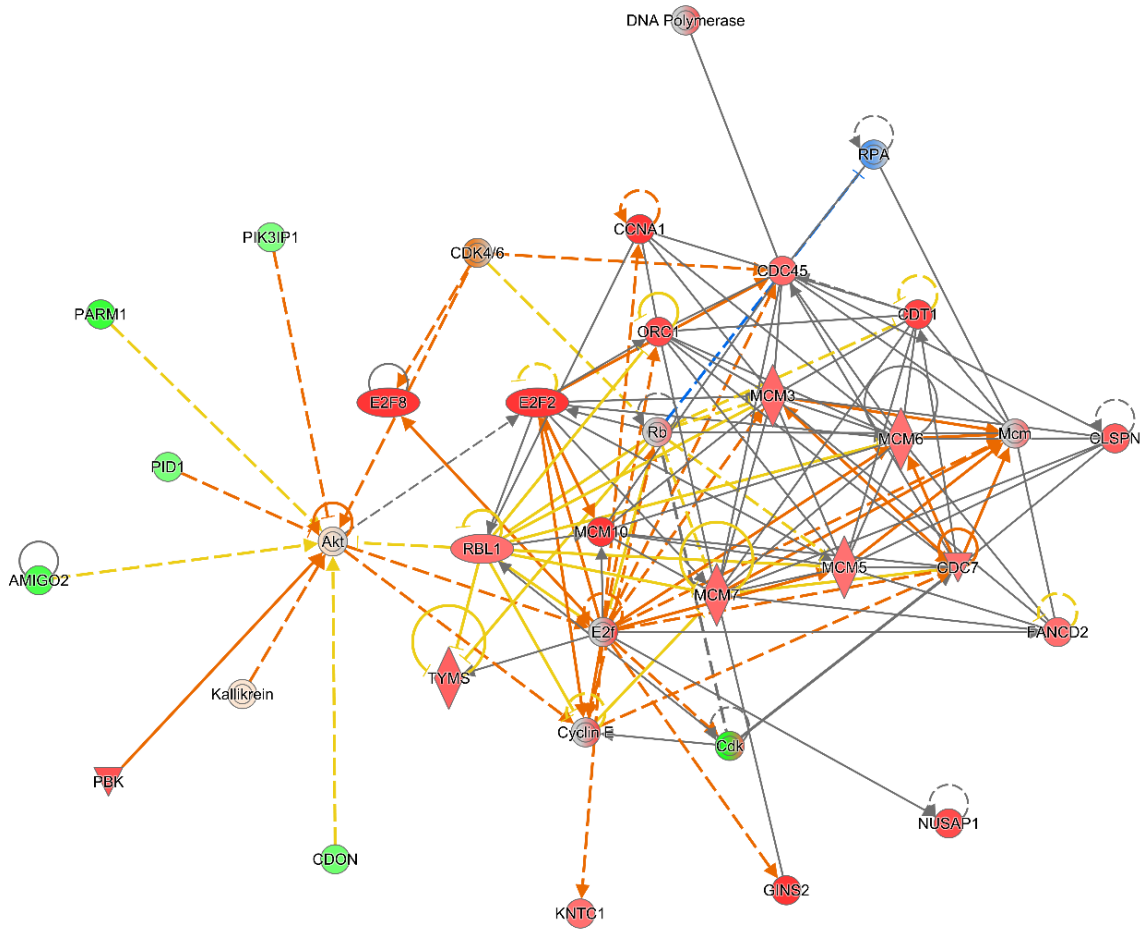

Figure 8. Network 4. The forth network of DEgenes had functions related to *Cell Cycle, Connective Tissue Disorders, and Developmental Disorder*. Of particular interest, *CCNA1*, *Rb*, and *E2F* were identified as primary nodes in this network.

3.5 Discussion

Primary hMPCs are an important research model used to understand skeletal muscle biology and the regenerative process. Additionally, hMPCs have the potential to be used for therapy. However, there are recognized challenges in using primary hMPCs for both research and therapy, including the limited understanding of human cells (14). There is also a large degree of variation in the expansion capacity among donor cultures, which limits the potential for use of hMPCs. Using K-means cluster analysis and measurements of culture population doubling time and saturation density, we are the first to unbiasedly cluster cultures with similar growth parameters, which allowed us to identify drivers of expansion capacity that weren't related to categorical age or sex. It is important to note that the participants whose cultures clustered into the FAST cluster were significantly younger on average than participants whose cultures clustered into the SLOW cluster. However, the age range for both clusters included both young and old participants. Additionally, a greater percentage of females clustered into the SLOW cluster compared to the FAST cluster. These observations agree with previous research which suggests reduced myoblast proliferation with advancing age (113, 159) and in female (vs male) cultures (108). While sex differences in proliferation may be attributable to differences in sex hormones, increasing evidence suggests these differences may be innate (7, 41). Furthermore, using this methodology, we determined that the transcript profile can distinguish donor cultures based on their expansion capacity (FAST and SLOW). Our primary findings demonstrate that cultures with enhanced expansion capacity have DEgenes enriched in functional classifications, pathways and networks that suggest promotion of the cell cycle, reduced apoptosis and cellular senescence, and enhanced DNA replication. Novel and known regulators of the cell cycle emerged as having important roles in these functional pathways.

3.5.1 Promotion of the cell cycle

As expected, when DEgenes were analyzed for functional classifications, pathways, and networks, we identified that FAST had an enrichment of DEgenes that suggested activation/promotion of the cell cycle and proliferation. In total, 82.0% of genes related to *Cell Cycle Control of Chromosomal Replication* (the top canonical pathway) and 66.7% of genes related to *Mitotic Roles of Polo-Like Kinase* (the second canonical pathway) were upregulated in the FAST cluster. TRPA1 and CHI3L1 were two of the most highly upregulated genes in FAST cells. While the specific function of TRPA1 has not yet been determined, recent evidence suggests it promotes myoblast migration and plays a functional role in skeletal muscle repair (126). Similarly, CHI3L1 has been shown to activate myoblast proliferation (70). The prediction score of upstream regulators further supports promotion of the cell cycle in FAST and inhibition of the cell cycle in SLOW. We identified several novel upstream regulators, including RABL6, IRGM1, and AREG, which have been shown to promote cell proliferation in cancer models, but have not been associated with functional roles in hMPCs (47, 67, 158, 168). Intriguingly, FOXM1, another predicted upstream regulator, was recently shown to be essential for the proliferation and survival of satellite cells (30). These upstream regulators likely interact to enhance hMPC proliferation in the FAST cluster.

In agreement with previous literature, we also identified several known regulators of hMPC proliferation in our analysis. The fourth network identified by IPA had nodes related to two of the top upstream regulators, CDKN1A (p21) and Rb. CDKN1A induces cell cycle arrest by inhibiting cyclin dependent kinase activity, a key regulator of cell cycle initiation and progression (119). Machida and Booth demonstrated that SCs from aged animals, which have reduced proliferation, have increased nuclear $p21^{WAF1/CIP1}$ and $p27^{Kip1}$ (105). Rb also induces cell

cycle arrest by inhibiting transcription factors of the E2F family; E2F transcription factors push cells into S phase and promote progression through the cell cycle (119). E2F was predicted to be an "active" upstream regulator in the FAST and CDKN1A and Rb were predicted to be "inhibited". Thus, cells in the FAST cluster have predicted activation of cell cycle activators and predicted inhibition of cell cycle inhibitors.

An alternative hypothesis to reduced cell proliferation in SLOW (vs. FAST) is that SLOW cultures prematurely differentiate, despite the presence of growth factors in the growth medium. In support of this hypothesis, our data demonstrate that *MYOG*, a marker of muscle differentiation, is upregulated 9.8 fold in the SLOW hMPCs compared to FAST. Collectively our data suggest that reduced expansion capacity in SLOW cultures may be due to a combination of processes including reduced cell cycle progression, increased cellular apoptosis, increased cellular senescence, and perhaps premature differentiation.

3.5.2 Reduced apoptosis and cellular senescence

DEgenes were enriched in apoptosis, cellular senescence, and cell survival functional classifications; differences in gene expression support promotion of apoptosis and cellular senescence and suppression of cell survival in cultures with reduced expansion capacity (i.e. in the SLOW cultures). There are several possible reasons for increased cellular senescence or cell death in SLOW cells. As alluded to below, SLOW cells may have ineffective DNA repair mechanisms, leading to increased cellular apoptosis (149). Alternatively, SLOW cells may experience SC exhaustion, a feature that occurs when cells senesce and are no longer able to divide (111). SC exhaustion has been reported to occur secondary to aging (111). However, we demonstrate here that SC exhaustion may be a feature of not only older cells, but young cells as

well. Again, FOXM1 and AREG were identified as key upstream regulators for cell survival, reinforcing the importance of these regulators in hMPC expansion.

3.5.3 Enhanced DNA replication

One of the top functional classifications, based on network analysis of DEgenes, was *DNA replication, recombination, and repair*. The DEgenes suggest upregulation of checkpoint control, alignment of chromosomes, DNA replication, DNA synthesis, and DNA repair in FAST cells. These results further support that FAST cells are better able to enter into S phase and promote progression of the cell cycle. Additionally, 91.2% of genes associated with the role of BRCA1 in the DNA damage response were upregulated in the FAST cluster. BRCA1 is a well characterized tumor suppressor gene that functions in DNA damage repair, genomic stability, and apoptosis (189). Furthermore, a key central hub to the top network was ERK1/2. ERK1/2 has been shown to play critical roles in promoting cell proliferation, partly through promotion of the DNA damage response (184). Activation of the BRCA1 and ERK1/2 pathways in FAST cells may promote DNA repair and prevent apoptosis, thus enhancing hMPC expansion capacity.

3.5.4 DEgenes that are not specific to the expansion of hMPCs

PC1, which accounted for 85% of variability in the gene expression data, did not distinguish the growth parameter clusters. Intriguingly, PC1 did not distinguish cultures by age or sex either. The top genes of PC1 were related to signaling pathways that have been previously identified as important for SC expansion including TGFβ and Wnt signaling (2, 27). Thus, although PC1 identified several previously known regulators of SC expansion, the underlying cause of these differences in gene expression between samples remains unknown.

3.5.5 Clinical implications

In humans, the degree of skeletal muscle hypertrophy has been associated with SC expansion and incorporation of SCs, as new nuclei, into myofibers (myonuclear addition) (134). Adults who had an extreme response to resistance exercise training (RT) achieved significantly greater myofiber hypertrophy compared to individuals with modest or no/minimal (non) response. These extreme responders had a significantly greater number of SCs at baseline, a significant increase in the number of SCs following RT, and the greatest myonuclear addition compared to other responder groups. Intriguingly, the whole tissue SkM transcript profile that distinguished the extreme and non-responders prior to RT contained several of the same DEgenes that we identified in FAST during expansion (169). Because not all of the DEgenes between the two studies were regulated in the same direction, future studies are needed to understand the relationship between expansion capacity of the SC and the hypertrophic and myonuclear addition capacity.

3.5.6 Limitations

A potential limitation of our research is use of passage six hMPCs. It is recognized that proliferative capacity declines with passaging (106). However, it is intriguing that some hMPCs maintain their expansion capacity. We have tracked the hMPCs from passage 2 to passage 7; we observed no difference in expansion parameters between passage 2 and passage 7 (data not shown). We have not tracked expansion parameters beyond passage 7. We and others (66) have demonstrated that FACS conducted on tissue digest provides only 10-15 satellite cells per milligram of skeletal muscle tissue. Thus, distinguishing populations of hMPCs that maintain expansion capacity is necessary for addressing scientific inquiries and utilization in therapies.

3.7 Conclusion

The regenerative capacity of hMPCs differs by many conditions including chronological age (38, 64) and perhaps the sex (165) of the donor. However, there is a large degree of variability in expansion capacity that comes from an unknown origin. Using a novel model of hMPC expansion and unsupervised approaches, we identified that a transcript profile underlies the culture to culture variability in hMPC expansion. We identified functional pathways and key regulators that distinguish cultures with greater expansion capacity. The transcript profile suggests maintenance of the cell cycle in FAST but an induction of cell cycle inhibitors in SLOW cultures.

3.8 Acknowledgments

We thank Jennifer Grenier from the Cornell University, RNA Sequencing Core for her help with RNA sequencing and analysis. We thank the Cornell University, Biotechnology Resource Center Imaging Facility for their help with fluorescence activated cell sorting. We thank Heather Roman for her assistance with maintaining the *h*MPC cultures. We also thank Melinda Lem for her help with participant recruitment. Finally, we thank the participants for their time and participation in the study. This study was funded by PCCW and Cornell Division of Nutritional Sciences.

CHAPTER 4: RNA TRANSCRIPT PROFILE DISTINGUISHES HUMAN MUSCLE PROGENITOR CELL INFLAMMATORY SUSCEPTIBILITY

Emily S Riddle, Erica L Bender, Anna E Thalacker-Mercer

Author Affiliations: Division of Nutritional Sciences, Cornell University, Ithaca, NY, 14853, USA (ER, EB, ATM)

Abbreviated Title for Running Head: Myoblast Inflammatory Susceptibility Transcriptome

Corresponding Author: Dr. Anna Thalacker-Mercer, aet74@cornell.edu, 109 Savage Hall, Cornell University, Ithaca, NY 14850

Emily S Riddle: Experimental design, data collection, data analysis, and interpretation
Erica L Bender: Data collection
Anna E Thalacker-Mercer: Experimental design, data collection, data analysis, and interpretation

Keywords: inflammation, variation, gene expression, muscle progenitor cells

4.1 Abstract

Acute inflammation following muscle injury is an integral component of the regenerative response. However, chronic muscle inflammation impairs the regenerative capacity of skeletal muscle (SkM). Previous research has identified muscle inflammatory susceptibility (MuIS), or the ability to manage and respond to inflammation, as a predictor of failed muscle regeneration and regrowth following surgery. We sought to determine the transcript profile that distinguishes human muscle progenitor cell (*h*MPC) cultures with high and low inflammatory susceptibility (MuIS+ and MuIS-, respectively). Sorted (CD56+/ CD29+) *h*MPC cultures from young adults were clustered using unbiased K-means and hierarchical clustering into MuIS+ and MuIS- clusters independent of sex. MuIS+ had greater expression of the inflammatory cytokines *TNFα, IL1β*, and *IL6* in the absence and presence of exogenous TNFα. RNAseq was conducted on RNA extracted after five days in differentiation media. Principal component analysis distinguished MuIS+ and MuIS- based on the transcript profile. There were 2269 DEgenes between MuIS+ and MuIS-, with fold change ≥ 2.0 and a q value (corrected for multiple hypothesis testing) ≤ 0.05, and 573 DEgenes that met a more stringent cutoff of $q \leq 0.001$ and $FC \geq 2.0$. DEgene enrichment suggested that MuIS+ cells had promotion of inflammatory pathways and inhibition of muscle differentiation pathways. MuIS+ cells also had significantly reduced expression of genes involved in the calcium signaling canonical pathway. Novel (*KISS1*) and known (*SMARCA4, MYOD1, IL1β*) genes emerged as regulators for identified functional pathways. Collectively the data suggest that *h*MPC inflammatory susceptibility is an intrinsic cell characteristic and occurs independent of the age or sex of the donor.

4.2 Introduction

Skeletal muscle (SkM) regeneration following muscle damage is imperative to maintain SkM structure and function throughout the lifespan (173). Regeneration requires a complex series of events involving acute inflammation, activation of SkM specific stem cells [satellite cells (SCs)], followed by proliferation and differentiation of committed myoblasts [muscle progenitor cells (MPCs)], and formation/repair of functional multinucleated muscle cells (29). Acute inflammation is essential for the regenerative response (192). Upon injury, macrophages secrete pro-inflammatory cytokines including tumor necrosis factor alpha (TNFα) and interleukin 1β (IL1β) (32). SkM cells can also synthesize TNFα, and TNFα acts in an autocrine/paracrine manner (96).

TNFα has positive effects on the early stages of myogenesis, promoting the proliferation and aggregation of myoblasts (166). To the contrary, chronic inflammation is associated with pathological remodeling of the SkM and muscle atrophy (37, 83). TNFα destabilizes MyoD protein, inhibiting differentiation, in an NFκB dependent manner (90). In animals, intraperitoneal exposure to TNFα (101) and local infusion of interleukin-6 (IL-6) (75) increase protein catabolism and decrease SkM mass; chronic TNFα exposure via intraperitoneal injections depletes body proteins in rats compared to pair fed control animals (55). Merritt et al. recently identified a state of heightened muscle inflammatory susceptibility (MuIS+) in older adults that was characterized by hyperactivity of TNFα, TWEAK, and/or IL-6 signaling in the SkM and in isolated SCs (112). In a follow-up study, Bamman et al. dichotomized patients into MuIS+ and MuIS- groups based on *TWEAK-R* mRNA levels and demonstrated that inflammation susceptibility discriminates muscle anabolic potential following surgery and may predict long-term muscle regrowth potential (10).

Although MuIS is an identified phenotype, the molecular mechanisms driving heightened MuIS remain unknown. Thus, the purpose of this study was to (i) determine the transcript profile that differentiates high inflammation susceptibility (MuIS+) from low inflammation susceptibility (MuIS-) in *h*MPCs and (ii) identify biological underpinnings of heightened muscle inflammatory susceptibility.

4.3 Methods

4.3.1 Ethical approval

All studies were approved by the Cornell University, Institutional Review Board. Written informed consent was obtained from all participants.

4.3.2 Human skeletal muscle procurement

*h*MPCs from healthy, ambulant young males (n=6) and females (n=5) were used to address the objectives of this research. All individuals completed a comprehensive health history and physical activity questionnaire and were independently ambulatory and cognitively intact (as determined by the examining nurse practitioner). Individuals were excluded for contagious infections and any chronic end-stage disease expected to limit life-expectancy to less than one year, induce anorexia, or restrict physical activity. Individuals with seated resting systolic blood pressure ≥140 mmHg or diastolic blood pressure ≥90 mmHg and individuals receiving anabolic (e.g., GH, IGF-I) therapy were also excluded.

4.3.3 Purified, primary human muscle progenitor cells

Primary human SCs were obtained from the vastus lateralis muscle using the

percutaneous biopsy technique. The biopsy tissue was cleaned of any extraneous fascia and adipose tissues. Approximately 75-100 mg of the total muscle biopsy was stored in Gibco® Hibernate®A (Thermo Fisher Scientific) at 4°C until tissue disassociation was performed. After mincing and washing via gravity with Ca-Mg free D-PBS, the tissue was disassociated in digest medium [2mg/mL Collagenase D (Roche) in low-glucose DMEM]. After 30 minutes in digest medium, fresh digest medium and Dispase (Sigma) were added. The disassociating pellet was titurated until a uniform slurry was achieved. Growth medium [(GM) Hams F12 + 20% FBS + 5ng/mL bFGF (Promega) + 1% Pen/Strep (Gibco)] was added to the slurry and passed through a 70 μm cell strainer into a sterile tube. The cell suspension was centrifuged. The pellet was resuspended in Recovery® freezing medium (Gibco) and cryopreserved at -80°C. Thawed cells were seeded on a type-I collagen coated culture dish (initial cell confluency ~15%). After 24 h, the GM was replaced with fresh GM and further replenished every 48 h. Once cells reached ~70% confluency, they were removed from the plate using 0.05% trypsin and passaged. Cells were expanded to passage four, then cryopreserved in 10% DMSO + GM.

4.3.4 Fluorescence activated cell sorting

Approximately 1-1.5 million cells were labeled with fluorescently-conjugated antibodies specific for myoblast cell surface antigens CD56 (NCAM; PE-Cy7-conjugated) and CD29 (β1-integrin; AlexaFluor488-conjugated) and the viability stain 7-Aminoactinomycin D (7AAD) (191). Individual samples yield 150,000 – 800,000 viable CD56+/CD29+ *h*MPCs per 1 million cells sorted using a BD FACS Aria™ Fusion flow cytometer. Sorted CD56+/CD29+ cells (>98% positive) were expanded in culture by passaging twice and then used in experiments; all *in vitro* experiments were performed using sorted cells at passage six.

4.3.5 Cell culture treatments

Sorted *h*MPCs were seeded at a density of approximately 10%. Throughout proliferation, GM was changed every 48 h. After 168 h of proliferation, *h*MPCs were switched to differentiation media [(DM) Ham's F12 (Gibco) supplemented with 2% heat inactivated equine serum]. After 72 h of differentiation, cells were treated for an additional 48 h with DM alone or DM + 10 ng/mL TNFα (recombinant human TNFα, Millipore). DM (+/- TNFα) was changed every 24 h. All cells were harvested after 120 h of differentiation.

4.3.6 RNA harvest and RT-PCR in differentiating cells

RNA was harvested from sorted cells using TRK lysis buffer (Omega) following manufacturer's instructions after 120 h of differentiation. Total RNA was purified using an EZNA total RNA kit (Omega) following manufacturer's instructions. Total RNA quantity and quality were determined spectrophotometrically, and an RNA quality number (RQN) was generated via sample quality control (QC). cDNA was synthesized using the High Capacity cDNA Reverse Transcription Kit (Applied Biosystems). We used real-time, quantitative PCR (RT-PCR) performed using the LightCycler 480 system (Roche) with the TaqMan Fast Advanced Master Mix and TaqMan® Gene Expression Assays (Applied Biosystems) to identify differences in gene expression of key targets related to inflammation (*IL6, IL1β, TNF*α), myogenesis (*MYOG*), and protein catabolism (*FBX032/Atrogin-1, TRIM63/MURF1*). Additionally, genes related to myogenesis and protein catabolism were selected for RNAseq validation. Primer/probes used were as follows: *IL6* (Hs00985639_m1), *TNF*α (Hs01113624_g1), *IL1β* (HS01555410_m1), *MYOG* (Hs01072232_m1), *FBX032* (Hs01041408_m1), and *TRIM63* (Hs00822387_m1). *18S* (Hs99999901_s1) was used as the

housekeeper.

4.3.7 Clustering via inflammatory profile

To determine the molecular signature differentiating MuIS+ from MuIS- cells, we evaluated the expression of inflammatory genes in differentiating *h*MPCs in the presence and absence of exogenous TNFα. It has previously been shown that SkM tissue that is MuIS+ has greater inflammation both at baseline and in response to injury, compared to MuIS- (10). Thus, we used K-means clustering with Euclidean distance to separate our samples, independent of age and sex into two clusters based on the gene expression of the inflammatory cytokines *IL6*, *IL1β*, and *TNF*α at baseline and post-TNFα treatment. We confirmed the results obtained with K-means cluster analysis with hierarchical clustering using Euclidean distance **(Figure 1)**. Four samples clustered as MuIS+, and seven samples clustered as MuIS-. *IL6, IL1β,* and *TNF*α mRNA levels in both clusters are shown in **Figure 2A-C**. Average weight, BMI, and age of participants in each group are presented in Table 1. There were no significant differences in age, weight, or BMI between the clusters. A subgroup of samples from each cluster was selected for RNA sequencing (RNAseq). The number of males and females as well as the average age, weight, and BMI of participants that were sequenced from each cluster are presented in Table 2.

Table 1. Participant Characteristics

Cluster	**M/F**	**Age (y)**	**Weight (kg)**	**BMI (kg/m^2)**
MuIS+	1/3	29 ± 7.3	62.6 ± 7.2	21.6 ± 1.2
MuIS-	5/2	28.1 ± 6.2	75.2 ± 18.7	24.5 ± 4.3

MuIS+ = muscle inflammatory susceptibility positive
MuIS- = muscle inflammatory susceptibility negative
BMI = body mass index

Table 2. Participant Characteristics of Samples Used for RNASeq

Cluster	M/F	Age (y)	Weight (kg)	BMI (kg/m^2)
MuIS+	1/3	29.0 ± 7.3	62.6 ± 7.2	21.6 ± 1.2
MuIS-	4/0	24.5 ± 3.5	80.4 ± 20.2	24.6 ± 4.3

MuIS+ = muscle inflammatory susceptibility positive
MuIS- = muscle inflammatory susceptibility negative
BMI = body mass index

4.3.8 Illumina library preparation and sequencing

To gain insight into the molecular pathways that may underlie *h*MPC inflammatory susceptibility, we performed RNAseq on a subset of samples from each group (MuIS+ n=4, MuIS- n=4). Total RNA quantity was determined spectrophotometrically, and an RQN number was generated via sample QC. All RNA samples used for RNAseq had an RQN >7. TruSeq-barcoded RNAseq libraries were generated with the NEBNext Ultra II RNA Library Prep Kit (New England Biolabs). Each library was quantified with a Qubit 2.0 (dsDNA HS kit; Thermo Fisher) and the size distribution was determined with a Fragment Analyzer (Advanced Analytical) prior to pooling. Libraries were sequenced on a NextSeq500 instrument (Illumina). At least 20M single-end 75bp reads were generated per library. Reads were trimmed for low quality and adaptor sequences with cutadapt v1.8 (parameters: parameters: -m 50 -q 20 -a AGATCGGAAGAGCACACGTCTGAACTCCAG --match-read-wildcards) (109). Reads were mapped to the reference genome/ transcriptome using tophat v2.1 (parameters: --library-type=fr-firststrand --no-novel-juncs -G <ref_genes.gtf>) (85). Cufflinks v2.2 (cuffnorm/cuffdiff) was used to generate Fragments Per Kilobase of transcript per Million mapped reads (FPKM) values and statistical analysis to determine differentially expressed gene (DEgenes) (176).

4.3.9 Principal Component Analysis

Principal component analysis (PCA) of the log2FPKM values was used to reduce the dimensionality and unbiasedly cluster the RNAseq data. Briefly, FPKM values were converted to log2FPKM values. The gene list was trimmed to include only genes for which at least two samples had FPKM ≥ 2 and the log2FPKM was at least a 2-fold absolute change across samples. JMP was used to complete the PCA on the covariances of the gene list. Eigenvectors, eigenvalues, and principal components were determined.

4.3.10 Pathway analysis

Ingenuity Pathway Analysis (IPA) was used to identify canonical pathways, functional classifications, upstream regulators, and networks discovery. The software was set to analyze transcripts with a fold change ≥ 2 and FDR corrected q value ≤ 0.001.

4.3.11 Puromycin

To measure protein synthesis, puromycin incorporation into newly synthesized proteins was quantified using the in-cell western technique (77). Briefly, after 120 h of differentiation with or without TNFα treatment during the last 48 h, puromycin was spiked to achieve a concentration of 0.5 ng/mL. After 30 min, culture media was aspirated, and cells were fixed with 4% paraformaldehyde and stored in sodium azide. Fixed cells were stained for puromycin using the following primary and secondary antibodies [Anti-Puromycin (MABE343, Millipore), Alexa-Fluor 488 goat anti-mouse IgG (A11029, Life Technologies)]. Images were quantified on the Li-Cor Odyssey® Imaging System. Puromycin was normalized to cell number in each well as determined by cell tag (926-41090, Licor 700 Stain).

4.3.12 RNAseq comparisons

Our RNAseq database was compared to two publically available databases downloaded from Gene Expression Omnibus (110, 169). Publically available RNAseq data was analyzed with GEO2R and uploaded into IPA. These data were then compared to our RNAseq database using the comparative analysis feature of IPA.

4.3.13 Statistical Methods

Statistical tests used to analyze differences in mRNA and puromycin were performed using R. For comparisons between groups, a two-way ANOVA (cluster-by-treatment) for unbalanced designs was performed. Main-effects of cluster or treatment are reported if significance was $p<0.05$. We did not observe any significant interactions.

4.4 Results

4.4.1 Identification of differentially expressed genes

PCA was used to determine whether the transcript profile, determined using RNAseq, could unbiasedly cluster the *h*MPC cultures into the same clusters as the inflammatory cytokine gene expression (MuIS+ and MuIS-). PC1 accounted for 80% of the variability while PC2 accounted for 13% of the variability in the transcript data **(Figure 3)**. PC2 separated the clusters into MuIS+ and MuIS-. The inflammatory genes and inflammation related predicted upstream regulators driving PC2 are presented in Table 3 and Table 4 respectively. These results confirm the MuIS+ and MuIS- clusters and suggest that PC2 separates the inflammatory groups. Interestingly, the transcript profiles also largely clustered by sex, with all 3 females clustering into the MuIS+ group.

Table 3. Inflammatory Genes Driving PC2

Target	Log Ratio
IL33	3.9
CXCL3	3.1
CXCL8	2.9
CXCL6	2.3
IL6	2.0
CXCL1	2.0
CXCL12	1.6
TNFRSF14	1.2

Table 4. Predicted Upstream Regulators of Genes Driving PC2

Upstream Regulator	Predicted Activation Score
LPS	5.8
TNF	5.0
IL1B	4.3
NF-kB Complex	4.0
IKBKB	4.0
IL1A	3.8
TGFB1	1.6

4.4.2 Validation of representative differentially expressed genes

To determine biological underpinnings for observed differences in MuIS, we determined DEgenes between MuIS+ and MuIS- clusters. Using RNAseq, we identified a total of 2269 DEgenes with fold change ≥ 2.0 and a q value (corrected for multiple hypothesis testing) ≤ 0.05. To validate our RNAseq results, we completed RT-PCR on five genes identified as differentially expressed via RNAseq. The original quantification of *IL6* and *IL1β* confirmed the RNAseq results. To further validate the RNAseq results, we measured mRNA levels for *MYOG*, *FBX032*, and *TRIM63* and compared fold change values between RT-PCR and RNAseq (**Figure 4**).

4.4.3 RNAseq and pathway enrichment

IPA was used for pathway enrichment of DEgenes. Of the 2269 DEgenes, IPA identified

573 DEgenes (178 down-regulated and 395 up-regulated in MuIS+/MuIS-) that met the cutoff of $q \leq 0.001$ and fold change ≥ 2.0. The most highly up- and down-regulated DEgenes are presented in Table 5.

Table 5. Up- and Down-Regulated DEgenes

Symbol	Expression Log Ratio	Q Value (FDR)
Downregulated in MuIS+		
KISS1	-4.4	8.01E-04
TSPAN7	-4.4	8.01E-04
MYH7	-4.3	8.01E-04
EEF1A2	-3.9	8.01E-04
MYH2	-3.9	8.01E-04
MYH1	-3.8	8.01E-04
FOLR1	-3.8	8.01E-04
MYH3	-3.7	8.01E-04
TSPAN33	-3.7	8.01E-04
ACTG2	-3.6	8.01E-04
Upregulated in MuIS+		
CXCL5	5.9	8.01E-04
EPB41L3	5.2	8.01E-04
MMP1	4.2	8.01E-04
PCOLCE2	4.2	8.01E-04
PENK	4.0	8.01E-04
IFI27	3.9	8.01E-04
GAP43	3.5	8.01E-04
IL13RA2	3.3	8.01E-04
ADAM33	3.3	8.01E-04
MALAT1	3.2	8.01E-04

A total of 54 functional classifications were identified at the $p<0.05$ level. Sub-functions within each functional classification are associated with a z-score that indicates predicted activation (increased or decreased) of the sub-function based on the directional change of the DEgenes. Of the top 10 functional classifications, four were of particular interest to us (*Organ Development, Organismal Development, Skeletal and Muscular System Development and*

Formation, and *Skeletal and Muscular Disorders*). The most highly activated and deactivated sub-functions within these functional classifications are reported in Table 6.

Table 6. Functional Classifications of DEgenes

Functional Pathway	Sub-function	P value	Activation z score	Number of molecules
Organ Development	Formation of Muscle	4.7E-35	-1.3	77
Skeletal and Muscular System Development and Function	Function of Muscle	1.1E-17	-2.2	48
	Contractility of muscle	2.4E-17	-3.0	35
	Differentiation of myoblasts	7.4E-08	-1.7	18
Skeletal and Muscular Disorders	Inflammation	2.6E-08	1.0	75
	Damage of muscle	1.3E-07	2.0	14

A total of 80 canonical pathways were identified at $p < 0.05$. Increased and decreased activity of canonical pathways is inferred based on the z-score. Inhibited canonical pathways included *Calcium Signaling* (z-score -3.1, p-value 7.7E-20), *ILK signaling* (z-score -3.0, p-value 9.0E-09), *Agrin Interactions at Neuromuscular Junction* (z score -2.8, p-value 1.4E-06), *Actin Cytoskeleton Signaling* (z-score -3.8, p-value 7.4E-06), and *PAK signaling* (z-score -2.7, p-value 1.1E-05). *RhoGD1 signaling* was the only canonical pathway significantly activated (z-score 3.1, p-value 7.1E-04).

Upstream regulators are predicted to control differentially expressed downstream effectors. We identified several upstream regulators using the Upstream Analysis tool in IPA (Table 7). Regulators that promote inflammation are upregulated in MuIS+ cells, and regulators that promote muscle cell differentiation are downregulated in MuIS+ cells. Several of these upstream regulators have been shown to induce inflammation (TNF, LPS, TNFSF12, IKBKB, IL1B) and muscle differentiation (MYOD1, TGFB1, MEF2C, MYOCD, MYOG, NOTCH1, SMARCA4) previously. We have also identified additional novel regulators, including DNMT3B, whose role in *h*MPCs has not yet been shown.

Table 7. Upstream Regulators Driving DEgenes

Upstream Regulator	Activation Z Score	P value
MYOD1	-5.0	4.9E-38
MEF2C	-3.8	6.1E-20
MYOCD	-3.6	5.7E-15
SMARCA4	-3.1	1.7E-09
MYOG	-2.9	1.2E-14
NOTCH1	-2.5	1.6E-10
TGFB1	-2.1	2.4E-21
Beta-estradiol	-1.3	6.1E-27
CHUK	1.5	2.1E-07
IL1B	2.9	5.5E-08
IKBKB	3.2	8.8E-09
DNMT3B	3.3	1.3E-14
TNFSF12	3.4	1.6E-08
TNF	3.5	3.7E-26
LPS	3.8	1.2E-11

4.4.4 Muscle regeneration markers

Successful muscle regeneration requires acute inflammation, proteolysis, protein synthesis, and myoblast differentiation. Knowing that MuIS+ cells have an elevated inflammatory response to proinflammatory cytokines, we also investigated the effect of MuIS with or without cytokine exposure on markers of proteolysis, differentiation, and protein synthesis in MuIS+ and MuIS- cells. We observed a main-effect of MuIS cluster for *FBX032* and *TRIM63*; MuIS+ cells had lower *FBX032* and *TRIM63* compared to MuIS- cells (Figure 8A,B). We observed no significant effect of MuIS on *MYOG* mRNA or puromycin (marker of protein synthesis) (Figure 8C, D).

4.4.5 Clinical relevance

To further explore the clinical relevance of the MuIS+ phenotype, we compared our

transcriptomics dataset with two others previously reported in the literature (110, 169). Previous work had identified a transcript profile in whole muscle that distinguished extreme responders from non-responders in response to progressive resistance exercise training (169). Importantly, all transcriptomics were completed on baseline samples, prior to the start of the resistance training. When compared to our dataset, non-responders and MuIS+ samples had significant overlap in transcript profiles. A list of canonical pathways up- and down-regulated in both datasets is presented in Table 8.

Table 8. Canonical Pathways Shared with Hypertrophic Responders to Resistance Exercise

Canonical Pathway	**Non-Responders vs. Extreme Responders**		**MuIS+ vs. MuIS-**	
	z-score	*p-value*	*z-score*	*p-value*
Actin Cytoskeleton Signaling	-3.2	1.5E-03	-3.8	7.4E-06
Regulation of Actin-based Motility by Rho	-1.5	3.0E-02	-3.3	5.2E-04
Calcium Signaling	-1.9	6.6E-04	-3.2	7.7E-20
RhoA Signaling	-1.5	3.3E-02	-3.2	3.7E-04
Signaling by Rho Family GTPases	-2.1	5.5E-02	-3.1	6.1E-03
ILK Signaling	-2.6	8.6E-02	-3.0	9.0E-09
GNRH Signaling	-2.0	9.9E-02	-1.6	2.8E-02
Opioid Signaling Pathway	-2.1	9.7E-02	-1.6	2.4E-02
RhoGDI Signaling	2.6	2.0E-02	3.1	7.1E-04

Previous work had also identified a transcript profile that distinguished young and old adult muscle (110). Melov et al. measured peak muscle strength and reported that older adults were 59% weaker than young adults. In a comparative analysis in IPA, genes differentially expressed in MuIS+ vs. MuIS- cultures from our dataset had significant overlap to genes differentially expressed in old vs. young adults, reported by Melov et al. Upstream regulators that are predicted to control the DEgene expression in both datasets are presented in Table 9.

Table 9. Upstream Regulators Shared with Older Adults

Upstream Regulator	**Old Adults vs. Young Adults**		**MuIS+ vs. MuIS-**	
	z-score	*p-value*	*z-score*	*p-value*
NR4A3	-1.9	4.2E-05	-3.7	2.2E-04
RB1	-7.6	2.5E-08	-3.3	1.6E-06
ESRRA	-2.8	5.6E-07	-3.0	1.8E-02
KMT2D	-2.4	3.3E-01	-2.8	2.3E-03
CD3	-2.6	4.3E-02	-1.7	3.3E-02
IGF1R	-1.6	3.1E-07	-1.5	2.8E-04
PDGF	2.9	1.5E-03	1.4	4.7E-03
CHUK	2.2	1.3E-02	1.5	2.1E-07
IL6	2.0	4.2E-02	1.5	2.6E-05
ESR2	2.0	1.3E-04	1.5	7.2E-16
IL17A	2.8	2.6E-02	1.6	6.4E-08
MGEA5	1.2	1.9E-07	2.2	3.0E-02
IL1	2.4	2.2E-01	2.5	4.2E-05
IKBKG	2.2	3.1E-02	2.8	2.8E-09
IL1B	1.2	1.0E-02	2.9	5.5E-08
TNFSF12	1.8	6.6E-02	3.4	1.6E-08
TNF	1.3	2.1E-05	3.5	3.7E-26
Lipopolysaccharide	1.4	1.0E-02	3.8	1.2E-11
KDM5A	4.0	3.4E-10	4.2	9.6E-09

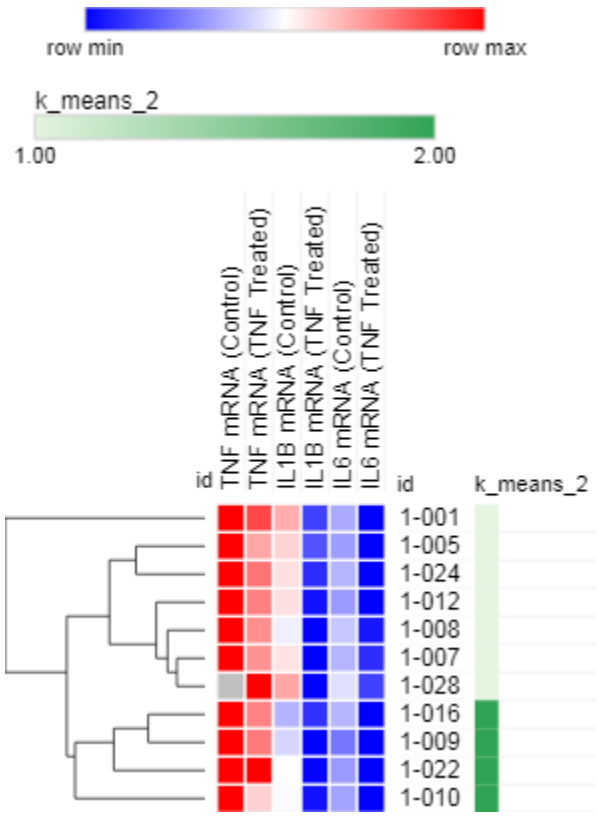

Figure 1. Inflammatory Susceptibility Clustering. K-means and hierarchical clustering on inflammatory cytokine mRNA levels from control and TNFα treated cells.

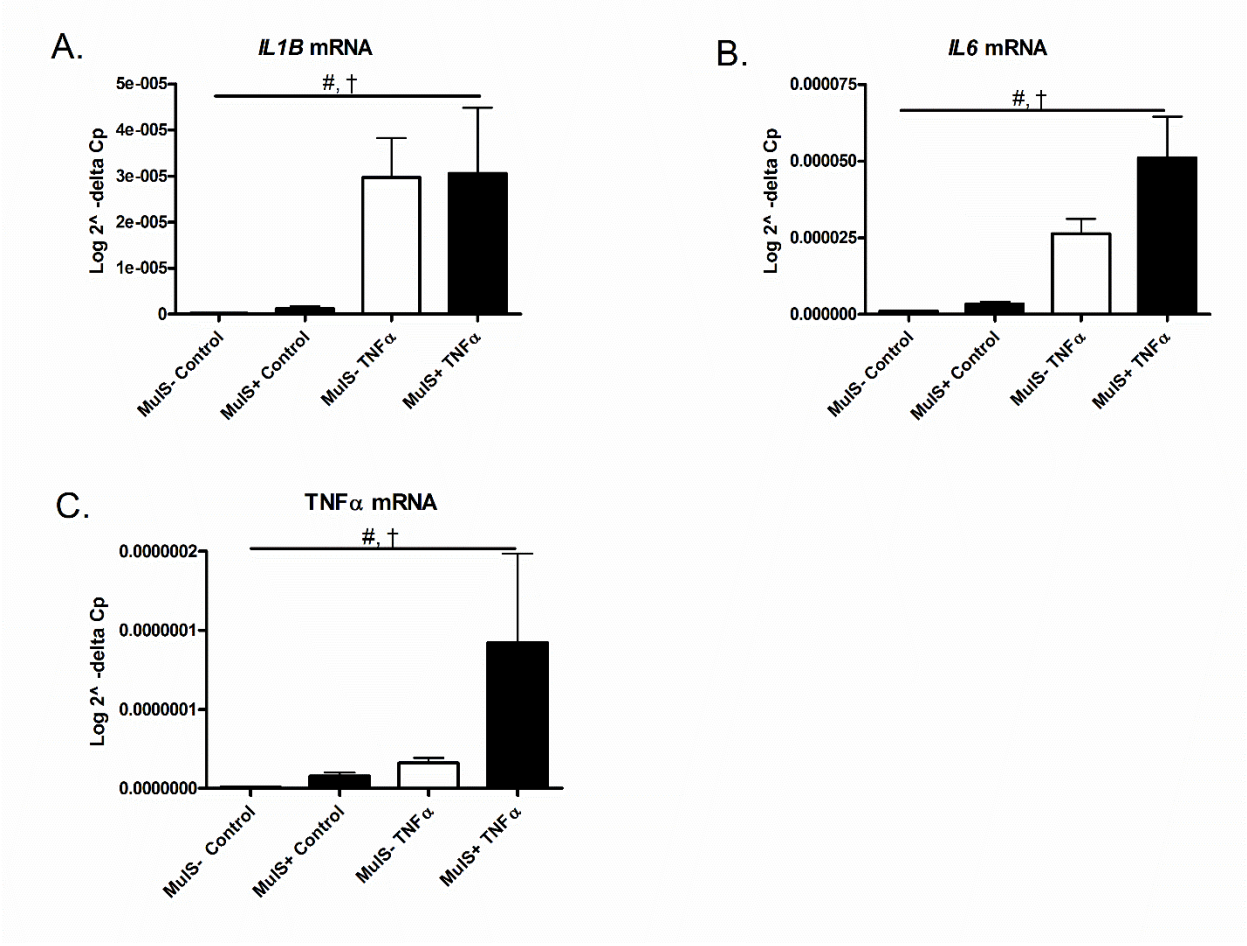

Figure 2. Inflammatory Cytokine mRNA Levels in MuIS+ and MuIS- *h*MPCs. A) *IL1β* mRNA, B) *IL6* mRNA, C) *TNFα* mRNA. For each transcript, the effect of 48 h of 10 ng/uL TNFα treatment on MuIS cluster was determined using a two-way ANOVA (cluster-by-treatment) for unbalanced designs. Main-effects are reported if significance $p<0.05$. # = main-effect of cluster (MuIS+ vs. MuIS-), † = main-effect of treatment (Control vs. TNFα treated).

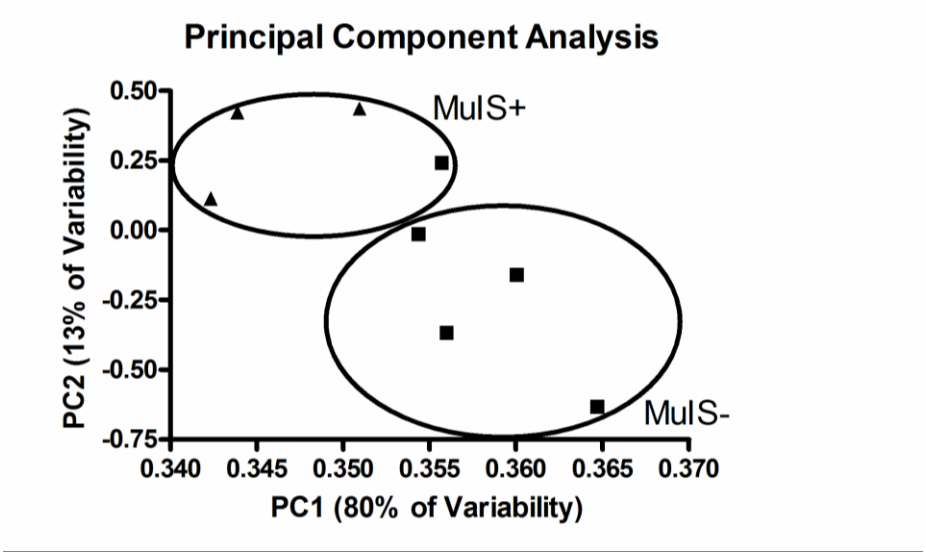

Figure 3. Principal Component Analysis of RNAseq Genes. Principle Component Analysis (PCA) revealed that 80% of the gene expression data could be explained by PC1. PC2 explained 13% of the variability. PCA on the RNAseq results separated the samples into the same clusters as the K-means and hierarchical clustering of cytokine expression data. ■ = Male-*h*MPCs, ▲= Female=*h*MPCs

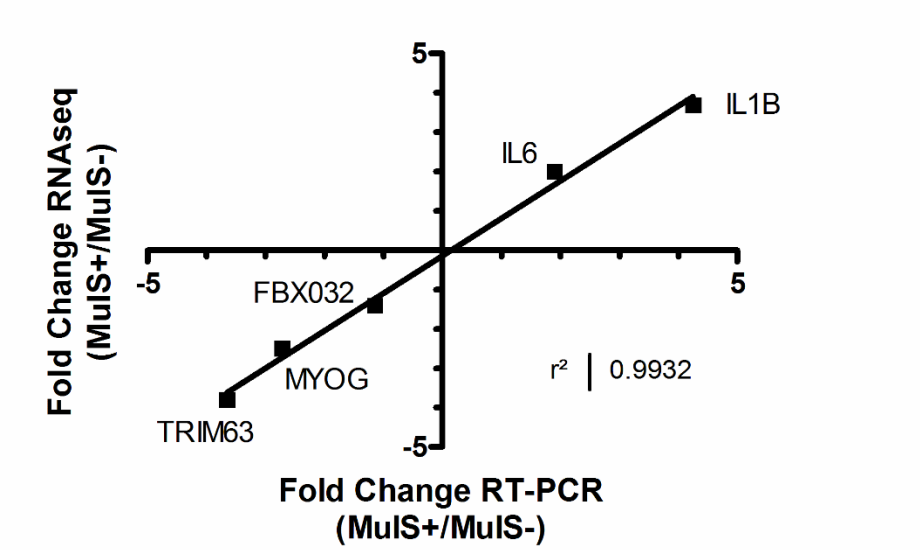

Figure 4. Validation of DEgenes. Plot comparing the fold-change between RT-PCR and RNAseq for five genes that were differentially expressed between MuIS+ and MuIS- clusters, at five days of differentiation under basal conditions.

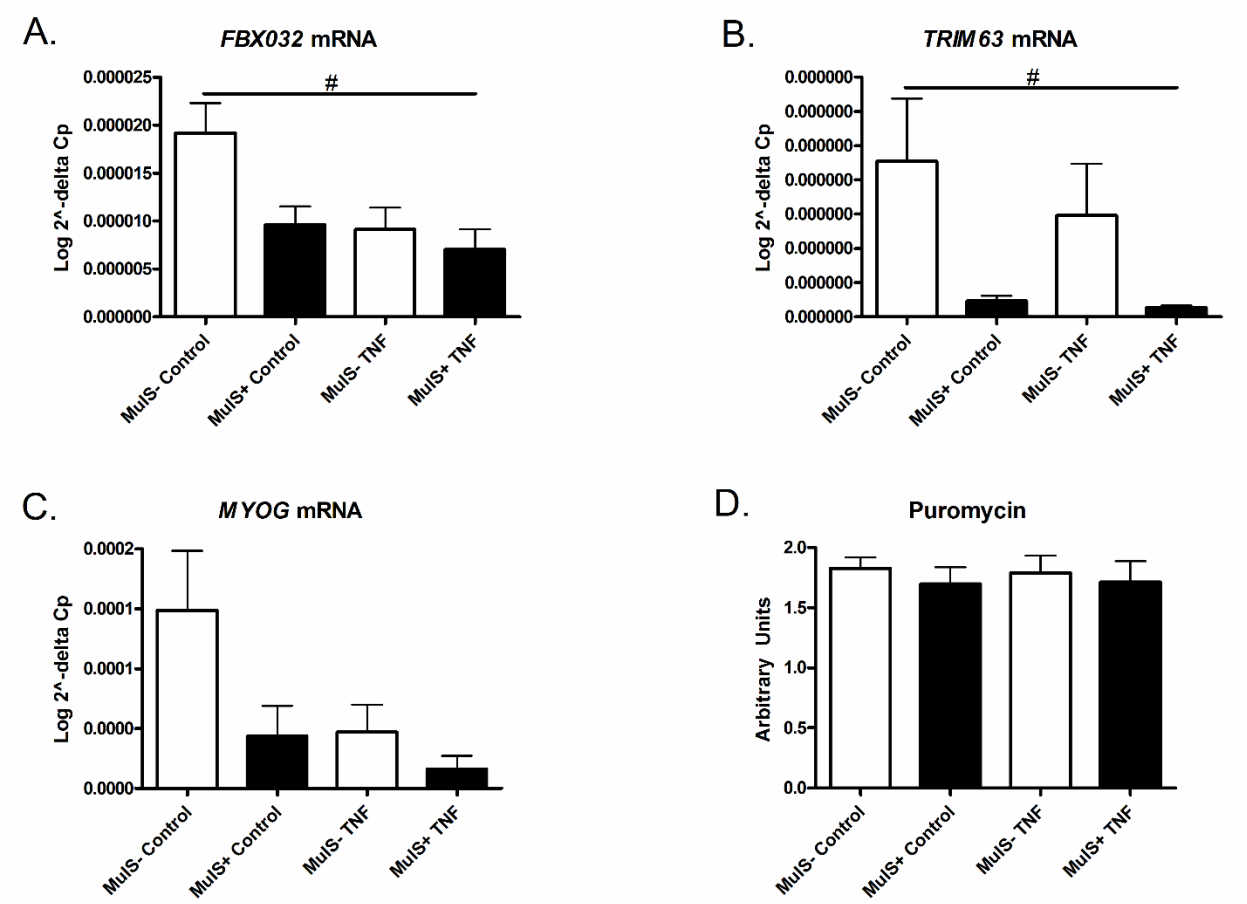

Figure 5. Markers of Muscle Regeneration. A) *FBX032* mRNA levels, B) *TRIM63* mRNA levels, C) *MYOG* mRNA levels, D) puromycin incorporation into newly synthesized proteins. For each marker, the effect of 48 h of 10 ng/uL TNFα treatment on MuIS cluster was determined using Two-way ANOVA (cluster-by-treatment) for unbalanced designs. Main-effects are reported if significance $p<0.05$. # = main-effect of cluster (MuIS+ vs. MuIS-).

4.5 Discussion

Using RNAseq, we are the first to identify a transcript profile that distinguishes *h*MPC cultures into MuIS clusters. Although inflammation following muscle damage is an integral part of the regenerative process, the ability of SkM to manage or respond to inflammation is

recognized as a major cause of impaired regeneration (10, 37, 112). Our primary findings demonstrate that MuIS+ cultures have DEgenes enriched in functional classifications, pathways and networks that suggest promotion of inflammatory signaling and inhibition of myoblast differentiation. In our analyses, novel and known regulators of inflammation and muscle cell differentiation have emerged as having important roles in inflammatory signaling and differentiation.

4.5.1 Inflammatory cytokines and muscle regulatory factors

As expected, when DEgenes were analyzed for functional classifications and pathways, we identified that MuIS+ cultures had an enrichment of DEgenes related to inflammation and muscle damage. These RNAseq results confirm our K-means clustering. It is important to highlight that RNAseq was performed on cells in the absence of an exogenous inflammatory exposure. Our results suggest that the inflammatory status of *h*MPCs is a characteristic intrinsic to the cells, which is in agreement with the results of others (10, 112).

MuIS+ cultures also had a downregulation of genes related to myoblast differentiation, formation of muscle, and function of muscle. In *h*MPCs, treatment with the inflammatory cytokine TNFα, promotes *h*MPC proliferation and inhibits *h*MPC differentiation and fusion (115). TNFα is known to downregulate the transcription of the pro-myogenic transcription factor MYOD through NF-κB (8). Similarly, our RNAseq results suggest greater proinflammatory signaling and reduced myotube formation in MuIS+ cells. Additionally, TNFα has also shown to induce apoptosis in C2C12 myotubes (175). However, despite the increased proinflammatory signaling in MuIS+ cultures, our RNAseq results suggest little change in apoptosis or necrosis pathways.

4.5.2 Hormones

Unexpectedly, kisspeptin-1 (*KISS1*) was the most highly DEgene between MuIS+ and MuIS- cells; *KISS1* was downregulated 21.4 fold in the MuIS+ compared to the MuIS- cultures. KISS1 is best known for its role in gonadotropic secretion and puberty (163). KISS1 is also known as a tumor metastasis suppressor in breast cancer cells; KISS1 inhibits TNFα mediated activation of NF-κB, which inhibits the TNFα enriched tumor microenvironment (31). While KISS1 has previously been reported in myocardium tissue (196), to our knowledge, we are the first to report the presence of KISS1 in human SkM cells. Our data suggest that KISS1 may play a novel and important role in the management of and response to inflammation during regeneration.

Estrogen has also been associated with a suppressed inflammatory response in SkM in response to injury. In our dataset, beta-estradiol signaling was predicted to be inhibited as an upstream regulator in the MuIS+ cluster. These results agree with previous literature; the protective effects of estrogen signaling have been shown *in vivo*. Estrogen reduced the inflammatory response after burn injury in human females (72) and reduced the inflammatory response to endotoxin exposure in post-menopausal women (136). However, despite the evidence for estrogen in suppressing the immune and inflammatory responses among females, our clusters did not depend on sex. In fact, 75% of the cultures that clustered into the MuIS+ group were female. Thus, in the absence of varying levels of exogenous estrogen, intrinsic differences in estrogen signaling, independent of sex, may play an important role in inflammation modulation.

4.5.3 Calcium signaling

Calcium signaling is the most significant and highly deactivated canonical pathway in MuIS+ cultures when compared to MuIS- cultures. Several components of the pathway, including the ryanodine receptor, calmodulin, calsequestrin, and the mitochondrial calcium uniporter, were downregulated in MuIS+ cells. Calcium acts as a second messenger and is required for the regulation of many cellular processes including gene transcription, proliferation, and immune responses (33). Ryanodine receptor mediated calcium dynamics are required for skeletal myogenesis (52, 53, 198), and perturbing calcium release from internal stores impairs regeneration and inhibits the activation and proliferation of SCs (177). Myoblast differentiation is also regulated by increases in intracellular calcium (86, 87, 100); calcium-calmodulin-dependent protein kinases (CaMK) and the calcium-calmodulin-dependent phosphatase, calcineurin, play significant roles in muscle cell differentiation by regulating the gene expression of *MEF2*, *MYOD*, and *MYOG* (57, 58, 103, 117). Aside from calcium's role in muscle differentiation, calcium has also been implicated in the pathogenesis of immune disorders, such as rheumatoid arthritis (78). Celastrol, a Chinese medicinal plant, has traditionally been used to treat autoimmune disease and chronic inflammation (23, 179); celastrol has recently been shown to increase intracellular and mitochondrial calcium mobilization (194) and to decrease the expression of genes associated with immunity/ inflammation (40). Thus, elevated calcium mobilization in MuIS- cultures may play important roles in modulating both myoblast differentiation and inflammation.

4.5.4 Epigenetics

One of the top predicted upstream regulators controlling DEgene expression is SMARCA4, a member of the SWI/SNF family of proteins that are thought to regulate the

transcription of certain genes by altering chromatin structure (188). In primary myoblasts, SMARCA4 is a positive regulator of cell proliferation and survival (129) and is required for activation of genes in myoblast differentiation (121). SMARCA4 remodels chromatin in a calcium dependent manner; inhibiting calcineurin blocks chromatin remodeling, myogenic gene expression, and muscle cell differentiation (121). SMARCA4 also modulates the immune response in a variety of tissues. SMARCA4 chromatin remodeling plays an integral role in regulating T cell suppression of inflammation (26). To the contrary, SMARCA4 promotes the expression of proinflammatory genes in nonalcoholic steatohepatitis (171). In endothelial cells, SMARCA4 is recruited to cell adhesion molecules (glycoproteins expressed on the cell surface that play important roles in inflammation) via NF-κB/p65, and β-estradiol antagonizes the activity of SMARCA4 (49). Although the role of SMARCA4 in inflammation in other cell types and in myoblast differentiation have been explored, the role of SMARCA4 in modulating inflammation in *h*MPCs remains unexplored.

4.5.5 Muscle remodeling

TNFα is known to promote the mRNA levels of *FBX032* and *TRIM63* and lead to the catabolism of muscle proteins (22, 84). Thus, we expected *FBX032* (*Atrogin-1*) and *TRIM 63* (*MuRF*) to be elevated in MuIS+ cells. To the contrary, we observed downregulated expression of both *FBX032* and *TRIM63* in MuIS+ cultures in both the RNAseq and PCR data. Aside from the role of FBX032 in muscle protein catabolism, FBX032 also plays a positive role in myoblast differentiation through inhibiting myocardin (82). Myocardin is a transcriptional coactivator transiently expressed in SkM progenitor cells with inhibitory effects on the expression of *MYOG* (82). Thus, elevated *FBX032* and *TRIM63* expression in MuIS+ cultures may reflect increased

protein remodeling and enhanced myoblast differentiation.

In vivo, muscle remodeling occurs secondary to exercise training (48). Inflammation appears to be closely tied to training outcomes; older adults who gain the most strength also have the largest decrease in *IL1β* following exercise (45). The inflammatory response to exercise has been shown to increase, decrease, or not change depending on specific haplotype patterns. The exercise-induced inflammatory response is also influenced by individual SNPs (44). Thus, although our data suggest that a transcript profile can distinguish those with high and low muscle inflammatory susceptibility, differences in genotype may also play a role in distinguishing the groups.

4.5.6 Clinical relevance

To further explore similarities of the MuIS+ phenotype with previously characterized phenotypes or disease states, we compared our transcriptomics dataset with two that have been published previously (110, 169). MuIS+ cultures share overlap in the gene expression profile to both individuals who do not respond to a progressive resistance exercise training and to older adults with diminished muscle strength. Importantly, all of our samples were from healthy young adults. This creates the question, "does the MuIS+ phenotype underlie impairment in muscle hypertrophy and predispose individuals to muscle loss even in the absence of old age?" Interestingly, when MuIS+ cultures were compared to whole tissue biopsies from those who do not respond to resistance training, both GnRH and calcium signaling came out as shared important canonical pathways. KISS-1 is known to activate GnRH signaling in other cell types, and KISS-1 alters the cytoskeleton in HEK293 cells (133). However, the role of KISS-1 or GnRH signaling in SkM has not been explored.

4.6 Conclusion

Acute muscle inflammation is an integral component of SC activation and muscle regeneration. However, there is a large degree of variability in the ability of MPCs to manage and respond to inflammatory cues. Using unsupervised approaches, we identified a transcript profile that underlies the culture-to-culture variability in MuIS. We identified key DEgenes, canonical pathways, and upstream regulators that distinguish cultures based on inflammatory susceptibility. Uncovering the molecular determinants of muscle inflammatory susceptibility and SkM regeneration is important to improving clinical outcomes following muscle injury.

4.7 Acknowledgments

We thank Jennifer Grenier from the Cornell University, RNA Sequencing Core for her help with RNA sequencing and analysis. We thank the Cornell University, Biotechnology Resource Center Imaging Facility for their help with fluorescence activated cell sorting. We thank Heather Roman for her assistance with maintaining the *h*MPC cultures. We also thank Melinda Lem for her help with participant recruitment. Finally, we thank the participants for their time and participation in the study. This study was funded by PCCW and Cornell Division of Nutritional Sciences.

CHAPTER 5: SUMMARY AND FUTURE DIRECTIONS

5.1. Summary and future research for the heterogeneity in expansion capacity

The research presented in this dissertation indicates that expansion capacity of human MPCs (*h*MPCs) is affected by age and sex of the cell donor. Although previous research has investigated the impact of age and sex on expansion capacity in animal models (108, 113, 159), relatively little research has focused on the impact of age (6, 128) and no previous research has focused on the impact of sex of MPCs obtained from human SkM. We hypothesized and confirmed that *h*MPCs from older donors have a reduced expansion capacity compared to *h*MPCs from younger donors (Chapter 2). *h*MPCs from young female donors also have a reduced expansion capacity compared to *h*MPCs from young male donors; however, this comparison was not maintained with age. Old male (OM)-*h*MPCs had the greatest impairment in expansion capacity with age while *h*MPCs from females were largely unaffected with age. *h*MPCs from old male donors also had the greatest percentage of cell death early in expansion. This is the first research to identify heightened cell death as the primary contributor to altered expansion capacity in *h*MPCs.

Catabolism of macronutrients provides the substrates and energy needed to support the generation of new cells and cellular structures (153). Thus, an impairment in the catabolism of macronutrients may negatively impact the expansion capacity of cells. To date, only one study has investigated the impact of chronological age (128) and no previous research has investigated the impact of sex on *h*MPC metabolic fuel preference throughout expansion. Our results suggest that oxidative phosphorylation (OXPHOS) is the predominant metabolic pathway used by healthy *h*MPCs during the expansion process (Chapter 2). Intriguingly, cultures from old male

donors had a significant disruption of OXPHOS during expansion and OM-*h*MPCs had the greatest impairment in expansion. Thus, we hypothesize that the elevated cell death and disruption in OXPHOS in *h*MPCs from old male donors contributed to the observed impaired expansion capacity. However, due to our experimental design, we can only state that altered OXPHOS is associated with impaired expansion capacity. To confirm that disruption in OXPHOS impairs expansion capacity, future research should inhibit OXPHOS through the use of small molecules (e.g. rotenone or antimycin A) and quantify changes in expansion capacity over time. If OXPHOS is the predominant energy source, we hypothesize that expansion capacity will be impaired over time.

Despite reporting main effects of age and sex on expansion capacity, our results indicate that not all old *h*MPCs have impaired expansion capacity and similarly, not all young *h*MPCs expand better than old *h*MPCs (Chapter 3). The research presented in this dissertation is the first to use both phenotype characteristics and transcriptomics to cluster *h*MPC cultures into FAST and SLOW expanders. Using K-means clustering, an unbiased statistical clustering tool, we were the first to cluster samples using phenotypic similarity (FAST versus SLOW expanders) instead of categorical similarity (age or sex) to investigate the biological underpinnings of expansion capacity. In agreement with our initial work (refer to Chapter 2), the average age of participants who clustered into the SLOW cluster were significantly older than the average age of participants who clustered into the FAST cluster. Additionally, a greater percentage of females clustered into the SLOW cluster compared to the FAST cluster. However, both FAST and SLOW clusters included young and old, male and female participants. Cultures with enhanced expansion capacity (i.e. FAST cluster) had DEgenes enriched in functional classifications, pathways, and networks that suggest enhanced cell cycle, reduced apoptosis and cellular

senescence, and enhanced DNA replication. We identified several novel upstream regulators, including RABL6, IRGM1, and AREG that have been shown to promote cell proliferation in other cell lines (47, 158, 168); however, these regulators have not been previously identified as playing a role in MPC expansion let alone in MPCs from human donors. Our dataset also identified FOXM1 as an important upstream regulator driving the DEgenes in our FAST and SLOW clusters. Very recently, FOXM1 was shown to directly regulate the long noncoding RNAs, Snhg8 and Gm26917, that significantly regulate the proliferation and apoptosis of SCs (30). In the same paper, Chen et al. demonstrated that Foxm1 knockout mice and Foxm1-knockdown C2C12 cells have decreased proliferation and increased apoptosis of SCs (30). Thus, one originally novel upstream regulator in our dataset has been confirmed as having an important functional role in SC proliferation. Future work should investigate the roles of the other novel upstream regulators identified in our dataset in *h*MPCs. Additionally, further exploration regarding the regulation of FOXM1 in SCs is warranted.

Although this dissertation reports on heterogeneity between cultures, the heterogeneity within cultures remains unknown. Do FAST cultures expand rapidly because all cells rapidly divide or is the effect driven by a subset of cells? If the effect is driven by a subset of cells, do these cells rely on OXPHOS or glycolysis more or less than cells that divide at a slower rate? These questions can be probed using single cell RNAseq, where the transcriptome from each cell is independently sequenced. The expression levels of biologically meaningful genes, such as cell cycle indicators or metabolic genes can be compared using this methodology. These questions can also be further explored using single cell clonal expansion. Using this technique, cells are sorted and one cell is placed into each well of a culture plate. The rate of expansion/colonization of each culture derived from a single cell could be compared. Further measures of metabolism,

gene expression, and protein expression/ activity from each clonal culture could also be compared. In this way, heterogeneity within FAST and SLOW cultures could be further evaluated.

5.2 Summary and future research for the heterogeneity in inflammatory susceptibility

Acute inflammation is an essential component of the muscle regenerative response (192). However, chronic inflammation is associated with pathological remodeling of the SkM, including muscle loss (37, 83). Muscle inflammatory susceptibility has been reported to vary between individuals and to discriminate muscle anabolic potential following surgery (10). We are the first to explore the molecular mechanisms driving heightened muscle inflammatory susceptibility. Heightened muscle inflammatory susceptibility (MuIS+) clusters have elevated levels of pro-inflammatory cytokines at baseline and in response to exogenous cytokine exposure (112). MuIS+ was initially identified by Merritt et al. in tissue and *h*MPCs from old adults compared to young adults. Unlike work done by Merritt et al., we report widespread inflammatory variability in *h*MPCs from young adults. Additionally, using RNAseq, we identified novel and known genes that are differentially expressed between MuIS+ and MuIS- clusters as well as novel and known upstream regulators of inflammation and differentiation.

Two interesting and novel results of this study were that in MuIS+ vs MuIS- cultures 1) *KISS-1* was the most highly differentially expressed and inhibited gene and 2) calcium signaling was the most significant and highly inhibited canonical pathway. When we compared our transcriptomics dataset to a dataset that differentiated extreme responders and non-responders to progressive resistance exercise training, GnRH signaling and calcium signaling were highlighted as important shared canonical pathways. Neither KISS-1 nor GnRH signaling have ever been

reported as present or functional in skeletal muscle. KISS-1 inhibits TNFα mediated activation of NF-κB in breast cancer cells (31) and thus may play an important role in mitigating inflammation in MuIS- cultures. Future research should investigate the role of KISS-1 and GnRH signaling as well as the regulation of KISS-1 expression at the SkM cell and tissue levels. Additionally, calcium signaling has known roles in myoblast differentiation (86) and inflammation in other tissues (78). Recent research suggests that calcium mobilization may improve chronic inflammation and be a viable therapy for autoimmune disease (78). However, the role of calcium signaling in muscle inflammation remains unknown. Future research should investigate the role of perturbed calcium signaling on muscle inflammation and subsequent effects on SkM regeneration.

As noted above, all samples used in this dissertation were from healthy individuals. Interestingly, despite being free of chronic disease, muscle inflammatory susceptibility varied widely, even in young adults. Exploring the molecular underpinnings of muscle inflammatory susceptibility will provide important insight into improving therapeutic outcomes following injury, even in young adults. Interestingly, the transcript profiles of MuIS+ cultures also had remarkable overlap with older adults with diminished muscle strength. This creates the question, "are those with MuIS+ predisposed to muscle loss, even in the absence of chronological old age?" Additionally, are those with MuIS+ at higher risk for the development of sarcopenia than those with MuIS-?

5.3 Additional uses of our model

For all experiments presented in this dissertation, we exclusively used MPCs from healthy human donors. Chronic diseases including diabetes are known to impact muscle health

(61). Diabetes impairs energy metabolism and induces SkM atrophy and muscle weakness (61). Ob/ob and db/db mice have impaired myoblast proliferation and delayed muscle regeneration (125). Although the effects of obesity and diabetes are well characterized in animal models, little work has been conducted in *h*MPCs. The experimental techniques used in this dissertation could similarly be applied to investigate the molecular underpinnings of impaired *h*MPC expansion and differentiation in various disease states.

5.4 Global summary

This dissertation highlights the heterogeneity that exists among *h*MPC cultures throughout the muscle regenerative process. Uncovering the molecular underpinnings of this heterogeneity is essential as the field of medicine moves towards precision therapies to improve human health. This dissertation utilizes –omics and unbiased clustering tools to cluster samples into phenotype categories aside from commonly used categorical bins, such as age and sex. Importantly, this dissertation highlights biologically meaningful data that would be lost if samples were binned using traditional techniques. Clustering samples unbiased based on phenotype provides insight into the pathways and regulators driving the phenotype. Although the phenotypes observed in *h*MPC cultures can also be reflected *in vivo*, this dissertation investigates intrinsic differences in *h*MPCs that remain outside of the tissue niche. Future research should follow up on the hypotheses generated in this dissertation and directly test the impact of altering key differentially DEgenes, upstream regulators, and canonical pathways on myoblast expansion and differentiation.

REFERENCES

1. **Aas V, Bakke SS, Feng YZ, Kase ET, Jensen J, Bajpeyi S, Thoresen GH, and Rustan AC.** Are cultured human myotubes far from home? *Cell Tissue Res* 354: 671-682, 2013.
2. **Abrigo J, Simon F, Cabrera D, Cordova G, Trollet C, and Cabello-Verrugio C.** Central Role of Transforming Ggrowth Factor Type Beta 1 in Skeletal Muscle Dysfunctions: an Update on Therapeutic strategies. *Curr Protein Pept Sci*, 2017.
3. **Adam-Vizi V and Chinopoulos C.** Bioenergetics and the formation of mitochondrial reactive oxygen species. *Trends Pharmacol Sci* 27: 639-645, 2006.
4. **Adams GR.** Satellite cell proliferation and skeletal muscle hypertrophy. *Appl Physiol Nutr Metab* 31: 782-790, 2006.
5. **Almada AE and Wagers AJ.** Molecular circuitry of stem cell fate in skeletal muscle regeneration, ageing and disease. *Nat Rev Mol Cell Biol* 17: 267-279, 2016.
6. **Alsharidah M, Lazarus NR, George TE, Agley CC, Velloso CP, and Harridge SD.** Primary human muscle precursor cells obtained from young and old donors produce similar proliferative, differentiation and senescent profiles in culture. *Aging Cell* 12: 333-344, 2013.
7. **Asakura A, Hirai H, Kablar B, Morita S, Ishibashi J, Piras BA, Christ AJ, Verma M, Vineretsky KA, and Rudnicki MA.** Increased survival of muscle stem cells lacking the MyoD gene after transplantation into regenerating skeletal muscle. *Proc Natl Acad Sci U S A* 104: 16552-16557, 2007.
8. **Bakkar N, Wang J, Ladner KJ, Wang H, Dahlman JM, Carathers M, Acharyya S, Rudnicki MA, Hollenbach AD, and Guttridge DC.** IKK/NF-kappaB regulates skeletal myogenesis via a signaling switch to inhibit differentiation and promote mitochondrial biogenesis. *J Cell Biol* 180: 787-802, 2008.
9. **Bales CW and Ritchie CS.** Sarcopenia, weight loss, and nutritional frailty in the elderly. *Annu Rev Nutr* 22: 309-323, 2002.
10. **Bamman MM, Ferrando AA, Evans RP, Stec MJ, Kelly NA, Gruenwald JM, Corrick KL, Trump JR, and Singh JA.** Muscle inflammation susceptibility: a prognostic index of recovery potential after hip arthroplasty? *Am J Physiol Endocrinol Metab* 308: E670-679, 2015.
11. **Bamman MM, Petrella JK, Kim JS, Mayhew DL, and Cross JM.** Cluster analysis tests the importance of myogenic gene expression during myofiber hypertrophy in humans. *J Appl Physiol (1985)* 102: 2232-2239, 2007.
12. **Baraibar MA, Hyzewicz J, Rogowska-Wrzesinska A, Bulteau AL, Prip-Buus C, Butler-Browne G, and Friguet B.** Impaired energy metabolism of senescent muscle satellite cells is associated with oxidative modifications of glycolytic enzymes. *Aging (Albany NY)* 8: 3375-3389, 2016.
13. **Barani AE, Durieux AC, Sabido O, and Freyssenet D.** Age-related changes in the mitotic and metabolic characteristics of muscle-derived cells. *J Appl Physiol (1985)* 95: 2089-2098, 2003.
14. **Bareja A and Billin AN.** Satellite cell therapy - from mice to men. *Skelet Muscle* 3: 2, 2013.
15. **Beccafico S, Riuzzi F, Puglielli C, Mancinelli R, Fulle S, Sorci G, and Donato R.** Human muscle satellite cells show age-related differential expression of S100B protein and RAGE. *Age (Dordr)* 33: 523-541, 2011.
16. **Bernet JD, Doles JD, Hall JK, Kelly Tanaka K, Carter TA, and Olwin BB.** p38

MAPK signaling underlies a cell-autonomous loss of stem cell self-renewal in skeletal muscle of aged mice. *Nat Med* 20: 265-271, 2014.
17. **Bjornholm M and Zierath JR.** Insulin signal transduction in human skeletal muscle: identifying the defects in Type II diabetes. *Biochem Soc Trans* 33: 354-357, 2005.
18. **Brack AS, Bildsoe H, and Hughes SM.** Evidence that satellite cell decrement contributes to preferential decline in nuclear number from large fibres during murine age-related muscle atrophy. *J Cell Sci* 118: 4813-4821, 2005.
19. **Brack AS, Conboy MJ, Roy S, Lee M, Kuo CJ, Keller C, and Rando TA.** Increased Wnt signaling during aging alters muscle stem cell fate and increases fibrosis. *Science* 317: 807-810, 2007.
20. **Brack AS and Munoz-Canoves P.** The ins and outs of muscle stem cell aging. *Skelet Muscle* 6: 1, 2016.
21. **Brooks SV and Faulkner JA.** Skeletal muscle weakness in old age: underlying mechanisms. *Med Sci Sports Exerc* 26: 432-439, 1994.
22. **Cai D, Frantz JD, Tawa NE, Jr., Melendez PA, Oh BC, Lidov HG, Hasselgren PO, Frontera WR, Lee J, Glass DJ, and Shoelson SE.** IKKbeta/NF-kappaB activation causes severe muscle wasting in mice. *Cell* 119: 285-298, 2004.
23. **Canter PH, Lee HS, and Ernst E.** A systematic review of randomised clinical trials of Tripterygium wilfordii for rheumatoid arthritis. *Phytomedicine* 13: 371-377, 2006.
24. **CDC.** Deaths: Final Data for 2011, edited by 7 T, 2011.
25. **Cerletti M, Jang YC, Finley LW, Haigis MC, and Wagers AJ.** Short-term calorie restriction enhances skeletal muscle stem cell function. *Cell Stem Cell* 10: 515-519, 2012.
26. **Chaiyachati BH, Jani A, Wan Y, Huang H, Flavell R, and Chi T.** BRG1-mediated immune tolerance: facilitation of Treg activation and partial independence of chromatin remodelling. *EMBO J* 32: 395-408, 2013.
27. **Chakkalakal J and Brack A.** Extrinsic Regulation of Satellite Cell Function and Muscle Regeneration Capacity during Aging. *J Stem Cell Res Ther* Suppl 11: 001, 2012.
28. **Chakravarthy MV, Davis BS, and Booth FW.** IGF-I restores satellite cell proliferative potential in immobilized old skeletal muscle. *J Appl Physiol (1985)* 89: 1365-1379, 2000.
29. **Charge SB and Rudnicki MA.** Cellular and molecular regulation of muscle regeneration. *Physiol Rev* 84: 209-238, 2004.
30. **Chen Z, Bu N, Qiao X, Zuo Z, Shu Y, Liu Z, Qian Z, Chen J, and Hou Y.** Forkhead Box M1 Transcriptionally Regulates the Expression of Long Noncoding RNAs Snhg8 and Gm26917 to Promote Proliferation and Survival of Muscle Satellite Cells. *Stem Cells*, 2018.
31. **Cho SG, Li D, Stafford LJ, Luo J, Rodriguez-Villanueva M, Wang Y, and Liu M.** KiSS1 suppresses TNFalpha-induced breast cancer cell invasion via an inhibition of RhoA-mediated NF-kappaB activation. *J Cell Biochem* 107: 1139-1149, 2009.
32. **Ciciliot S and Schiaffino S.** Regeneration of mammalian skeletal muscle. Basic mechanisms and clinical implications. *Curr Pharm Des* 16: 906-914, 2010.
33. **Clapham DE.** Calcium signaling. *Cell* 131: 1047-1058, 2007.
34. **Collins CA, Zammit PS, Ruiz AP, Morgan JE, and Partridge TA.** A population of myogenic stem cells that survives skeletal muscle aging. *Stem Cells* 25: 885-894, 2007.
35. **Conboy IM, Conboy MJ, Smythe GM, and Rando TA.** Notch-mediated restoration of regenerative potential to aged muscle. *Science* 302: 1575-1577, 2003.
36. **Cosgrove BD, Gilbert PM, Porpiglia E, Mourkioti F, Lee SP, Corbel SY, Llewellyn ME, Delp SL, and Blau HM.** Rejuvenation of the muscle stem cell population restores strength

to injured aged muscles. *Nat Med* 20: 255-264, 2014.
37. **Costamagna D, Costelli P, Sampaolesi M, and Penna F.** Role of Inflammation in Muscle Homeostasis and Myogenesis. *Mediators Inflamm* 2015: 805172, 2015.
38. **D'Souza DM, Zhou S, Rebalka IA, MacDonald B, Moradi J, Krause MP, Al-Sajee D, Punthakee Z, Tarnopolsky MA, and Hawke TJ.** Decreased Satellite Cell Number and Function in Humans and Mice With Type 1 Diabetes Is the Result of Altered Notch Signaling. *Diabetes* 65: 3053-3061, 2016.
39. **Day K, Shefer G, Shearer A, and Yablonka-Reuveni Z.** The depletion of skeletal muscle satellite cells with age is concomitant with reduced capacity of single progenitors to produce reserve progeny. *Dev Biol* 340: 330-343, 2010.
40. **de Seabra Rodrigues Dias IR, Mok SWF, Gordillo-Martinez F, Khan I, Hsiao WWL, Law BYK, Wong VKW, and Liu L.** The Calcium-Induced Regulation in the Molecular and Transcriptional Circuitry of Human Inflammatory Response and Autoimmunity. *Front Pharmacol* 8: 962, 2017.
41. **Deasy BM, Lu A, Tebbets JC, Feduska JM, Schugar RC, Pollett JB, Sun B, Urish KL, Gharaibeh BM, Cao B, Rubin RT, and Huard J.** A role for cell sex in stem cell-mediated skeletal muscle regeneration: female cells have higher muscle regeneration efficiency. *J Cell Biol* 177: 73-86, 2007.
42. **Decary S, Mouly V, Hamida CB, Sautet A, Barbet JP, and Butler-Browne GS.** Replicative potential and telomere length in human skeletal muscle: implications for satellite cell-mediated gene therapy. *Hum Gene Ther* 8: 1429-1438, 1997.
43. **Delmonico MJ, Harris TB, Visser M, Park SW, Conroy MB, Velasquez-Mieyer P, Boudreau R, Manini TM, Nevitt M, Newman AB, and Goodpaster BH.** Longitudinal study of muscle strength, quality, and adipose tissue infiltration. *Am J Clin Nutr* 90: 1579-1585, 2009.
44. **Dennis RA, Trappe TA, Simpson P, Carroll C, Huang BE, Nagarajan R, Bearden E, Gurley C, Duff GW, Evans WJ, Kornman K, and Peterson CA.** Interleukin-1 polymorphisms are associated with the inflammatory response in human muscle to acute resistance exercise. *J Physiol* 560: 617-626, 2004.
45. **Dennis RA, Zhu H, Kortebein PM, Bush HM, Harvey JF, Sullivan DH, and Peterson CA.** Muscle expression of genes associated with inflammation, growth, and remodeling is strongly correlated in older adults with resistance training outcomes. *Physiol Genomics* 38: 169-175, 2009.
46. **Doherty TJ.** Invited review: Aging and sarcopenia. *J Appl Physiol (1985)* 95: 1717-1727, 2003.
47. **Dong H, Tian L, Li R, Pei C, Fu Y, Dong X, Xia F, Wang C, Li W, Guo X, Gu C, Li B, Liu A, Ren H, and Xu H.** IFNg-induced Irgm1 promotes tumorigenesis of melanoma via dual regulation of apoptosis and Bif-1-dependent autophagy. *Oncogene* 34: 5363-5371, 2015.
48. **Egan B and Zierath JR.** Exercise metabolism and the molecular regulation of skeletal muscle adaptation. *Cell Metab* 17: 162-184, 2013.
49. **Fang F, Chen D, Yu L, Dai X, Yang Y, Tian W, Cheng X, Xu H, Weng X, Fang M, Zhou J, Gao Y, Chen Q, and Xu Y.** Proinflammatory stimuli engage Brahma related gene 1 and Brahma in endothelial injury. *Circ Res* 113: 986-996, 2013.
50. **Faulkner JA, Larkin LM, Claflin DR, and Brooks SV.** Age-related changes in the structure and function of skeletal muscles. *Clin Exp Pharmacol Physiol* 34: 1091-1096, 2007.
51. **Fazelzadeh P, Hangelbroek RW, Tieland M, de Groot LC, Verdijk LB, van Loon LJ, Smilde AK, Alves RD, Vervoort J, Muller M, van Duynhoven JP, and Boekschoten**

MV. The Muscle Metabolome Differs between Healthy and Frail Older Adults. *J Proteome Res* 15: 499-509, 2016.
52. **Ferrari MB, Ribbeck K, Hagler DJ, and Spitzer NC.** A calcium signaling cascade essential for myosin thick filament assembly in Xenopus myocytes. *J Cell Biol* 141: 1349-1356, 1998.
53. **Ferrari MB, Rohrbough J, and Spitzer NC.** Spontaneous calcium transients regulate myofibrillogenesis in embryonic Xenopus myocytes. *Dev Biol* 178: 484-497, 1996.
54. **Fiatarone MA, Marks EC, Ryan ND, Meredith CN, Lipsitz LA, and Evans WJ.** High-intensity strength training in nonagenarians. Effects on skeletal muscle. *JAMA* 263: 3029-3034, 1990.
55. **Fong Y, Moldawer LL, Marano M, Wei H, Barber A, Manogue K, Tracey KJ, Kuo G, Fischman DA, Cerami A, and et al.** Cachectin/TNF or IL-1 alpha induces cachexia with redistribution of body proteins. *Am J Physiol* 256: R659-665, 1989.
56. **Fortin M, Videman T, Gibbons LE, and Battie MC.** Paraspinal muscle morphology and composition: a 15-yr longitudinal magnetic resonance imaging study. *Med Sci Sports Exerc* 46: 893-901, 2014.
57. **Friday BB, Horsley V, and Pavlath GK.** Calcineurin activity is required for the initiation of skeletal muscle differentiation. *J Cell Biol* 149: 657-666, 2000.
58. **Friday BB, Mitchell PO, Kegley KM, and Pavlath GK.** Calcineurin initiates skeletal muscle differentiation by activating MEF2 and MyoD. *Differentiation* 71: 217-227, 2003.
59. **Frontera WR and Ochala J.** Skeletal muscle: a brief review of structure and function. *Calcif Tissue Int* 96: 183-195, 2015.
60. **Fry CS, Lee JD, Mula J, Kirby TJ, Jackson JR, Liu F, Yang L, Mendias CL, Dupont-Versteegden EE, McCarthy JJ, and Peterson CA.** Inducible depletion of satellite cells in adult, sedentary mice impairs muscle regenerative capacity without affecting sarcopenia. *Nat Med* 21: 76-80, 2015.
61. **Fujimaki S, Wakabayashi T, Takemasa T, Asashima M, and Kuwabara T.** Diabetes and stem cell function. *Biomed Res Int* 2015: 592915, 2015.
62. **Fukada S, Uezumi A, Ikemoto M, Masuda S, Segawa M, Tanimura N, Yamamoto H, Miyagoe-Suzuki Y, and Takeda S.** Molecular signature of quiescent satellite cells in adult skeletal muscle. *Stem Cells* 25: 2448-2459, 2007.
63. **Garcia-Prat L, Martinez-Vicente M, Perdiguero E, Ortet L, Rodriguez-Ubreva J, Rebollo E, Ruiz-Bonilla V, Gutarra S, Ballestar E, Serrano AL, Sandri M, and Munoz-Canoves P.** Autophagy maintains stemness by preventing senescence. *Nature* 529: 37-42, 2016.
64. **Garcia-Prat L, Sousa-Victor P, and Munoz-Canoves P.** Functional dysregulation of stem cells during aging: a focus on skeletal muscle stem cells. *FEBS J* 280: 4051-4062, 2013.
65. **Garcia-Prat L, Sousa-Victor P, and Munoz-Canoves P.** Proteostatic and Metabolic Control of Stemness. *Cell Stem Cell* 20: 593-608, 2017.
66. **Garcia SM, Tamaki S, Lee S, Wong A, Jose A, Dreux J, Kouklis G, Sbitany H, Seth R, Knott PD, Heaton C, Ryan WR, Kim EA, Hansen SL, Hoffman WY, and Pomerantz JH.** High-Yield Purification, Preservation, and Serial Transplantation of Human Satellite Cells. *Stem Cell Reports*, 2018.
67. **Gemenetzidis E, Elena-Costea D, Parkinson EK, Waseem A, Wan H, and Teh MT.** Induction of human epithelial stem/progenitor expansion by FOXM1. *Cancer Res* 70: 9515-9526, 2010.
68. **Gheller BJ, Riddle ES, Lem MR, and Thalacker-Mercer AE.** Understanding Age-

Related Changes in Skeletal Muscle Metabolism: Differences Between Females and Males. *Annu Rev Nutr* 36: 129-156, 2016.
69. **Goodpaster BH, Park SW, Harris TB, Kritchevsky SB, Nevitt M, Schwartz AV, Simonsick EM, Tylavsky FA, Visser M, and Newman AB.** The loss of skeletal muscle strength, mass, and quality in older adults: the health, aging and body composition study. *J Gerontol A Biol Sci Med Sci* 61: 1059-1064, 2006.
70. **Gorgens SW, Hjorth M, Eckardt K, Wichert S, Norheim F, Holen T, Lee S, Langleite T, Birkeland KI, Stadheim HK, Kolnes KJ, Tangen DS, Kolnes AJ, Jensen J, Drevon CA, and Eckel J.** The exercise-regulated myokine chitinase-3-like protein 1 stimulates human myocyte proliferation. *Acta Physiol (Oxf)* 216: 330-345, 2016.
71. **Green CJ, Pedersen M, Pedersen BK, and Scheele C.** Elevated NF-kappaB activation is conserved in human myocytes cultured from obese type 2 diabetic patients and attenuated by AMP-activated protein kinase. *Diabetes* 60: 2810-2819, 2011.
72. **Gregory MS, Duffner LA, Faunce DE, and Kovacs EJ.** Estrogen mediates the sex difference in post-burn immunosuppression. *J Endocrinol* 164: 129-138, 2000.
73. **Grounds MD and Yablonka-Reuveni Z.** Molecular and cell biology of skeletal muscle regeneration. *Mol Cell Biol Hum Dis Ser* 3: 210-256, 1993.
74. **Guttridge DC, Mayo MW, Madrid LV, Wang CY, and Baldwin AS, Jr.** NF-kappaB-induced loss of MyoD messenger RNA: possible role in muscle decay and cachexia. *Science* 289: 2363-2366, 2000.
75. **Haddad F, Zaldivar F, Cooper DM, and Adams GR.** IL-6-induced skeletal muscle atrophy. *J Appl Physiol (1985)* 98: 911-917, 2005.
76. **Hawke TJ and Garry DJ.** Myogenic satellite cells: physiology to molecular biology. *J Appl Physiol (1985)* 91: 534-551, 2001.
77. **Henrich CJ.** A Microplate-Based Nonradioactive Protein Synthesis Assay: Application to TRAIL Sensitization by Protein Synthesis Inhibitors. *PLoS One* 11: e0165192, 2016.
78. **Izquierdo JH, Bonilla-Abadia F, Canas CA, and Tobon GJ.** Calcium, channels, intracellular signaling and autoimmunity. *Reumatol Clin* 10: 43-47, 2014.
79. **Janssen I, Heymsfield SB, and Ross R.** Low relative skeletal muscle mass (sarcopenia) in older persons is associated with functional impairment and physical disability. *J Am Geriatr Soc* 50: 889-896, 2002.
80. **Janssen I, Heymsfield SB, Wang ZM, and Ross R.** Skeletal muscle mass and distribution in 468 men and women aged 18-88 yr. *J Appl Physiol (1985)* 89: 81-88, 2000.
81. **Javan R, Horvath JJ, Case LE, Austin S, Corderi J, Dubrovsky A, Kishnani PS, and Bashir MR.** Generating color-coded anatomic muscle maps for correlation of quantitative magnetic resonance imaging analysis with clinical examination in neuromuscular disorders. *Muscle Nerve* 48: 293-295, 2013.
82. **Jiang Y, Singh P, Yin H, Zhou YX, Gui Y, Wang DZ, and Zheng XL.** Opposite roles of myocardin and atrogin-1 in L6 myoblast differentiation. *J Cell Physiol* 228: 1989-1995, 2013.
83. **Jo E, Lee SR, Park BS, and Kim JS.** Potential mechanisms underlying the role of chronic inflammation in age-related muscle wasting. *Aging Clin Exp Res* 24: 412-422, 2012.
84. **Karalaki M, Fili S, Philippou A, and Koutsilieris M.** Muscle regeneration: cellular and molecular events. *In Vivo* 23: 779-796, 2009.
85. **Kim D, Pertea G, Trapnell C, Pimentel H, Kelley R, and Salzberg SL.** TopHat2: accurate alignment of transcriptomes in the presence of insertions, deletions and gene fusions. *Genome Biol* 14: R36, 2013.

86. **Konig S, Beguet A, Bader CR, and Bernheim L.** The calcineurin pathway links hyperpolarization (Kir2.1)-induced Ca2+ signals to human myoblast differentiation and fusion. *Development* 133: 3107-3114, 2006.
87. **Konig S, Hinard V, Arnaudeau S, Holzer N, Potter G, Bader CR, and Bernheim L.** Membrane hyperpolarization triggers myogenin and myocyte enhancer factor-2 expression during human myoblast differentiation. *J Biol Chem* 279: 28187-28196, 2004.
88. **Kuang S, Charge SB, Seale P, Huh M, and Rudnicki MA.** Distinct roles for Pax7 and Pax3 in adult regenerative myogenesis. *J Cell Biol* 172: 103-113, 2006.
89. **Langen RC, Schols AM, Kelders MC, Wouters EF, and Janssen-Heininger YM.** Inflammatory cytokines inhibit myogenic differentiation through activation of nuclear factor-kappaB. *FASEB J* 15: 1169-1180, 2001.
90. **Langen RC, Van Der Velden JL, Schols AM, Kelders MC, Wouters EF, and Janssen-Heininger YM.** Tumor necrosis factor-alpha inhibits myogenic differentiation through MyoD protein destabilization. *FASEB J* 18: 227-237, 2004.
91. **Larsson L and Ansved T.** Effects of ageing on the motor unit. *Prog Neurobiol* 45: 397-458, 1995.
92. **Latil M, Rocheteau P, Chatre L, Sanulli S, Memet S, Ricchetti M, Tajbakhsh S, and Chretien F.** Skeletal muscle stem cells adopt a dormant cell state post mortem and retain regenerative capacity. *Nat Commun* 3: 903, 2012.
93. **Leary SC, Battersby BJ, Hansford RG, and Moyes CD.** Interactions between bioenergetics and mitochondrial biogenesis. *Biochim Biophys Acta* 1365: 522-530, 1998.
94. **Lepper C, Partridge TA, and Fan CM.** An absolute requirement for Pax7-positive satellite cells in acute injury-induced skeletal muscle regeneration. *Development* 138: 3639-3646, 2011.
95. **Li YP.** TNF-alpha is a mitogen in skeletal muscle. *Am J Physiol Cell Physiol* 285: C370-376, 2003.
96. **Li YP and Reid MB.** Effect of tumor necrosis factor-alpha on skeletal muscle metabolism. *Curr Opin Rheumatol* 13: 483-487, 2001.
97. **Lindle RS, Metter EJ, Lynch NA, Fleg JL, Fozard JL, Tobin J, Roy TA, and Hurley BF.** Age and gender comparisons of muscle strength in 654 women and men aged 20-93 yr. *J Appl Physiol (1985)* 83: 1581-1587, 1997.
98. **Ling PR, Schwartz JH, and Bistrian BR.** Mechanisms of host wasting induced by administration of cytokines in rats. *Am J Physiol* 272: E333-339, 1997.
99. **Liu C, McFarland DC, and Velleman SG.** Effect of genetic selection on MyoD and myogenin expression in turkeys with different growth rates. *Poult Sci* 84: 376-384, 2005.
100. **Liu JH, Konig S, Michel M, Arnaudeau S, Fischer-Lougheed J, Bader CR, and Bernheim L.** Acceleration of human myoblast fusion by depolarization: graded Ca2+ signals involved. *Development* 130: 3437-3446, 2003.
101. **Llovera M, Lopez-Soriano FJ, and Argiles JM.** Effects of tumor necrosis factor-alpha on muscle-protein turnover in female Wistar rats. *J Natl Cancer Inst* 85: 1334-1339, 1993.
102. **Lu A, Proto JD, Guo L, Tang Y, Lavasani M, Tilstra JS, Niedernhofer LJ, Wang B, Guttridge DC, Robbins PD, and Huard J.** NF-kappaB negatively impacts the myogenic potential of muscle-derived stem cells. *Mol Ther* 20: 661-668, 2012.
103. **Lu J, McKinsey TA, Nicol RL, and Olson EN.** Signal-dependent activation of the MEF2 transcription factor by dissociation from histone deacetylases. *Proc Natl Acad Sci U S A* 97: 4070-4075, 2000.

104. **Lunt SY and Vander Heiden MG.** Aerobic glycolysis: meeting the metabolic requirements of cell proliferation. *Annu Rev Cell Dev Biol* 27: 441-464, 2011.
105. **Machida S and Booth FW.** Increased nuclear proteins in muscle satellite cells in aged animals as compared to young growing animals. *Exp Gerontol* 39: 1521-1525, 2004.
106. **Machida S, Spangenburg EE, and Booth FW.** Primary rat muscle progenitor cells have decreased proliferation and myotube formation during passages. *Cell Prolif* 37: 267-277, 2004.
107. **MacIntyre DL, Reid WD, and McKenzie DC.** Delayed muscle soreness. The inflammatory response to muscle injury and its clinical implications. *Sports Med* 20: 24-40, 1995.
108. **Manzano R, Toivonen JM, Calvo AC, Miana-Mena FJ, Zaragoza P, Munoz MJ, Montarras D, and Osta R.** Sex, fiber-type, and age dependent in vitro proliferation of mouse muscle satellite cells. *J Cell Biochem* 112: 2825-2836, 2011.
109. **Martin M.** Cutadapt removes adapter sequences from high-throughput sequencing reads. . *EMBnetjournal* 17: 10-12, 2011.
110. **Melov S, Tarnopolsky MA, Beckman K, Felkey K, and Hubbard A.** Resistance exercise reverses aging in human skeletal muscle. *PLoS One* 2: e465, 2007.
111. **Mendelsohn AR and Larrick JW.** Rejuvenating Muscle Stem Cell Function: Restoring Quiescence and Overcoming Senescence. *Rejuvenation Res* 19: 182-186, 2016.
112. **Merritt EK, Stec MJ, Thalacker-Mercer A, Windham ST, Cross JM, Shelley DP, Craig Tuggle S, Kosek DJ, Kim JS, and Bamman MM.** Heightened muscle inflammation susceptibility may impair regenerative capacity in aging humans. *J Appl Physiol (1985)* 115: 937-948, 2013.
113. **Mesires NT and Doumit ME.** Satellite cell proliferation and differentiation during postnatal growth of porcine skeletal muscle. *Am J Physiol Cell Physiol* 282: C899-906, 2002.
114. **Miller AE, MacDougall JD, Tarnopolsky MA, and Sale DG.** Gender differences in strength and muscle fiber characteristics. *Eur J Appl Physiol Occup Physiol* 66: 254-262, 1993.
115. **Miller SC, Ito H, Blau HM, and Torti FM.** Tumor necrosis factor inhibits human myogenesis in vitro. *Mol Cell Biol* 8: 2295-2301, 1988.
116. **Minet AD and Gaster M.** Cultured senescent myoblasts derived from human vastus lateralis exhibit normal mitochondrial ATP synthesis capacities with correlating concomitant ROS production while whole cell ATP production is decreased. *Biogerontology* 13: 277-285, 2012.
117. **Miska EA, Karlsson C, Langley E, Nielsen SJ, Pines J, and Kouzarides T.** HDAC4 deacetylase associates with and represses the MEF2 transcription factor. *EMBO J* 18: 5099-5107, 1999.
118. **Mitnitski A, Song X, Skoog I, Broe GA, Cox JL, Grunfeld E, and Rockwood K.** Relative fitness and frailty of elderly men and women in developed countries and their relationship with mortality. *J Am Geriatr Soc* 53: 2184-2189, 2005.
119. **Mohan A and Asakura A.** CDK inhibitors for muscle stem cell differentiation and self-renewal. *J Phys Fit Sports Med* 6: 65-74, 2017.
120. **Musatov A and Robinson NC.** Susceptibility of mitochondrial electron-transport complexes to oxidative damage. Focus on cytochrome c oxidase. *Free Radic Res* 46: 1313-1326, 2012.
121. **Nasipak BT, Padilla-Benavides T, Green KM, Leszyk JD, Mao W, Konda S, Sif S, Shaffer SA, Ohkawa Y, and Imbalzano AN.** Opposing calcium-dependent signalling pathways control skeletal muscle differentiation by regulating a chromatin remodelling enzyme. *Nat*

Commun 6: 7441, 2015.
122. **Neal A, Boldrin L, and Morgan JE.** The satellite cell in male and female, developing and adult mouse muscle: distinct stem cells for growth and regeneration. *PLoS One* 7: e37950, 2012.
123. **Nehlin JO, Just M, Rustan AC, and Gaster M.** Human myotubes from myoblast cultures undergoing senescence exhibit defects in glucose and lipid metabolism. *Biogerontology* 12: 349-365, 2011.
124. **Nelson JW, Ferdaus MZ, McCormick JA, Minnier J, Kaul S, Ellison DH, and Barnes AP.** Endothelial transcriptomics reveals activation of fibrosis-related pathways in hypertension. *Physiol Genomics* 50: 104-116, 2018.
125. **Nguyen MH, Cheng M, and Koh TJ.** Impaired muscle regeneration in ob/ob and db/db mice. *ScientificWorldJournal* 11: 1525-1535, 2011.
126. **Osterloh M, Bohm M, Kalbe B, Osterloh S, and Hatt H.** Identification and functional characterization of TRPA1 in human myoblasts. *Pflugers Arch* 468: 321-333, 2016.
127. **Oustanina S, Hause G, and Braun T.** Pax7 directs postnatal renewal and propagation of myogenic satellite cells but not their specification. *EMBO J* 23: 3430-3439, 2004.
128. **Paasuke R, Eimre M, Piirsoo A, Peet N, Laada L, Kadaja L, Roosimaa M, Paasuke M, Martson A, Seppet E, and Paju K.** Proliferation of Human Primary Myoblasts Is Associated with Altered Energy Metabolism in Dependence on Ageing In Vivo and In Vitro. *Oxid Med Cell Longev* 2016: 8296150, 2016.
129. **Padilla-Benavides T, Nasipak BT, and Imbalzano AN.** Brg1 Controls the Expression of Pax7 to Promote Viability and Proliferation of Mouse Primary Myoblasts. *J Cell Physiol* 230: 2990-2997, 2015.
130. **Pasiakos SM, Cao JJ, Margolis LM, Sauter ER, Whigham LD, McClung JP, Rood JC, Carbone JW, Combs GF, Jr., and Young AJ.** Effects of high-protein diets on fat-free mass and muscle protein synthesis following weight loss: a randomized controlled trial. *FASEB J* 27: 3837-3847, 2013.
131. **Pasiakos SM, Margolis LM, and Orr JS.** Optimized dietary strategies to protect skeletal muscle mass during periods of unavoidable energy deficit. *FASEB J* 29: 1136-1142, 2015.
132. **Pedersen BK.** Muscle as a secretory organ. *Compr Physiol* 3: 1337-1362, 2013.
133. **Perrett RM and McArdle CA.** Molecular mechanisms of gonadotropin-releasing hormone signaling: integrating cyclic nucleotides into the network. *Front Endocrinol (Lausanne)* 4: 180, 2013.
134. **Petrella JK, Kim JS, Mayhew DL, Cross JM, and Bamman MM.** Potent myofiber hypertrophy during resistance training in humans is associated with satellite cell-mediated myonuclear addition: a cluster analysis. *J Appl Physiol (1985)* 104: 1736-1742, 2008.
135. **Prothro JW and Rosenbloom CA.** Body measurements of black and white elderly persons with emphasis on body composition. *Gerontology* 41: 22-38, 1995.
136. **Puder JJ, Freda PU, Goland RS, and Wardlaw SL.** Estrogen modulates the hypothalamic-pituitary-adrenal and inflammatory cytokine responses to endotoxin in women. *J Clin Endocrinol Metab* 86: 2403-2408, 2001.
137. **Rahmatallah Y, Emmert-Streib F, and Glazko G.** Comparative evaluation of gene set analysis approaches for RNA-Seq data. *BMC Bioinformatics* 15: 397, 2014.
138. **Rantanen T, Guralnik JM, Sakari-Rantala R, Leveille S, Simonsick EM, Ling S, and Fried LP.** Disability, physical activity, and muscle strength in older women: the Women's

Health and Aging Study. *Arch Phys Med Rehabil* 80: 130-135, 1999.
139. **Rappolee DA and Werb Z.** Macrophage-derived growth factors. *Curr Top Microbiol Immunol* 181: 87-140, 1992.
140. **Rathbone CR, Wenke JC, Warren GL, and Armstrong RB.** Importance of satellite cells in the strength recovery after eccentric contraction-induced muscle injury. *Am J Physiol Regul Integr Comp Physiol* 285: R1490-1495, 2003.
141. **Ravaglia G, Forti P, Maioli F, Bastagli L, Chiappelli M, Montesi F, Bolondi L, and Patterson C.** Metabolic Syndrome: prevalence and prediction of mortality in elderly individuals. *Diabetes Care* 29: 2471-2476, 2006.
142. **Relaix F, Montarras D, Zaffran S, Gayraud-Morel B, Rocancourt D, Tajbakhsh S, Mansouri A, Cumano A, and Buckingham M.** Pax3 and Pax7 have distinct and overlapping functions in adult muscle progenitor cells. *J Cell Biol* 172: 91-102, 2006.
143. **Riddle ES, Bender EL, and Thalacker-Mercer A.** Transcript profile distinguishes variability in human myogenic progenitor cell expansion capacity. *Physiol Genomics*, 2018.
144. **Roberts BM, Lavin KM, Many GM, Thalacker-Mercer A, Merritt EK, Bickel CS, Mayhew DL, Tuggle SC, Cross JM, Kosek DJ, Petrella JK, Brown CJ, Hunter GR, Windham ST, Allman RM, and Bamman MM.** Human neuromuscular aging: Sex differences revealed at the myocellular level. *Exp Gerontol* 106: 116-124, 2018.
145. **Robertson TA, Maley MA, Grounds MD, and Papadimitriou JM.** The role of macrophages in skeletal muscle regeneration with particular reference to chemotaxis. *Exp Cell Res* 207: 321-331, 1993.
146. **Rochard P, Rodier A, Casas F, Cassar-Malek I, Marchal-Victorion S, Daury L, Wrutniak C, and Cabello G.** Mitochondrial activity is involved in the regulation of myoblast differentiation through myogenin expression and activity of myogenic factors. *J Biol Chem* 275: 2733-2744, 2000.
147. **Rocheteau P, Gayraud-Morel B, Siegl-Cachedenier I, Blasco MA, and Tajbakhsh S.** A subpopulation of adult skeletal muscle stem cells retains all template DNA strands after cell division. *Cell* 148: 112-125, 2012.
148. **Rodgers JT, King KY, Brett JO, Cromie MJ, Charville GW, Maguire KK, Brunson C, Mastey N, Liu L, Tsai CR, Goodell MA, and Rando TA.** mTORC1 controls the adaptive transition of quiescent stem cells from G0 to G(Alert). *Nature* 510: 393-396, 2014.
149. **Roos WP and Kaina B.** DNA damage-induced cell death: from specific DNA lesions to the DNA damage response and apoptosis. *Cancer Lett* 332: 237-248, 2013.
150. **Rossi CA, Pozzobon M, Ditadi A, Archacka K, Gastaldello A, Sanna M, Franzin C, Malerba A, Milan G, Cananzi M, Schiaffino S, Campanella M, Vettor R, and De Coppi P.** Clonal characterization of rat muscle satellite cells: proliferation, metabolism and differentiation define an intrinsic heterogeneity. *PLoS One* 5: e8523, 2010.
151. **Roth D and Oron U.** Repair mechanisms involved in muscle regeneration following partial excision of the rat gastrocnemius muscle. *Exp Cell Biol* 53: 107-114, 1985.
152. **Rowe RW and Goldspink G.** Muscle fibre growth in five different muscles in both sexes of mice. *J Anat* 104: 519-530, 1969.
153. **Ryall JG.** Metabolic reprogramming as a novel regulator of skeletal muscle development and regeneration. *FEBS J* 280: 4004-4013, 2013.
154. **Ryall JG, Dell'Orso S, Derfoul A, Juan A, Zare H, Feng X, Clermont D, Koulnis M, Gutierrez-Cruz G, Fulco M, and Sartorelli V.** The NAD(+)-dependent SIRT1 deacetylase translates a metabolic switch into regulatory epigenetics in skeletal muscle stem cells. *Cell Stem*

Cell 16: 171-183, 2015.
155. **Sadeh M.** Effects of aging on skeletal muscle regeneration. *J Neurol Sci* 87: 67-74, 1988.
156. **Sajko S, Kubinova L, Cvetko E, Kreft M, Wernig A, and Erzen I.** Frequency of M-cadherin-stained satellite cells declines in human muscles during aging. *J Histochem Cytochem* 52: 179-185, 2004.
157. **Sayer AA, Syddall HE, Martin HJ, Dennison EM, Roberts HC, and Cooper C.** Is grip strength associated with health-related quality of life? Findings from the Hertfordshire Cohort Study. *Age Ageing* 35: 409-415, 2006.
158. **Schmucker H, Blanding WM, Mook JM, Wade JF, Park JP, Kwist K, Shah H, and Booth BW.** Amphiregulin regulates proliferation and migration of HER2-positive breast cancer cells. *Cell Oncol (Dordr)*, 2017.
159. **Schultz E and Lipton BH.** Skeletal muscle satellite cells: changes in proliferation potential as a function of age. *Mech Ageing Dev* 20: 377-383, 1982.
160. **Seale P, Sabourin LA, Girgis-Gabardo A, Mansouri A, Gruss P, and Rudnicki MA.** Pax7 is required for the specification of myogenic satellite cells. *Cell* 102: 777-786, 2000.
161. **Shefer G, Van de Mark DP, Richardson JB, and Yablonka-Reuveni Z.** Satellite-cell pool size does matter: defining the myogenic potency of aging skeletal muscle. *Dev Biol* 294: 50-66, 2006.
162. **Sin J, Andres AM, Taylor DJ, Weston T, Hiraumi Y, Stotland A, Kim BJ, Huang C, Doran KS, and Gottlieb RA.** Mitophagy is required for mitochondrial biogenesis and myogenic differentiation of C2C12 myoblasts. *Autophagy* 12: 369-380, 2016.
163. **Skorupskaite K, George JT, and Anderson RA.** The kisspeptin-GnRH pathway in human reproductive health and disease. *Hum Reprod Update* 20: 485-500, 2014.
164. **Snow MH.** The effects of aging on satellite cells in skeletal muscles of mice and rats. *Cell Tissue Res* 185: 399-408, 1977.
165. **Stolting MN, Hefermehl LJ, Tremp M, Azzabi F, Sulser T, and Eberli D.** The role of donor age and gender in the success of human muscle precursor cell transplantation. *J Tissue Eng Regen Med* 11: 447-458, 2017.
166. **Szalay K, Razga Z, and Duda E.** TNF inhibits myogenesis and downregulates the expression of myogenic regulatory factors myoD and myogenin. *Eur J Cell Biol* 74: 391-398, 1997.
167. **Tang AH and Rando TA.** Induction of autophagy supports the bioenergetic demands of quiescent muscle stem cell activation. *EMBO J* 33: 2782-2797, 2014.
168. **Tang H, Ji F, Sun J, Xie Y, Xu Y, and Yue H.** RBEL1 is required for osteosarcoma cell proliferation via inhibiting retinoblastoma 1. *Mol Med Rep* 13: 1275-1280, 2016.
169. **Thalacker-Mercer A, Stec M, Cui X, Cross J, Windham S, and Bamman M.** Cluster analysis reveals differential transcript profiles associated with resistance training-induced human skeletal muscle hypertrophy. *Physiol Genomics* 45: 499-507, 2013.
170. **Thompson LV.** Age-related muscle dysfunction. *Exp Gerontol* 44: 106-111, 2009.
171. **Tian W, Xu H, Fang F, Chen Q, Xu Y, and Shen A.** Brahma-related gene 1 bridges epigenetic regulation of proinflammatory cytokine production to steatohepatitis in mice. *Hepatology* 58: 576-588, 2013.
172. **Tidball JG.** Inflammatory cell response to acute muscle injury. *Med Sci Sports Exerc* 27: 1022-1032, 1995.
173. **Tidball JG.** Mechanisms of muscle injury, repair, and regeneration. *Compr Physiol* 1: 2029-2062, 2011.

174. **Tierney MT, Stec MJ, Rulands S, Simons BD, and Sacco A.** Muscle Stem Cells Exhibit Distinct Clonal Dynamics in Response to Tissue Repair and Homeostatic Aging. *Cell Stem Cell* 22: 119-127 e113, 2018.
175. **Tolosa L, Morla M, Iglesias A, Busquets X, Llado J, and Olmos G.** IFN-gamma prevents TNF-alpha-induced apoptosis in C2C12 myotubes through down-regulation of TNF-R2 and increased NF-kappaB activity. *Cell Signal* 17: 1333-1342, 2005.
176. **Trapnell C, Hendrickson DG, Sauvageau M, Goff L, Rinn JL, and Pachter L.** Differential analysis of gene regulation at transcript resolution with RNA-seq. *Nat Biotechnol* 31: 46-53, 2013.
177. **Tu MK and Borodinsky LN.** Spontaneous calcium transients manifest in the regenerating muscle and are necessary for skeletal muscle replenishment. *Cell Calcium* 56: 34-41, 2014.
178. **Uezumi A, Nakatani M, Ikemoto-Uezumi M, Yamamoto N, Morita M, Yamaguchi A, Yamada H, Kasai T, Masuda S, Narita A, Miyagoe-Suzuki Y, Takeda S, Fukada S, Nishino I, and Tsuchida K.** Cell-Surface Protein Profiling Identifies Distinctive Markers of Progenitor Cells in Human Skeletal Muscle. *Stem Cell Reports* 7: 263-278, 2016.
179. **Venkatesha SH, Yu H, Rajaiah R, Tong L, and Moudgil KD.** Celastrus-derived celastrol suppresses autoimmune arthritis by modulating antigen-induced cellular and humoral effector responses. *J Biol Chem* 286: 15138-15146, 2011.
180. **von Maltzahn J, Jones AE, Parks RJ, and Rudnicki MA.** Pax7 is critical for the normal function of satellite cells in adult skeletal muscle. *Proc Natl Acad Sci U S A* 110: 16474-16479, 2013.
181. **Wagatsuma A and Sakuma K.** Mitochondria as a potential regulator of myogenesis. *ScientificWorldJournal* 2013: 593267, 2013.
182. **Wagers AJ and Conboy IM.** Cellular and molecular signatures of muscle regeneration: current concepts and controversies in adult myogenesis. *Cell* 122: 659-667, 2005.
183. **Wang Z, Gerstein M, and Snyder M.** RNA-Seq: a revolutionary tool for transcriptomics. *Nat Rev Genet* 10: 57-63, 2009.
184. **Wei F, Yan J, and Tang D.** Extracellular signal-regulated kinases modulate DNA damage response - a contributing factor to using MEK inhibitors in cancer therapy. *Curr Med Chem* 18: 5476-5482, 2011.
185. **Welle S, Tawil R, and Thornton CA.** Sex-related differences in gene expression in human skeletal muscle. *PLoS One* 3: e1385, 2008.
186. **Wen X, Wu J, Wang F, Liu B, Huang C, and Wei Y.** Deconvoluting the role of reactive oxygen species and autophagy in human diseases. *Free Radic Biol Med* 65: 402-410, 2013.
187. **West LA, Cole S, Goodkind D, and He W.** 65+ in the United States: 2010. In: *Current Population Reports*: United States Census Bureau, 2014, p. 23-212.
188. **Wilson BG and Roberts CW.** SWI/SNF nucleosome remodellers and cancer. *Nat Rev Cancer* 11: 481-492, 2011.
189. **Wu J, Lu LY, and Yu X.** The role of BRCA1 in DNA damage response. *Protein Cell* 1: 117-123, 2010.
190. **Xu Q, Ni S, Wu F, Liu F, Ye X, Mougin B, Meng X, and Du X.** Investigation of variation in gene expression profiling of human blood by extended principle component analysis. *PLoS One* 6: e26905, 2011.
191. **Xu X, Wilschut KJ, Kouklis G, Tian H, Hesse R, Garland C, Sbitany H, Hansen S,**

Seth R, Knott PD, Hoffman WY, and Pomerantz JH. Human Satellite Cell Transplantation and Regeneration from Diverse Skeletal Muscles. *Stem Cell Reports* 5: 419-434, 2015.
192. **Yang W and Hu P.** Skeletal muscle regeneration is modulated by inflammation. *J Orthop Translat* 13: 25-32, 2018.
193. **Yin H, Price F, and Rudnicki MA.** Satellite cells and the muscle stem cell niche. *Physiol Rev* 93: 23-67, 2013.
194. **Yoon MJ, Lee AR, Jeong SA, Kim YS, Kim JY, Kwon YJ, and Choi KS.** Release of Ca2+ from the endoplasmic reticulum and its subsequent influx into mitochondria trigger celastrol-induced paraptosis in cancer cells. *Oncotarget* 5: 6816-6831, 2014.
195. **Zamboni M, Zoico E, Scartezzini T, Mazzali G, Tosoni P, Zivelonghi A, Gallagher D, De Pergola G, Di Francesco V, and Bosello O.** Body composition changes in stable-weight elderly subjects: the effect of sex. *Aging Clin Exp Res* 15: 321-327, 2003.
196. **Zhang Y, Hou Y, Wang X, Ping J, Ma Z, Suo C, Lei Z, Li X, Zhang Z, Jia C, and Su J.** The effects of kisspeptin-10 on serum metabolism and myocardium in rats. *PLoS One* 12: e0179164, 2017.
197. **Zushi K and Yamazaki T.** The Effect of Reloading on Disuse Muscle Atrophy: Time Course of Hypertrophy and Regeneration Focusing on the Myofiber Cross-sectional Area and Myonuclear Change. *J Jpn Phys Ther Assoc* 15: 1-8, 2012.
198. **Zvaritch E, Depreux F, Kraeva N, Loy RE, Goonasekera SA, Boncompagni S, Kraev A, Gramolini AO, Dirksen RT, Franzini-Armstrong C, Seidman CE, Seidman JG, and Maclennan DH.** An Ryr1I4895T mutation abolishes Ca2+ release channel function and delays development in homozygous offspring of a mutant mouse line. *Proc Natl Acad Sci U S A* 104: 18537-18542, 2007.

APPENDIX

Satellite Cell Isolation

Biopsy processing

1. Prepare digest medium. Warm PBS and DMEM in 37°C water bath.
2. Remove the 60-100 mg of fresh tissue stored for 24-48h in Hibernate A (Gibco) from the 4°C refrigerator.
3. Transfer tissue from Hibernate A to sterile petri dish in biological safety cabinet.
4. Mince into approximately $1mm^3$ pieces using sterile scalpel blades.
5. Transfer minced tissue to 15mL falcon® tube containing 10mL calcium-magnesium free Dulbecco's PBS (CMF-DPBS) and allow to settle via gravity.
6. Aspirate the supernatant, being careful not to touch the pellet.
7. Resuspend the pellet in 10mL CMF-DPBS; Repeat steps 4-5.
8. Resuspend the pellet in 10mL Low Glucose DMEM (Gibco); Repeat steps 4-5.
9. Resuspend pellet in 3mL digest medium.
10. Place suspension in water bath at 37°C for 30 min, resuspending pellet every 10-15 min.
11. Add 83µL fresh digest medium and 24µL Dispase stock to the suspension. Return to the water bath.
12. Triturate every 5-10 min using a wide bore pipet tip until a uniform slurry is achieved. Note: do not incubate suspension longer than 1.5 h. The majority of the tissue should be digested within an hour. If not, check the age and concentration of the collagenase and dispase stocks.
13. Add 6mL Growth medium to the slurry and pass through a filter by pipetting the suspension through 70µm cell strainer (BD falcon 352350) into a sterile 50mL conical tube. Rinse the strainer with an additional 4mL growth medium.

14. Centrifuge 300rcf for 5 minutes at room temperature (RT).
15. Aspirate supernatant, being careful not to disturb pellet.

    Note: To prevent clumping, “flick” the pellet in minimal media, using the surface tension at the meniscus to disrupt the pellet prior to resuspending in liquid.
16. Resuspend the pellet gently in 1.5mL Recovery® freezing medium (Gibco) and place in a controlled rate chiller (1°C/min) for a minimum of 2 hours at -80C before transferring to storage box (-80C) or liquid nitrogen.

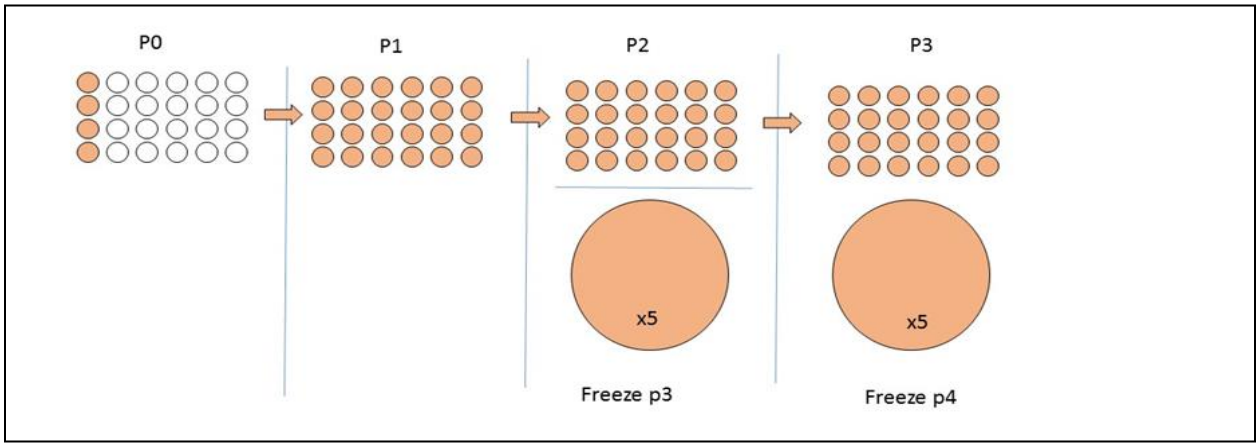

Scheme to produce high yields of low passage number cultures enriched for MPCs using the Celigo S Imaging Cytometer

The total surface area of a 24 well plate and a 10 cm plate are the same. The reason for using the 24 well plate is to continue rapidly scanning wells daily to confirm confluence (24 well plates scan much more rapidly than the 10 cm plates on the Celigo). Also the time of the scan can be shortened by only scanning a fraction of the wells, making each confluence scan last between 3-5 minutes before the plate is returned to the incubator. The 10cm plates are not scanned daily, but their total cell counts are compared to the total cell counts of the 24 well plate and have shown not to differ significantly. This shows that the rate of proliferation of the cells does not vary with the size (or edge effect) of the vessels. Due to the highly motile nature of the cells, yielding variable coverage of the well, much more precise measurements of cell confluence are obtained with the Celigo as the entire wells are scanned, instead of portions of wells. To save cells, we only measure confluence so the cells are not sacrificed. However, total nuclei counts could also be performed on single wells, thus sacrificing a very small percentage of cells per passage if using the 24 well plates.

Collagen Coating

Collagen solution

Prepare at time of use. Keep on ice. Do not store.

1. Make 20mM Acetic Acid (add glacial acetic acid to 10mOhm water in fume hood).

Water	HoAc	Collagen
200 ml	230µL	2.8mL
300	345	4.2
50	57.5	0.700

2. Add Type 1 Rat Tail Collagen (Corning) to a final concentration of 50µg/mL.
3. Filter through a 0.22µm filter.

   Note: Collagen solution comes at varying concentration. Be sure to dilute appropriately.

   Note: Make only the amount of collagen solution necessary to coat the desired number of plates. Keep solution on ice prior to plating.

Collagen coating culture vessels

1. Apply 5µg/cm^2 freshly prepared **collagen solution** to vessels.
   - 50µL to each well of 96 well plate
   - 250µL each well of to 24 well plate
   - 2mL to each well of 6 well plate
   - 8mL to 10cm plate
2. Cover plates and leave in BSC for 12 hours (overnight).

3. Aspirate collagen solution and set plates on their lids, leaving them open in the BSC until completely dry.
4. Store at 4°C in a sealed bag or container to maintain sterility for up to one month.

   Note: many protocols say to rinse the collagen coated wells with PBS before drying, but we have found that this can disrupt the collagen gel and leave a precipitate of salts on the surface. The purpose of rinsing is to remove any acid from the wells during the coating process. This is taken care of by the pre-equilibration step prior to culture.

Passaging Cells

Passage 0: Using the processed biopsy slurry ("Participant" stored in Recovery® at -80°C after biopsy processing)

1. For each biopsy slurry, add 250µL freshly prepared GM to each of 4 wells of a collagen coated 24-well plate. Pre-equilibrate for 1-2h at 37°C/5%CO2/Air. To prevent evaporation, fill unused wells with 500µL F12 or PBS. At the same time, place freshly prepared GM in glass in the incubator. Leave bottle cap loose as with autoclaving to allow gas to reach the media.
2. Rapidly thaw vial of P0 slurry in 37°C water bath until only very small ice crystals remain.

   Note: Thaw less than 5 minutes. Make sure water is NOT above 40°C. Never trust the thermostat. Use a thermometer.
3. Transfer contents of tube to a 15mL falcon tube containing 10mL Ham's F12 + 20% FBS and gently but rapidly mix by inversion.
4. Centrifuge at 300rcf for 5 min at RT in swinging bucket rotor.

5. Aspirate supernatant, being careful not to disturb the pellet.

   Note: **Dislodge/loosen the pellet** by gently "flicking" the tube, using the surface tension of the small amount of media remaining to help dislodge the pellet. This will help prevent clumping and cell death due to shear forces.

   Note: Keep cell suspensions on ice when not working with them to prevent clumping and adhesion to the centrifuge tube. Tubes of cells can be handled and centrifuged at RT.
6. Gently resuspend pellet in 1mL GM.
7. Seed P0 culture by pipetting 250µL cell suspension into each of 4 wells containing pre-equilibrated GM in a 24 well plate.
8. Incubate 37C/5%CO2/Air for 24 hours.
9. Aspirate media containing debris and dead cells; replace with 500µL fresh GM.
10. Perform baseline **confluence scan** using Celigo® S imaging cytometer; return to incubator.
11. Replace GM containing fresh bFGF every 2 days.
12. Perform **confluence scan** daily until confluence reaches 70-75%.

    Note: Passage 0 cells will often show a 2-3 day lag phase.

Passage 1: Trypsinization and splitting of passage 0 cultures (24 well plates)

1. When confluence scan shows cells to be 75-80% confluent in all four wells of the passage 0 culture, pre-equilibrate one entire collagen coated 24 well plate for a minimum of two hours, using 250µL GM per well (total 6mL GM).
2. Aspirate media from the 4 passage 0 wells
3. Add 250µL 0.25% Trypsin-EDTA to each of 4 wells.

4. Return to incubator for 3-5 minutes, checking periodically for the state of detachment using a phase contrast microscope (EVOS).
5. As soon as cells have rounded up and detached from the plate surface, pool the contents of the wells and transfer the resulting 1mL of cells suspended in 0.25% Trypsin-EDTA to 5mL fresh GM in a 15mL Falcon tube to inactivate trypsin.
6. Rinse all wells with fresh GM and pool with cell suspension in Falcon tube.
7. Place on ice until centrifugation if processing more than one participant culture. This will prevent cell clumping.
8. Centrifuge at 300 rcf for 5 min at RT.
9. Aspirate supernatant, loosen pellet, gently resuspend with 6 mL GM.
10. Seed each well of a 24 well plate with 250 μL suspended cells (this is a 1:6 split).
11. Incubate 37°C/5%CO2/Air for 24 hours.
12. Perform passage 1 baseline **confluence scan** using Celigo® S imaging cytometer; return to incubator.
13. Aspirate media, replace with 500mL GM containing fresh bFGF every 2 days.
14. Perform **confluence scan** daily until confluence reaches 70-75%.

    Note: Passage 1 cultures often do not have a lag phase.

Passage 2: Trypsinization and splitting of passage 1 cultures

1. When confluence scan shows cells to be 75-80% confluent in all 24 wells of the passage 1 culture, pre-equilibrate passage 2 vessels: one entire collagen coated 24 well plate with 250μL GM per well and five (5) collagen coated 10cm plates with 8mL GM per plate per participant culture for a minimum of two hours.

2. Add 250µL 0.25% Trypsin-EDTA to each of the 24 wells of the passage 1 plate.
3. Return to incubator for 3-5 minutes, checking periodically for the state of detachment using a phase contrast microscope (EVOS).
4. As soon as cells have rounded up and detached from the plate surface, pool the contents of the wells and transfer the resulting 6mL of cells suspended in 0.25% Trypsin-EDTA to a 15mL Falcon.
5. Rinse all wells with an additional 6mL (250µL per well) fresh GM and add to falcon tube.
6. Place on ice until centrifugation if processing more than one participant culture. This will prevent cell clumping.
7. Centrifuge at 300rcf for 5min at RT.
8. Aspirate supernatant, loosen pellet, gently resuspend with 6 mL GM. Place on ice until seeding.
9. To each of the five 10 cm plates containing 8mL pre-equilibrated GM, add 1 mL cell suspension. Be sure to gently mix the suspension before pipetting as the cells will settle rapidly. Distribute cells equally by moving the plate as described above.
10. Add 5mL GM to the remaining 1mL cell suspension in the Falcon tube and mix gently to resuspend cells.
11. Seed each well of a 24 well plate containing 250µL pre-equilibrated media per well with 250 µL suspended cells.
12. Incubate 37C/5%CO2/Air for 24 hours.
13. Perform passage 1 baseline **confluence scan** using Celigo® S imaging cytometer; return to incubator.

14. Aspirate media and replace with 500mL GM containing fresh bFGF every 2 days.
15. Perform **confluence scan** daily until confluence reaches 70-75%.

    Note: Passage 2 cultures often do not have a lag phase.

Passage 3: Trypsinization, splitting and cryopreservation of passage 2 cultures

1. When confluence scan shows cells to be 75-80% confluent in all 24 wells of the passage 1 culture, pre-equilibrate one entire collagen coated 24 well plate with 250µL GM per well and five (5) collagen coated 10cm plates with 8mL GM per plate for a minimum of two hours.
2. Aspirate media from the 24 passage 2 wells.
3. Add 250µL 0.25% Trypsin-EDTA to each of 24 wells.
4. Return to incubator for 3-5 minutes, placing each plate in direct contact with the metal shelf of the incubator.
5. Remove the five 10cm plates from the incubator and aspirate the media.
6. Add 2mL 0.25% Trypsin-EDTA to each 10 cm plate, ensuring the media is distributed evenly over the entire surface.
7. Return the five 10 cm plates to the incubator, placing each plate in direct contact with the metal shelf of the incubator.
8. Immediately check the 24 well plate for detachment using the EVOS. The cells should be detached by this time.
9. Pool the contents of the 24 wells and transfer the resulting 6mL of cells suspended in 0.25% Trypsin-EDTA to a 15mL Falcon.

10. Rinse all wells with an additional 6mL (250µL per well) fresh GM and add to falcon tube labeled with the participant number and “24”.
11. Place on ice.
12. Immediately check one 10 cm plate for detachment using the EVOS. The cells should be detached by this time.
13. Remove the cells from each 10cm dish by holding the plate at an angle and rinsing the plate surface with the 2 mL trypsin solution, allowing it to collect at the bottom edge of the dish. Transfer the contents of each dish to a 15mL falcon tube (10mL total) labeled with the participant number and “10”.
14. Add 2mL FBS to the falcon tube to neutralize the trypsin and balance the tube with the pooled cells from the 24 well plate. Place on ice.
15. Centrifuge both tubes at 300rcf for 5min at RT.
16. Aspirate supernatant from each pellet and dislodge the pellet. The pellet from the “10” tube should be approximately 5 times the size of the “24” tube.
17. Resuspend each pellet with 1mL GM per “10 cm plate”, meaning resuspend the “24” pellet in 1 mL GM and resuspend the “10” pellet with 5 mL GM.
18. Place both suspensions on ice.
19. Dilute 10µL from each cell suspension 1:10 in Moxi Z Diluent and determine the number of cells in each culture. There should be the same number of cells per mL at this point. Record the cell concentration.
20. Pool the two suspensions into one tube and mix gently.
21. Cryopreservation

a. For passage 3 cryopreservation, prepare 8 sterile cryovials and label **(Side: Study ID, Participant number, P3, Date; Top (insert) Participant number, P3).** In the BSC, open all of the tubes and place them in a white Styrofoam rack.
b. In a 50mL Falcon tube, prepare cryopreservation media by combining 3mL GM with 800µL DMSO. Chill on ice.
c. Working rapidly but pipetting gently, transfer 5mL of the cell suspension to the prepared cryopreservation media and mix by gentle trituration. The concentration of DMSO is now 10%.
d. Immediately distribute the suspension equally to the open cryotubes, cap the tubes, transfer them to a controlled rate isopropanol chiller (Mr. Frosty) and place in a -80°C freezer for a minimum of 4 h before transferring cultures to storage boxes.

22. Add 5mL GM to the remaining 1mL cell suspension in the Falcon tube and mix gently to resuspend cells.
23. Retrieve the five 10 cm plates containing 8 mL pre-equilibrated GM from the incubator and add 1mL cell suspension to each. Be sure to gently mix the suspension before pipetting as the cells will settle rapidly. Distribute cells equally by moving the plate as described above. Return plates to the incubator.
24. Add 5mL GM to the remaining 1mL cell suspension in the Falcon tube and mix gently to resuspend cells.
25. Retrieve the prepared 24 well plate containing 250µL pre-equilibrated media per well from the incubator and seed each well with 250µL suspended cells. Return plate to incubator.

26. Incubate 37C/5%CO2/Air for 24 h.
27. Perform passage 3 baseline **confluence scan** using Celigo® S imaging cytometer; return to incubator.
28. Aspirate media, replace with 500mL GM containing fresh bFGF every 2 days.
29. Perform **confluence scan** daily until confluence reaches 70-75%.

Passage 4: Trypsinization and cryopreservation of passage 3 cultures

1. When the confluence scan shows cells to be 75-80% confluent in all 24 wells of the passage 1 culture, prepare 18 cryovials **(Side: Study ID, Participant number, P4, Date; Top Participant number, P4).**
2. Aspirate media from the 24 passage 2 wells.
3. Add 250µL 0.25% Trypsin-EDTA to each of 24 wells.
4. Return to incubator for 3-5 min, placing each plate in direct contact with the metal shelf of the incubator.
5. Remove the five 10cm plates from the incubator and aspirate the media.
6. Add 2mL 0.25% Trypsin-EDTA to each 10 cm plate, ensuring the media is distributed evenly over the entire surface.
7. Return the five 10 cm plates to the incubator, placing each plate in direct contact with the metal shelf of the incubator.
8. Immediately check the 24 well plate for detachment using the EVOS. The cells should be detached by this time.
9. Pool the contents of the 24 wells and transfer the resulting 6mL of cells suspended in 0.25% Trypsin-EDTA to a 15mL Falcon tube.

10. Rinse all wells with an additional 6mL (250µL per well) fresh GM and add to falcon tube labeled with the participant number and “24”.
11. Place on ice.
12. Immediately check one 10 cm plate for detachment using the EVOS. The cells should be detached by this time.
13. Remove the cells from each 10cm dish by holding the plate at an angle and rinsing the plate surface with the 2 ml trypsin solution, allowing it to collect at the bottom edge of the dish. Transfer the contents of each dish to a 15mL falcon tube (10mL total) tube labeled with the participant number and “10”.
14. Add 2mL FBS to the falcon tube to neutralize the trypsin and balance the tube with the pooled cells from the 24 well plate. Place on ice.
15. Centrifuge both tubes at 300rcf for 5min at RT.
16. Aspirate supernatant from each pellet and dislodge the pellet. The pellet from the “10” tube should be approximately 5 times the size of the “24” tube.
17. Resuspend each pellet with 1mL GM per “10 cm plate”, meaning resuspend the “24” pellet in 1 ml GM and resuspend the “10” pellet with 5 mL GM.
18. Place both suspensions on ice.
19. Dilute 10µL from each cell suspension 1:10 in Moxi Z Diluent and determine the number of cells in each culture. There should be the same number of cells per mL at this point. Record the cell concentration.
20. Cryopreservation:

a. For passage 4 cryopreservation, prepare 16 sterile cryovials and label **(Side: Study ID, Participant number, P4, Date; Top Participant number, P4).** In the BSC, open all of the tubes and place them in a white Styrofoam rack.
b. In a 50mL Falcon tube, prepare cryopreservation media by combining 10mL GM with 1600µL DMSO. Chill on ice.
c. Working rapidly but pipetting gently, transfer all 6mL of the cell suspension to the prepared cryopreservation media and mix by gentle trituration. The concentration of DMSO is now 10%.
d. Immediately distribute the suspension equally to the open cryotubes, cap the tubes, transfer them to a controlled rate isopropanol chiller (Mr. Frosty) and place in a -80°C freezer for a minimum of 4 h before transferring cultures to storage boxes.

FACS sorting cultures to obtain homogeneous living MPCs (CD56+/CD29+)

1. Pre-equilibrate plates for culture after sorting. Place in incubator 1x24 well 500µL per well, 2x10cm, 9mL per plate for each culture.
2. Two hours prior to sorting, rapidly thaw 1-1.5 million cryopreserved passage 4 cells (1-2 vials).

   Note: If sorting cultures from more than one participant, handle each culture independently, keeping all cell suspensions on ice when not being processed.
3. Transfer entire contents of cryovials to 15mL falcon tube containing 10mL GM 10mL GM into labeled 15mL Falcon tube, labeled with participant number.

4. Mix gently by inversion and place on ice until centrifugation if preparing more than one culture.
5. Centrifuge at 300rcf for 5min at RT.
6. Aspirate supernatant and dislodge pellet.

   Note: 1-2 million cells should produce a visible pellet. If pellet is not visible, perform a cell count with the Moxi and thaw more vials of cells if necessary. Be sure you have sufficient cells before processing.
7. Resuspend pellet in 3mL FACS buffer.
8. Centrifuge at 300rcf for 5min at RT.
9. Aspirate supernatant, dislodge pellet.
10. Resuspend pellet in 250µL FACS buffer. Place on ice.
11. For Live/Dead controls, pool 50µL from each tube of resuspended cells in a 1.7mL microfuge tube. Place on ice until step 16.
12. From this point on, turn off lights in BSC and protect samples from direct light or sunlight.
13. Prepare antibody cocktail consisting of 5µL CD56 AF488 and 8µL CD56 PE-Cy7 per culture (for four cultures combine 21µL CD56 AF488 and 33.6 µL CD56 PE-Cy7).
14. Add 13µL antibody cocktail to the suspended cells and incubate 30 min in the dark on ice.
15. Prepare Compensation controls for fluorochrome gating.
    a. Vortex eBeads, one drop =50µL. Prepare a separate control for each antibody.
    b. Combine 1 drop eBeads with 1µL antibody in 1.7mL microfuge tube.
    c. Incubate in the dark on ice for a minimum of 15 min.

d. Add 1.5mL FACS buffer to beads and vortex.

e. Centrifuge 500rcf in microfuge for 5min at RT (to save time, this step can be performed at the same time as step 16e).

f. Locate the pellet. It will move to the bottom of the tube and be difficult to see. Aspirate supernatant, and resuspend beads in 200µL FACS buffer.

g. Transfer antibody conjugated beads to culture tube. Keep on ice in dark.

16. Prepare live/dead gating controls.

a. Evenly divide the total volume of pooled cell suspension from step 11 into two 1.7mL Microfuge tubes.

b. Label one tube "dead" and add 500µL 70% ethanol to the cell suspension.

c. Label another tube "live" and add 1.5 ml FACS buffer to the tube.

d. Add 1mL FACS buffer to the "dead" tube.

e. Centrifuge 500rcf in microfuge for 5min at RT (to save time, this step can be performed at the same time as step 15e).

f. Aspirate the supernatants. Resuspend each pellet in 150µL FACS buffer.

g. Pool "live" and "dead" cells in a culture tube. Keep on ice in dark.

17. Wash cultures stained with antibody cocktail.

a. Add 10mL FACS buffer to each culture.

b. Centrifuge 300rcf for 5min at RT.

c. Aspirate supernatant and dislodge pellet.

d. Resuspend each pellet in 300µL FACS buffer and transfer to labeled culture tube.

e. Store on ice in the dark.

18. Prepare collection tubes for each culture by pipetting 300μL FACS into two culture tubes per culture to be sorted. Label each with the participant number. One should be labeled CD56+/CD29+ (++) and the other CD56-/CD29+ (+-).
19. Perform live/dead staining on live/dead controls and cultures stained with antibody cocktail just prior to leaving for the FACS facility.
    a. Add 1μL 7AAD to each culture to be sorted.
    b. Add 1μL 7AAD to live/dead control prepared in step 16.
20. Transport all samples to FACS facility on ice in the dark. Follow university guidelines and regulations for transport.
21. FACS sort cultures.
    a. Use ND2 filter for mammalian cells.
    b. Compensation beads for CD56, check voltage, record.
    c. Compensation beads for CD29, check voltage, record.
    d. Run compensation controls (each AB and live dead).
    e. Gate based on side/forward scatter and 7AAD negativity.
    f. Sort living cells into ++ and +- populations, and record number of events in each category. Use these numbers when seeding cells back into culture plates.
22. As soon as possible, resuspend the sorted ++ cells for each culture in GM.
23. Centrifuge at 300rcf for 5min at RT.
24. Aspirate supernatant, dislodge pellet and resuspend in 1mL GM.
25. Based on the event count from the FACS sort, seed all cells at recommended densities in pre-equilibrated, collagen coated plates.

a. Seed all wells of the 24 well plate (if possible) with 10,000 cells per well for Celigo Scanning.
b. Seed 10cm plates with the remainder of the cells (if there are any) at a density of ~175,000 cells per plate.

Note: As a rule of thumb, seed one well/plate at higher than the recommended density if there are not enough cells to seed two at the recommended density.

26. Return plates to incubator and culture 37°C/5%CO2/Air for 24 h.
27. Perform passage 4 ++ baseline **confluence scan** using Celigo® S imaging cytometer; return to incubator.
28. Aspirate media, replace with 500mL GM containing fresh bFGF every 2 days.
29. Perform **confluence scan** daily until confluence reaches 70-75%.

Passage 5: Trypsinization and splitting of cultures

At this point we find that the rate of proliferation will slow significantly for the CD56+/CD29+ culture. These cultures will also show a lag phase, and may also reach a growth plateau before reaching 75% confluence. Daily confluence scans will make this easily detectible. If the culture shows a growth plateau after exponential growth for two successive days, split the culture. Some cultures may proliferate very slowly without reaching a plateau or 75%. If this is the case split the culture after 7 days.

1. When confluence scan shows the ++ cells for a participant culture to be an average of 75-80% confluent in the 24 well plate, pre-equilibrate one entire collagen coated 24 well plate with 250µL GM per well and five (5) collagen coated 10cm plates with 8mL GM per plate per sorted culture for a minimum of two hours. If any 10 cm plates were

seeded, prepare two labeled cryovials per 10 cm plate **(Side: Study ID, Participant number, P5++, Date; Top (insert) Participant number, P5++).**

2. Aspirate media from the passage 4++ wells of the 24 well plate.
3. Add 250µL 0.25% Trypsin-EDTA to each of Passage 4 ++ wells of the 24 well plate.
4. Return to incubator for 3-5 min, placing each plate in direct contact with the metal shelf of the incubator.
5. Remove 10cm plate(s) from the incubator and aspirate the media.
6. Add 2mL 0.25% Trypsin-EDTA to each 10 cm plate, ensuring the media is distributed evenly over the entire surface.
7. Return the 10 cm plate(s) to the incubator, placing each plate in direct contact with the metal shelf of the incubator.
8. Immediately check the 24 well plate for detachment using the EVOS. The cells should be detached by this time.
9. Pool the contents of the 24 wells and transfer the resulting 6mL of cells suspended in 0.25% Trypsin-EDTA to a 15mL Falcon.
10. Rinse all wells with an additional 6mL (250µL per well) fresh GM and add to falcon tube labeled with the participant number and "24".
11. Place on ice.
12. Immediately check one 10 cm plate for detachment using the EVOS. The cells should be detached by this time.
13. Remove the cells from each 10 cm dish by holding the plate at an angle and rinsing the plate surface with the 2 mL trypsin solution, allowing it to collect at the bottom edge of

the dish. Transfer the contents of each dish to a 15mL falcon tube labeled with the participant number, and "10". Add GM to the tube to match the volume of the "24" tube.

14. Keep cells on ice if processing more than one participant culture. Process all cultures separately, and keep on ice until centrifugation. It is very rare that all four sorted cultures will reach the same stage of confluence on the same day. It is often best to process 1-2 cultures per day/interval, as more than that will lead to mistakes and extended times out of the incubator.
15. Centrifuge for 300rcf for 5min at RT.
16. Aspirate supernatants, dislodge pellets.
17. Resuspend "10" pellet in 1mL GM and place on ice until step 22.
18. Resuspend "24" pellet in 6mL GM, seed plates, and mix gently to resuspend cells.
19. Retrieve the five 10 cm plates containing 8mL pre-equilibrated GM from the incubator and add 1 mL cell suspension to each. Be sure to gently mix the suspension before pipetting as the cells will settle rapidly. Distribute cells equally by moving the plate as described above. Return plates to the incubator.
20. Add 5mL GM to the remaining 1mL cell suspension in the Falcon tube and mix gently to resuspend cells.
21. Retrieve the prepared 24 well plate containing 250µL pre-equilibrated media per well from the incubator and seed each well with 250µL suspended cells. Return plate to incubator.
22. Count and cryopreserve any additional cells from the 10 cm plates.
    a. Gently resuspend the cells in the "10" tube and dilute 10µL 1:10 in Moxi Z Dilutent and determine the number of cells per mL in the tube.

b. In the BSC, open the two prepared cryovials and place them in a white Styrofoam rack.
c. In a 15 ml falcon tube, prepare cryopreservation medium by combining 1mL GM with 200µL DMSO and chill on ice.
d. Add the 1mL "10" cell suspension to the cold cryoprpreservation medium and mix gently by pipetting. The concentration of DMSO is now 10%.
e. Immediately distribute the suspension equally to the prepared cryotubes, cap the tubes, transfer them to a controlled rate isopropanol chiller (Mr. Frosty), and place in a -80°C freezer for a minimum of 4 h before transferring cultures to storage boxes.

23. Incubate the seeded passage 5++ cells at 37°C/5%CO2/Air for 24 h.
24. Perform passage 5++ baseline **confluence scan** using Celigo® S imaging cytometer; return to incubator.
25. Aspirate media, replace with 500mL GM containing fresh bFGF every 2 days.
26. Perform **confluence scan** daily until confluence reaches 70-75%.

Passage 6: Trypsinization and cryopreservation of passage 6++ cultures. (This is the same as Passage 4.)

1. When the confluence scan shows cells to be 75-80% confluent in all 24 wells of the passage 5++ culture, prepare 16 cryovials. **(Side: Study ID, Participant number, P6++, Date; Top (insert) Participant number, P6++).**
2. Aspirate media from the 24 passage 5++ wells.
3. Add 250µL 0.25% Trypsin-EDTA to each of 24 wells.

4. Return to incubator for 3-5 minutes, placing each plate in direct contact with the metal shelf of the incubator.
5. Remove the five 10cm plates from the incubator and aspirate the media.
6. Add 2mL 0.25% Trypsin-EDTA to each 10 cm plate, ensuring the media is distributed evenly over the entire surface.
7. Return the five 10 cm plates to the incubator, placing each plate in direct contact with the metal shelf of the incubator.
8. Immediately check the 24 well plate for detachment using the EVOS. The cells should be detached by this time.
9. Pool the contents of the 24 wells and transfer the resulting 6mL of cells suspended in 0.25% Trypsin-EDTA to a 15mL Falcon tube.
10. Rinse all wells with an additional 6mL (250µL per well) fresh GM and add to falcon tube labeled with the participant number and "24".
11. Place on ice.
12. Immediately check one 10 cm plate for detachment using the EVOS. The cells should be detached by this time.
13. Remove the cells from each 10cm dish by holding the plate at an angle and rinsing the plate surface with the 2 mL trypsin solution, allowing it to collect at the bottom edge of the dish. Transfer the contents of each dish to a 15mL falcon tube (10mL total) tube labeled with the participant number and "10".
14. Add 2mL FBS to the falcon tube to neutralize the trypsin and balance the tube with the pooled cells from the 24 well plate. Place on ice.
15. Centrifuge both tubes at 300rcf for 5min at RT.

16. Aspirate supernatant from each pellet and dislodge the pellet. The pellet from the “10” tube should be approximately 5 times the size of the “24” tube.
17. Resuspend each pellet with 1mL GM per “10 cm plate”, meaning resuspend the “24” pellet in 1 mL GM and resuspend the “10” pellet with 5 mL GM.
18. Place both suspensions on ice.
19. Dilute 10µL from each cell suspension 1:10 in Moxi Z Diluent and determine the number of cells in each culture. There should be the same number of cells per mL at this point. Record the cell concentration.
20. Cryopreservation:
    a. In the BSC, open all 16 of the prepared cryovials and place them in a white Styrofoam rack.
    b. In a 50mL Falcon tube, prepare cryopreservation media by combining 10mL GM with 1600µL DMSO. Chill on ice.
    c. Working rapidly but pipetting gently, transfer all 6mL of the cell suspension to the prepared cryopreservation media and mix by gentle trituration. The concentration of DMSO is now 10%.
    d. Immediately distribute the suspension equally to the open cryotubes, cap the tubes, transfer them to a controlled rate isopropanol chiller (Mr. Frosty) and place in a -80°C freezer for a minimum of 4 hours before transferring cultures to storage boxes.

FACS Protocol

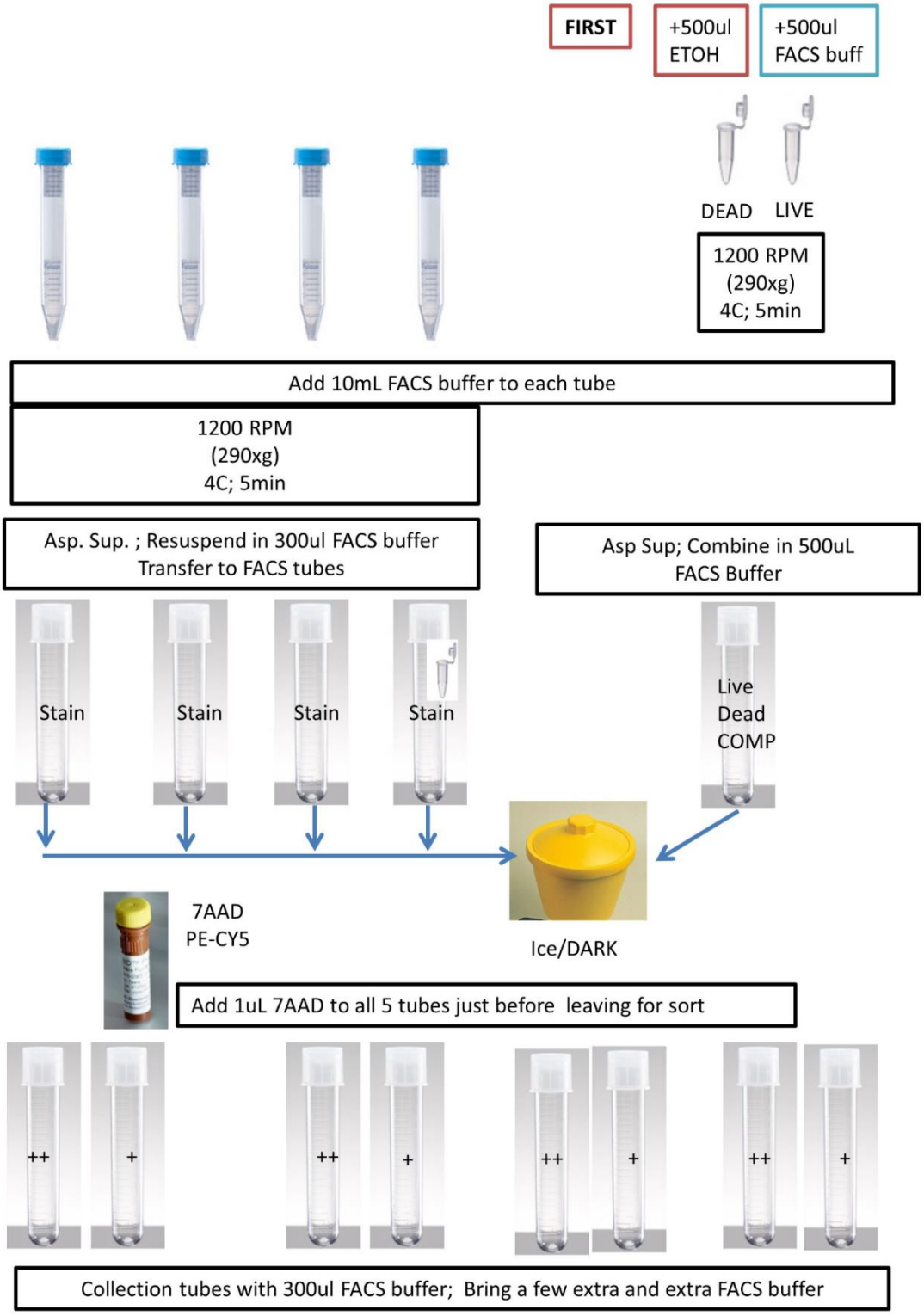

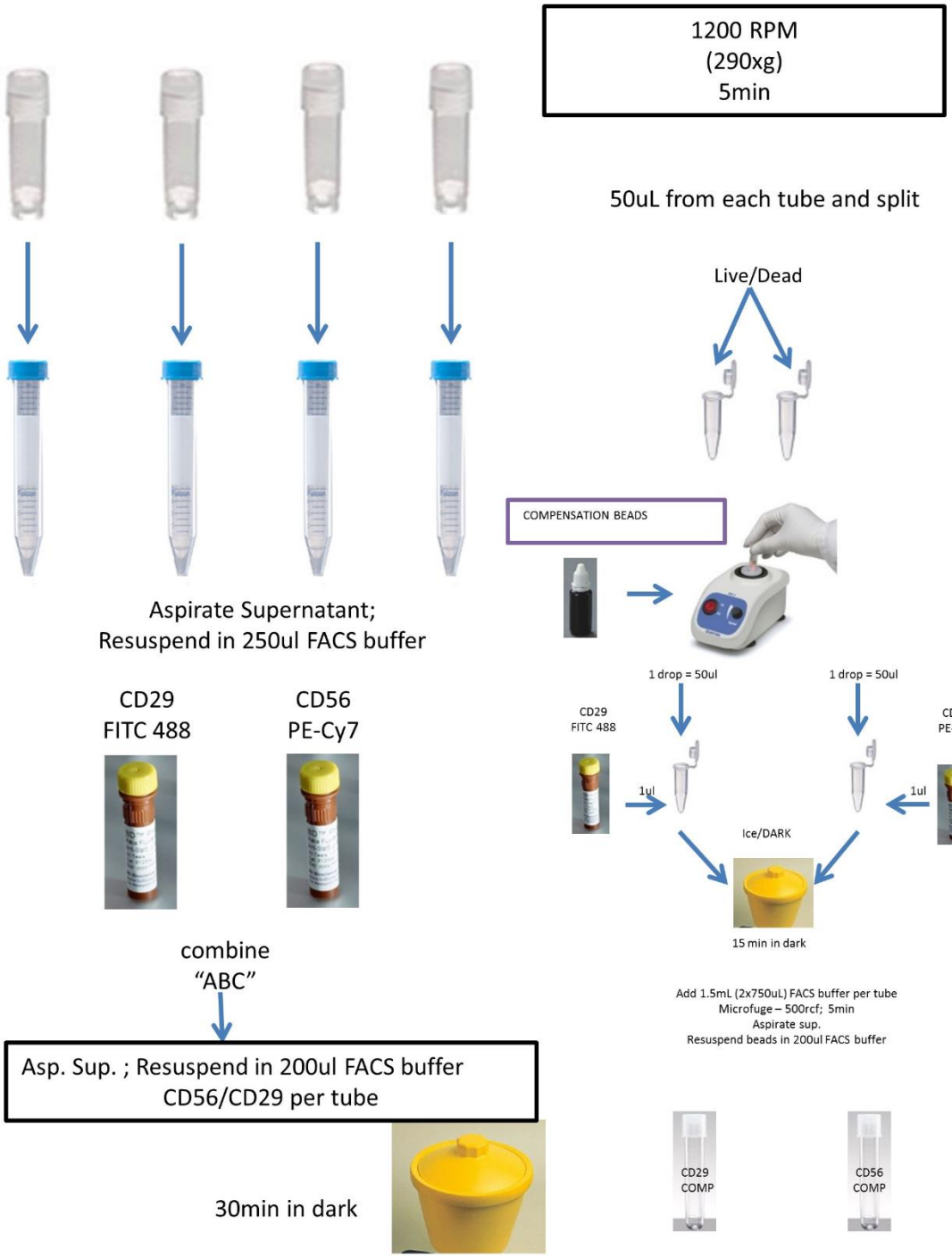
1200 RPM
(290xg)
5min
50uL from each tube and split
Live/Dead
COMPENSATION BEADS
Aspirate Supernatant;
Resuspend in 250ul FACS buffer
CD29
FITC 488
CD56
PE-Cy7
1 drop = 50ul
1 drop = 50ul
CD29
FITC 488
CD56
PE-Cy7
1ul
1ul
Ice/DARK
15 min in dark
combine
"ABC"
Add 1.5mL (2x750uL) FACS buffer per tube
Microfuge – 500rcf; 5min
Aspirate sup.
Resuspend beads in 200ul FACS buffer
Asp. Sup. ; Resuspend in 200ul FACS buffer
CD56/CD29 per tube
30min in dark
CD29
COMP
CD56
COMP

Live/Dead Staining

Cell staining

1. Prepare propidium iodide and Hoechst mixed dye solution (6mL F12 + 6μL propidium iodide + 2 μL Hoechst).
2. Remove media from all wells and add 200 μL of mixed dyes solution.
3. Incubate cells for 20 min at 5% CO_2, 37 °C.
4. Remove media from all wells and add 200 μL of F12.
5. As cells are live in the wells, the place should be imaged immediately on the Celigo.

Celigo imaging

1. Create a new scan and name file appropriately
2. Scan Tab: Select Celigo Application: Cell Viability (live + dead + total)
3. Setup Live Channel
    a. Select Brightfield Channel
    b. Auto exposure
    c. Register Auto
4. Setup Dead Channel
    a. Select Red illumination for Propidium Iodide stain
    b. Auto exposure
    c. Set offset
5. Setup Total Channel
    a. Select Blue illumination for Hoescht stain
    b. Auto exposure
    c. Set offset

6. Start scan

RNA Isolation

1. Heat water to 56°C
2. Run lysate (prepared with buffer TRK) through homogenizer column
3. Spin; 10,000 g; 1 minute (keep filtrate!)
4. Add one volume 70% ethanol; mix gently by repipetting
5. Transfer to spin column (orange); 10,000 g; 1 minute
6. Discard filtrate (the RNA is now attached to filter column)
7. Add 250 μL RNA wash buffer 1 to orange column reservoir; 10,000 g; 1 minute
8. Discard filtrate
9. DNAse Digest: Apply 75 μL DNAse solution to the column membrane; incubate 15 min on bench
    a. Prepare DNAse solution: 10 μL DNAse stock + 70 μL buffer RDD for each sample to be treated
    b. 6 samples: 60 μL DNAse stock + 42 μL buffer RDD
10. Add 250 μL RNA wash buffer 1 to column reservoir; 10,000 g; 1 minute
11. Discard filtrate
12. Add 500 μL wash buffer II to column reservoir; 10,000 g; 1 minute
13. Discard filtrate
14. Add 500 μL wash buffer II to column reservoir; 10,000 g; 1 minute
15. Discard filtrate
16. Spin empty column 10,000 g; 2 minutes

17. Apply 50 μL RNAse free water to column membrane heated to 56 degrees; incubate 5-15 minutes on bench – this will allow the RNA to detach from the membrane in the column
18. Elute RNA by spinning into clean conical tube (cut the top off) 10,000g; 1 minute
19. Keep RNA on ice or colder

Spectromax

1. Plate reader has 24 spots
2. Top left corner, put blank
3. Set machine to blank to that
4. Load samples (2.5 μL)
5. Protocol on desktop (5 mm RNA?)
6. Run

cDNA Synthesis from RNA by Reverse Transcription

RNA can be reverse transcribed into cDNA using reverse transcriptase. RNA expression can then be quantified using the cDNA and quantitative PCR (RT-qPCR).

1. Determine RNA dilutions: Using the High Capacity cDNA Synthesis Kit from Applied Biosciences, you can load a maximum of 2 μg of RNA per reaction. If you have low concentrations or volumes of RNA, load 1 μg (or less) of RNA per reaction instead
2. Label tubes: Use the small 0.2 mL thin walled PCR tubes , one tube per sample. Also get one larger tube for the RT master mix. A no template control should also be made with 10μL of RT master mix and 10 μL nanopure water.
3. Prepare 2X RT master mix: Make enough for 1 extra reaction to account for pipetting error. Use filter tips for PCR.

Component	Volume per reaction (μL)	Volume for ___ reactions (μL)
10X RT Buffer	2.0	
25X dNTP mix	0.8	
10X RT random primers	2.0	
Multiscribe Reverse Transcriptase	1.0	
Nuclease-free H2O	4.2	
TOTAL	10.0	

4. Add water and RNA sample: Use the RNA dilutions sheet to load the appropriate amount of nanopure water, followed by the RNA sample. There should be 10 μL total of RNA + water.
5. Add 10 μL of 2X RT Master Mix to each tube.
6. Program the Bio-Rad Thermal cycler: Using the Bio-Rad T100-Thermocycler in room 140 Kinzelberg and run pr otocol: AB-HC-RT. The program should have the following parameters:

   1. 25^0 C for 10 minutes

   2. 37^0 C for 120 minutes

   3. 85^0 C for 5 minutes

   4. 4^0 C
7. Load samples and run RT reaction: Spread out your samples evenly. Start the PCR run, and come back in two hours for your cDNA.

RT-PCR

The following directions were written for TaqMan Fast Advanced Master Mix

1. Thaw Taqman Fast Advanced Master Mix, Taqman Prime/probes and dilute cDNA sample at room temperature
2. Use the PCR MM Calculator (see ATM Lab Protocol Folder > RT-PCR for a copy) to calculate appropriate volumes
3. In one tube make enough master mix (water + Taqman Master Mix + Primer/probe) for all samples
4. Vortex and spin the master mix
5. Aliquot 64.8 µL to a set of tubes – one tube for each sample
6. Vortex and spin the cDNA
7. Add 7.2µL cDNA to each tube of aliquoted master mix
8. Vortex and spin each reaction tube (master mix + cDNA)
9. Pipette 20µL of each reaction into 3 wells of a 96 well plate
10. Cover the plate with a clear cover
11. Spin the plate on the centrifuge on the second floor at 1000 rpm for 1 minute
12. Read the plate on the LightCycler480 on the 3rd floor

Seahorse Flux Analysis

1. Hydrate cartridge 12+ hours prior to assay in non CO2 incubator
2. Prepare unbuffered assay medium: pH to7.4 @ 37 degrees
3. Warm assay medium to 37 degrees in non-CO2 incubator
4. Prepare injectable compounds using assay medium to 7.4 @ 37 degrees

a. 50 μL oligomycin + 50 μL FCCP + 400 μL medium

5. Check cells under microscope
6. Replace cell culture medium with assay medium
7. Place cells in assay medium into non-CO2 incubator for 30+ minutes prior to assay run
8. Load injectable compounds (56 μL) into port A
9. Place cartridge and utility plate with calibration buffer into XF Analyzer
10. Run protocol from template to calibrate cartridge
11. Upon completion of cartridge calibration, load cell culture plate into instrument
12. Continue to run assay protocol
13. Upon completion of run, complete live/dead stain
    a. 1 mL media + 20 μL propidium iodide + 5 μL Hoescht → spike 25 μL per well
    b. Incubate 20-30 minutes
    c. Read on Celigo
14. Normalize ECAR and OCR readings to live cell count in each well

Glucose Uptake

1. Make 2DPG Detection Reagent 1 hr prior to use
    a. Luciferase, 3300 μL
    b. NADP+, 33 μL
    c. G6PDH, 82.5 μL
    d. Reductase, 16.5 μL
    e. Reductase substrate, 2.06 μL
2. Remove media, wash with 100 μL glucose free media

3. Add 50 µL 2DG Detection Reagent media/well
4. Add 50 µL glucose free media to background wells
5. Spike 25 µL Hoescht dilution in normalization row → incubate → read celigo
6. Wash normalization row and add 50 µL glucose free media
7. After 1 hr of 2DG incubation, add stop buffer, neutralization buffer, detection buffer
8. Read luminescence after 1 hour incubation

Puromycin

1. Stock = 25 mg/mL
2. Dilute 1:1000
3. Add 202.5 µL of 1:1000 diluted stock + 922.5 µL media
4. Spike 25 µL of dilution into each well
5. Leave 20 min
6. Aspirate
7. Add 150 µL Paraformaldehyde
8. Leave 20 min
9. Aspirate
10. Add 150 µL sodium azide per well
11. Wrap plate with parafilm and store in refrigerator
12. Wash 5x with 200 µL 0.1% Triton X-100 solution in 1X PBS at RT
13. Block with 150 µL Odyssey Blocking Buffer for 1.5 h at RT

14. Add 50 µL diluted antibody (1:1000) to all wells except controls. Add 50 µL Odyssey Blocking Buffers to control wells. Incubate for 2.5 h at RT or overnight at 4 degrees C with gently shaking.
15. Wash 5x with 200 µL 0.1% Tween 20 in 1x PBS solution at RT
16. Add 50 µL diluted secondary antibody/ cell tag 700 to all wells except the control well. Add 50 µL diluted secondary antibody to the control wells. Wash 5x with 200 µL 0.1% Tween 20 in 1x PBS solution at RT
17. After final wash, completely remove solution from wells; scan immediately on Licor or store from light at 4°C

R Code

Code for Paper: Expansion capacity of human muscle progenitor cells differs by age, sex, and metabolic fuel preference

- For variables: percent dead tAUC, live nuclei nAUC, confluency nAUC, saturation density, population doubling time, baseline OCR, stressed OCR, OCR metabolic potential, baseline ECAR, stressed ECAR, ECAR metabolic potential, OCR/ECAR ratio, and glucose uptake:

```
library(lme4)
library(ggplot2)
library(lsmeans)
library(pbkrtest)
my_data<-read.csv("Growth_Metabolic_R.csv")
str(my_data)
table(my_data$Age, my_data$Sex)
```

```
install.packages("car")
library(car)
View(my_data)
#Run the ANOVA
ANOVA_PDT<-aov(PDT ~ Age*Sex, data=my_data)
Anova(ANOVA_PDT, type="III")
#Compute summary statistics
model.tables(ANOVA_PDT, type="mean", se=TRUE)
#Multiple comparisons if interaction is significant
TukeyHSD(ANOVA_PDT)
#Check homogeneity of variance assumption
plot(ANOVA_PDT)
leveneTest(PDT ~ Age*Sex, data=my_data)
plot(ANOVA_PDT,2)
#extract residuals
aov_residuals<-residuals(object=ANOVA_PDT)
shapiro.test(x=aov_residuals)
```

- For variables: percent dead, live nuclei count, and percent confluency over time:

```
library(lme4)
library(ggplot2)
library(lsmeans)
library(pbkrtest)
```

```
library(emmeans)
my_data<-read.csv("Curves_For_R.csv")
str(my_data)
table(my_data$Age, my_data$Sex)
install.packages("car")
library(car)
View(my_data)
#Run the ANOVA
ANOVA_Nuclei<-aov(Confluency ~ Group*as.factor(Time), data=my_data)
Anova(ANOVA_Nuclei, type="III")
#For pairwise testing in linear model at each time point
Nuclei.lm<-lmer(Confluency ~ Group*as.factor(Time) +(1|Sample), data=my_data)
Anova(Nuclei.lm, type="III")
emmeans(Nuclei.lm, pairwise~Group|as.factor(Time), at=list(Time=c(24,48,72,96,120)))

#Pairwise and adjust
Nuclei.emm<-emmeans(Nuclei.lm, pairwise~Group|as.factor(Time),adjust="bonferroni")
Nuclei.summary<-summary(Nuclei.emm$contrast)
Nuclei.summary
```

- For variables: mRNA levels of *PPARGC1α*, *CD36*, *GLUT1*, and *GLUT4* over time:

```
library(lme4)
library(ggplot2)
```

```
library(lsmeans)
library(pbkrtest)
my_data<-read.csv("PCR_Metabolic_R.csv")
str(my_data)
table(my_data$Age, my_data$Sex)
install.packages("car")
library(car)
View(my_data)
#convert time to a factor
my_data$Time<-factor(my_data$Time, levels=c(1,2))
#Run the ANOVA
ANOVA_GLUT4<-aov(GLUT4 ~ Age*Sex*Time, data=my_data)
Anova(ANOVA_GLUT4, type="III")
#If interaction is not significant, replace * with + (additive model)
#Compute summary statistics
model.tables(ANOVA_LN_96, type="mean", se=TRUE)
#Multiple comparisons if interaction is significant
TukeyHSD(ANOVA_GLUT4)
#Check homogeneity of variance assumption
plot(ANOVA_PDT)
leveneTest(PDT ~ Age*Sex, data=my_data)
plot(ANOVA_PDT,2)
#extract residuals
```

```
aov_residuals<-residuals(object=ANOVA_GLUT1)
shapiro.test(x=aov_residuals)
```

Code for Paper: Transcript profile distinguishes variability in human myogenic progenitor cell expansion capacity

- For variables: confluency, live nuclei count, and percent dead over time:

```
library(lme4)
library(ggplot2)
library(lsmeans)
library(pbkrtest)
library(emmeans)
my_data<-read.csv("Curves_For_R.csv")
str(my_data)
table(my_data$Age, my_data$Sex)
install.packages("car")
library(car)
View(my_data)
#Run the ANOVA
ANOVA_Nuclei<-aov(Confluency ~ Group*as.factor(Time), data=my_data)
Anova(ANOVA_Nuclei, type="III")
#For pairwise testing in linear model at each time point
Nuclei.lm<-lmer(Confluency ~ Group*as.factor(Time) +(1|Sample), data=my_data)
```

```
Anova(Nuclei.lm, type="III")

emmeans(Nuclei.lm, pairwise~Group|as.factor(Time), at=list(Time=c(24,48,72,96,120)))


#Pairwise and adjust

Nuclei.emm<-emmeans(Nuclei.lm, pairwise~Group|as.factor(Time),adjust="bonferroni")

Nuclei.summary<-summary(Nuclei.emm$contrast)

Nuclei.summary
```

Code for Paper: RNA Transcript profile distinguishes human muscle progenitor cell inflammatory susceptibility

- For variables puromycin and mRNA:

```
library(lme4)

library(ggplot2)

library(lsmeans)

library(pbkrtest)

my_data<-read.csv("PCR_and_Puromycin.csv")

str(my_data)

table(my_data$Age, my_data$Sex)

install.packages("car")

library(car)

View(my_data)

#Run the ANOVA

ANOVA_PDT<-aov(PDT ~ Age*Sex, data=my_data)
```

```
Anova(ANOVA_PDT, type="III")

#If interaction is not significant, replace * with + (additive model)

#Compute summary statistics

model.tables(ANOVA_Con_408, type="mean", se=TRUE)

#Multiple comparisons if interaction is signifcant

TukeyHSD(ANOVA_PDT)

#Check homogeneity of variance assumption

plot(ANOVA_PDT)

leveneTest(PDT ~ Age*Sex, data=my_data)

plot(ANOVA_PDT,2)

#extract residuals

aov_residuals<-residuals(object=ANOVA_PDT)

shapiro.test(x=aov_residuals)
```